ELECTRON TRANSFER REACTION BETWEEN SELECTED AROMATIC AMINES AND Cu^{2+} IN ACETONITRILE; KINETIC, SPECTROSCOPIC AND MECHANISTIC INVESTIGATIONS

THESIS SUBMITTED TO
THE UNIVERSITY OF KERALA
FOR THE DEGREE OF
DOCTOR OF PHILOSOPHY
IN CHEMISTRY
UNDER THE FACULTY OF SCIENCE

By

SREENATH K.

UNDER THE SUPERVISION OF

Dr. K. R. GOPIDAS

PHOTOSCIENCES AND PHOTONICS
CHEMICAL SCIENCES AND TECHNOLOGY DIVISION
NATIONAL INSTITUTE FOR INTERDISCIPLINARY SCIENCE AND TECHNOLOGY
COUNCIL OF SCIENTIFIC AND INDUSTRIAL RESEARCH
TRIVANDRUM 695019
KERALA, INDIA

FEBRUARY 2010

STATEMENT

I hereby declare that the matter embodied in the thesis entitled, “**Electron Transfer Reaction between Selected Aromatic Amines and Cu^{2+} in Acetonitrile; Kinetic, Spectroscopic and Mechanistic Investigations”** are results of investigations carried out by me at the Photosciences and Photonics Section, Chemical Sciences and Technology Division of the National Institute for Interdisciplinary Science and Technology, Council of Scientific and Industrial Research, Trivandrum, under the supervision of Dr. K. R. Gopidas and the same has not been submitted elsewhere for a degree.

In keeping with the general practice of reporting scientific observations, due acknowledgement has been made wherever the work described is based on the findings of other investigators.

Sreenath K.

राष्ट्रीय अंतर्विषयी विज्ञान तथा प्रौद्योगिकी संस्थान
(पहले - क्षेत्रीय अनुसंधान प्रयोगशाला)
वैज्ञानिक एवं औद्योगिक अनुसंधान परिषद्
NATIONAL INSTITUTE FOR INTERDISCIPLINARY SCEINCE AND TECHNOLOGY
(*Formerly*-REGIONAL RESEARCH LABORATORY)
COUNCIL OF SCIENTIFIC AND INDUSTRIAL RESEARCH
इन्डस्ट्रियल इस्टेट डाक घर, तिरुवनंन्तपुरम् -695 019, भारत
Industrial Estate P. O., Thiruvanthapuram-695 019
KERALA, INDIA

डॉ. के. आर. गोपिदास
वैज्ञानिक
Dr. K. R. GOPIDAS
Head
Photosciences and Photonics
Chemical Sciences and Technology Division

February 16, 2010

CERTIFICATE

This is to certify that the work embodied in the thesis entitled, "**Electron Transfer Reaction between Selected Aromatic Amines and Cu^{2+} in Acetonitrile; Kinetic, Spectroscopic and Mechanistic Investigations**" has been carried out by Mr. Sreenath K., under my supervision and the same has not been submitted elsewhere for a degree.

K. R. Gopidas
(Thesis Supervisor)

ACKNOWLEDGEMENTS

It is with immense pleasure that I express my deep sense of gratitude to my research supervisor Dr. K. R. Gopidas, for suggesting the research topic and for his guidance, constant support and encouragement that led to the successful completion of this work.

I express my sincere thanks to Professor M. V. George for his inspiration, motivation and moral support during the course this work.

I thank Dr. Suresh Das, Director, NIIST, Trivandrum and former Directors Dr. B. C. Pai and Prof. T. K. Chandrasekhar for providing me the necessary facilities for carrying out this work.

My sincere thanks are also due to,

- *Dr. A. Ajayaghosh, Dr. D. Ramaiah and Dr. K. George Thomas, the Scientists of Photosciences and Photonics Section, for their help and support.*
- *Professor Robert A. Flowers II, Lehigh University, USA, for help and support during my visit to Lehigh University under DST-NSF collaboration.*
- *Mr. Robert Philip and Mrs. Sarada Nair for general help and support.*
- *Mrs. Soumini Mathew and Mr. B. Adarsh for NMR; Mrs. Viji for HRMS analysis.*
- *My seniors, Dr. E. Prasad, Dr. S. Sumalekshmy, Dr. Bijitha Balan, and Dr. G. Ajayakumar for their help and support.*
- *My colleagues Mr. C. V. Suneesh, Mr. V. K. Ratheesh Kumar, Mrs. Deepthi. L. Sivadas, Ms. A. M. Rakhi, Mr. K. Retheesh, Mr. M. V. Vinayak, Mr. Tony George Thomas, Ms. K. Sreedevi and all other members of Photosciences and Photonics for their help and affection.*
- *All friends in other divisions of NIIST for their help and support.*
- *Council of Scientific and Industrial Research (CSIR) for research fellowship, Department of Science and Technology (DST), Government of India and National Science Foundation (NSF), USA, for the financial assistance.*

- *I am deeply grateful to my parents and my sister for their constant love and care, which have been a great source of inspiration. I would also like to thank all my teachers for their help and blessings.*

Finally, I thank the Almighty for everything.

Sreenath K.

CONTENTS

Chapter 1 **An Overview of Aromatic Amine Radical Cations**

Chapter 2 Generation of Aromatic Amine Radical Cations by Reaction with Cu^{2+} in Acetonitrile: Kinetic and Mechanistic Aspects

Chapter 3 Reactivity Patterns of a few Aromatic Amine Radical Cations

Chapter 4 Cu^{2+} Mediated Generation of Dications of a few Selected Aromatic Amines and Design of a Selective Cu^{2+} Sensor

PREFACE

Radical cations of amines are important intermediates in a large number of single electron transfer reactions. They are formed by the one electron oxidation of amines and are involved in the synthesis of amino acids, alkaloids and several other nitrogen containing compounds of biological and pharmaceutical importance. Amine radical cations are also important intermediates in several technological applications such as imaging and photo-polymerization. Hence, generation of amine radical cations and study of their structural and reactivity aspects are extremely important.

The thesis consists of four chapters. Chapter 1 is a review of the different methods available for generating amine radical cations. These include treatment of the substrates with oxidizing metals, Lewis acids, protic acids and stable radicals. Other methods include anodic oxidation, photo-ionization, photo-induced electron transfer (PET), γ-irradiation and inclusion in zeolite cavities. Even though a variety of methods are available for the generation of aromatic amine radicals, these methods are synthetically not very useful.

Recently our group introduced an easy and effective method for the generation of aromatic amine radical cations. The reaction involves mixing of aromatic amine with Cu^{2+} in acetonitrile. The radical cations generated were characterized by absorption and ESR spectroscopy. Chapter 2 of the thesis deals with a study of the kinetics of the electron transfer reaction between aromatic amine and Cu^{2+} as a function of driving force and temperature. A broad range of triphenylamine derivatives (**TPA**) were studied, and the driving force for the electron-transfer reaction ranged from +3.67 to -8.56 kcal M^{-1} with rate constants varying from 1.09×10^2 to 2.15×10^5 M^{-1} s^{-1} for these systems. Fitting of the rate data to the Marcus equation using different values of the electronic coupling matrix element H_{el} provided a good fit with H_{el} =100 cm^{-1} suggesting that electron transfer in the **TPA**/Cu^{2+} system conforms to the Marcus-type electron transfer.

Third chapter of the thesis deals with the synthetic utility of the above reaction. We observed that amine radical cations undergo dimerization to give benzidines in very good yields. In the presence of nucleophiles, the radical cations undergo nucelophilic substitution to give *para*-substituted products in good to excellent yield. Suitable mechanisms are proposed for dimerization and substitution reaction.

We observed that easily oxidizable aromatic amines reacted with excess Cu^{2+} to generate dications. Some of the dications are very stable and a few are highly reactive. The stability and reactions of dicationic species were studied using common spectroscopic technique. The play of colors shown by tris(4-methoxyphenyl)amine/Cu^{2+} was utilized as a simple tool for detecting and quantifying micro molar amounts of Cu^{2+} in water:acetonitrile (1:9) mixture. Details of the study are presented in the fourth Chapter.

…………………………………………………………………………………..

Note: The Number of the various compounds given in each chapter corresponds to those given under the respective chapters.

Chapter 1

An Overview of Aromatic Amine Radical Cations

1.1. Introduction

Reactive intermediates occupy a fascinating place in Organic Chemistry. Most commonly observed reactive intermediates are carbocations, carbanions, radicals, carbenes and nitrenes. A vast variety of organic reactions take place via these intermediates. These reactive intermediates are formed by cleavage of carbon-carbon or carbon-heteroatom bonds. For example, radicals are formed by the homolytic cleavage of C-C or C-X bonds, whereas heterolytic bond cleavages in the above systems lead to carbocations or carbanions. Formation of carbenes and nitrenes requires two successive heterolytic bond cleavages. Several books and reviews are available that deal with the generation, structure and reactivity studies of these reactive intermediates.[1]

In 1928 E. Z. Weitz introduced two other reactive intermediates namely, cation radical and anion radical, which are formed from neutral molecules by the removal or addition of one electron as shown in Scheme 1.1.[2]

$$\mathbf{R\text{-}X} \;-\; \mathbf{e^-} \longrightarrow [\mathbf{R\text{-}X}]^{+\bullet} \qquad \textbf{Cation radical}$$

$$\mathbf{R\text{-}X} \;+\; \mathbf{e^-} \longrightarrow [\mathbf{R\text{-}X}]^{-\bullet} \qquad \textbf{Anion radical}$$

Scheme 1.1

In the above reactions no bonds are formed or broken and the ion radicals differed from the parent molecules only in the number of electrons. Although the terms ‘cation radical’ and ‘anion radical’ were used originally, usage of the alternate terms ‘radical cation’ and ‘radical anion’ is also very common. Radical ions were considered as ‘interesting’, but synthetically ineffectual intermediates. Hence, compared to other reactive intermediates (carbocations, carbanions etc), the chemistry of radical ions were much less explored.

Organic molecules can be designated as ‘donors’ or ‘acceptors’ depending on the energy levels of the highest occupied (HOMO) and lowest unoccupied (LUMO) molecular orbitals. Molecules with a high energy HOMO (donors) will have low oxidation potentials and would exhibit a tendency to lose an electron from the HOMO. The resulting radical cation will be positively charged and would have an unpaired electron in the HOMO as shown in Figure 1.1. In a similar way, molecules with low energy LUMO will exhibit a tendency to accept electrons into its LUMO. The radical anion thus formed would have an unpaired electron in the LUMO and will have a negative charge as shown in Figure 1.1.

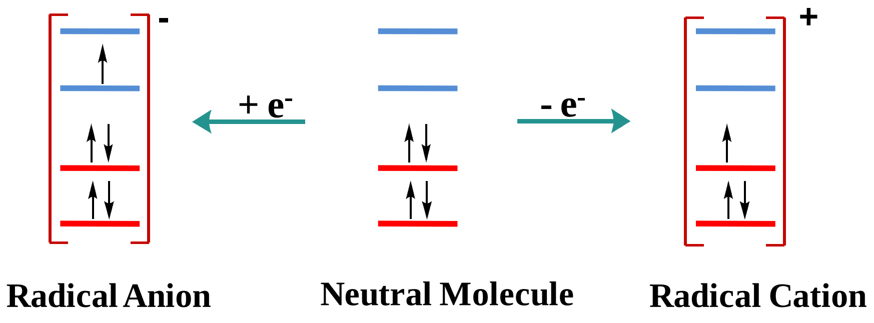

Figure 1.1 Electronic configurations for neutral molecule, radical cation and radical anion.

As is evident from Figure 1.1, ion radicals have dual character. They contain an unpaired electron and are, therefore, close to radicals. Since they contain a charge, they also behave like ions and will react with oppositely charged species.

In this thesis we are mainly focused on aromatic amine radical cations. These are formed by one electron oxidation of aromatic amines, which are very good electron donors. Schmittel and Burghart have classified electron donors based on the orbital from which electron is removed during the oxidation process.[3] The atom or group of atoms exhibiting the largest HOMO coefficient was designated as 'electrophore' and based on the nature of the electrophore, donors were classified as σ, π or n donors. Thus, toluene is a π donor, triethylamine is an n donor and cyclopropane is a σ donor.

The generation of radical cations and study of their reactivity patterns have gained considerable attention in recent years.[3,4] It is now established that radical cations can undergo a variety of reactions. For example, they can undergo isomerization, ring closure, bond cleavage, and deprotonation reactions.

They can also react with neutral substrates or undergo nucleophilic reactions. However, compared to the well-known chemistry of cations and radicals, many aspects of radical cation chemistry still need to be explored.

Among the large family of radical cations, aromatic amine radical cations are especially interesting because they are found as important intermediates in a large number of single electron transfer reactions[5] and also in the synthesis of various biologically and pharmaceutically important compounds, such as amino acids, alkaloids and other nitrogen-containing compounds.[6] Amine radical cation intermediates are also involved in technical applications such as photopolymerization[7] and imaging.[8] The most important reactions of amine radical cations include dimerization and reactions with nucleophiles. Several papers dealing with mechanistic studies of these reactions have appeared recently.[9]

In this thesis we describe a simple method for the generation and study of aromatic amine radical cations. The method involves treatment of the amine with copper(II) in acetonitrile. Mechanistic and spectroscopic aspects of this reaction are explored in some detail. We have also explored the utility of this reaction in synthetic applications. In order to put our work in proper perspective, the literature on amine radical cations is reviewed in the following section. Methods currently available for the generation of amine radical cations are described. This is followed by a description of the techniques available for the characterization of amine radical cations. A few reactions where amine radical cations are involved as intermediates are then presented.

1.2. Generation of Aromatic Amine Radical Cations

One electron oxidation of aromatic amines could be achieved by a variety of methods such as chemical oxidation, photochemical oxidation, or electrochemical oxidation. Other methods include pulse radiolysis and electron impact ionization. In this section some of these methods are described.

1.2.1. Chemical Oxidation

A variety of chemical oxidants were employed for the generation of radical cations. These include, Brønsted acids, Lewis acids, the halogens, certain zeolites, numerous metal ions, metal oxides and stable organic radical cations. Sulphuric acid was the first Brønsted acid used for this purpose. In one of the early experiments, Laurent treated diphenylamine (**1**), isolated from bitter almonds, with sulphuric acid, which resulted in the formation of a blue coloured solution. The blue colour was attributed to diphenylamine radical cation ($\mathbf{1}^{\bullet+}$).[10]

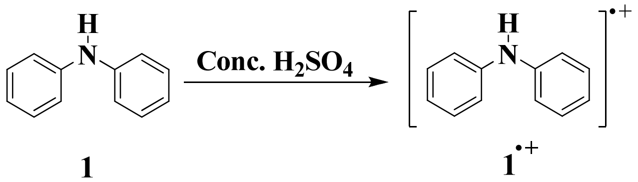

Scheme 1.2

In 1915 Kehrmann used the same reagent for the one and two electron oxidations of phenothiazine (**2**), and thoroughly characterized the radical cation by absorption spectroscopy.[11]

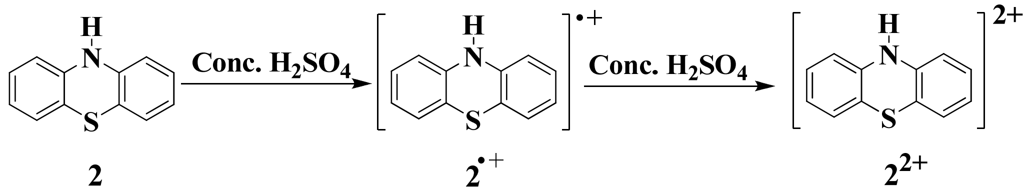

Scheme 1.3

Lewis acids such as $SbCl_5$, $AlCl_3$, PF_5 and SO_3 have been used effectively to generate a variety of radical cations. Hilpert and Wolf utilized $SbCl_5$ to generate radical cations of hydrocarbons such as benzene and anthracene.[12] Kainer and Hausser reacted 4,4'-dimethoxydiphenylamine (**3**) with $SbCl_5$ and obtained the $SbCl_6^-$ salt of $\mathbf{3}^{\bullet+}$ as shown in Scheme 1.4.[13]

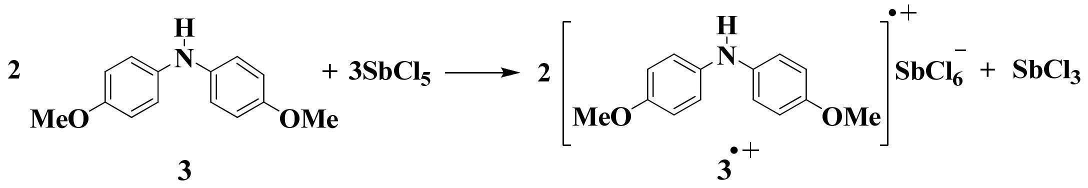

Scheme 1.4

In the above reaction actual oxidizing agent is $SbCl_4^+$ which is formed as a result of disproportionation of $SbCl_5$ as shown in Scheme 1.5.

$$2SbCl_5 \longrightarrow SbCl_6^- + SbCl_4^+$$

$$SbCl_4^+ + \text{amine} \longrightarrow SbCl_4^\bullet + \text{amine}^{\bullet+}$$

$$2SbCl_4^\bullet \longrightarrow SbCl_5 + SbCl_3$$

Scheme 1.5

Among the halogens bromine was found to be a more useful oxidizing reagent than chlorine and iodine. Iodine is not a good enough oxidant, while chlorine engages in electrophilic substitution. In 1879 the German chemist Casimir Wurster employed bromine for oxidizing *N,N'*-dimethyl-*p*-phenylenediamine (**4**) and *N,N,N',N'*-tetramethyl-*p*-phenylenediamine (**5**) to their radical cations.[14]

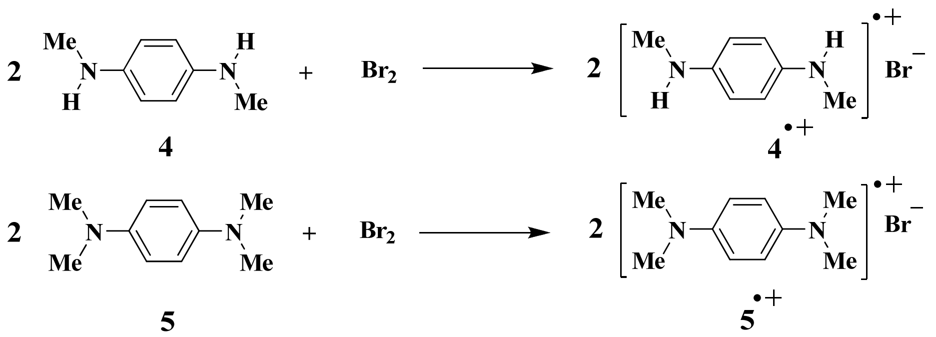

Scheme 1.6

Later Wieland used Br_2 to generate aminium salts of triphenylamine (**6**), *N,N,N',N'*-tetraphenyl-*p*-benzidine (**7**) and their derivatives.[15] Even though bromine acts as an oxidizing agent, its tendency to add readily to unsaturated and strained ring systems, limits its use in these reactions.

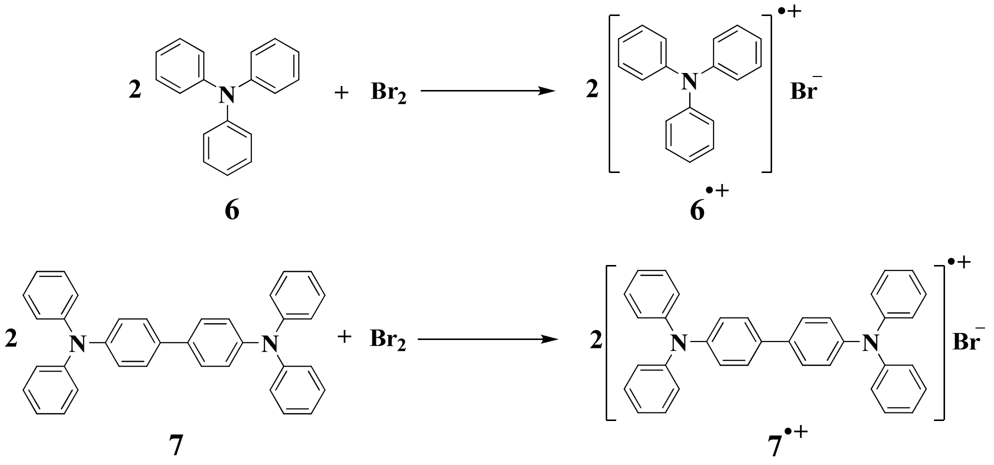

Scheme 1.7

The generation of organic radical cations by appropriately treated zeolites is well documented in the literature.[16] Zeolites are crystalline aluminum silicates, whose lattice consists of networks of SiO_4^{4-} and AlO_4^{4-} tetrahedra. There are numerous naturally occurring and synthetic zeolites, each with a unique structure. Some of the important zeolites are faujasite, linde type A, chabazite, offertite, phillipsite, erionite, linde type L, mordenite, ZSM-11, and ZSM-5.[17]An important characteristic of these crystals is that cations of different sizes and charges can be substituted in the lattice, without affecting lattice parameters. Zeolites possess large cavities that can incorporate molecules of appropriate shape and size. The incorporated molecules can be oxidized via cationic sites, heat or by exposure to ionizing radiation. The resulting radical cation remains within the cavity and hence is protected from bimolecular scavenging reactions.

Molecules having low ionization potentials, such as arylamines, polynuclear aromatic hydrocarbons, and phenylalkenes gave radical cations when adsorbed into faujasite type zeolites.[18] Stamires and Turkevich generated radical cations of triphenylamine (**6**) inside sodium zeolite.[18a] The radical ion so produced was identified through its hyperfine structure in electron spin resonance (ESR) spectrum. Chen and Fripiat observed the formation of aniline (**8**) radical cation on H-mordenite and H-faujasite type zeolites and studied the role of oxygen in the oxidizing ability of these zeolites.[19] Adsorption into H-mordenite cavities generated aniline radical cation ($\mathbf{8}^{\bullet+}$) and its ESR signal was found to be significantly enhanced on admitting molecular oxygen into the sample. In H-faujasite, ESR signal of $\mathbf{8}^{\bullet+}$ appeared only after molecular oxygen was introduced. This study showed that for generation of $\mathbf{8}^{\bullet+}$ inside mordenite, co-adsorption of oxygen is not a prerequisite, where as the assistance of oxygen is a prerequisite for radical cation generation in faujasite.

Flockhart *et al.* generated radical cation of **1** by adsorbing the amine on faujasite zeolite. $\mathbf{1}^{\bullet+}$ was identified by a weak, broad ESR spectrum. In the presence of polar liquid, $\mathbf{1}^{\bullet+}$ underwent radical-radical coupling leading to the formation of *N,N'*-diphenyl-*p*-benzidine (**9**).[20] Borkowski *et al.* observed conversion of $\mathbf{1}^{\bullet+}$ to diphenylnitroxyl radical in alkali metal exchanged zeolite and found that this reaction was more prominent on K^+ exchanged zeolites.[21] Incorporation of *N,N,N',N'*-tetramethyl-*p*-benzidine (**10**) into sodium zeolite, led to generation of its radical cation.[22] Similarly, tris(*p*-bromophenyl)amine (**11**) also was converted to its radical cation on zeolite.[23] But hydrazine (**12**) failed to generate radical cations in zeolite. However radical cation formation was observed if the hydrazine-zeolite sample is irradiated at -40 ^{0}C[24] (Scheme 1.8). Although zeolites generate long lived organic radical cations, monitoring reactions of radical cations inside zeolites is rarely reported and often times difficult to achieve.

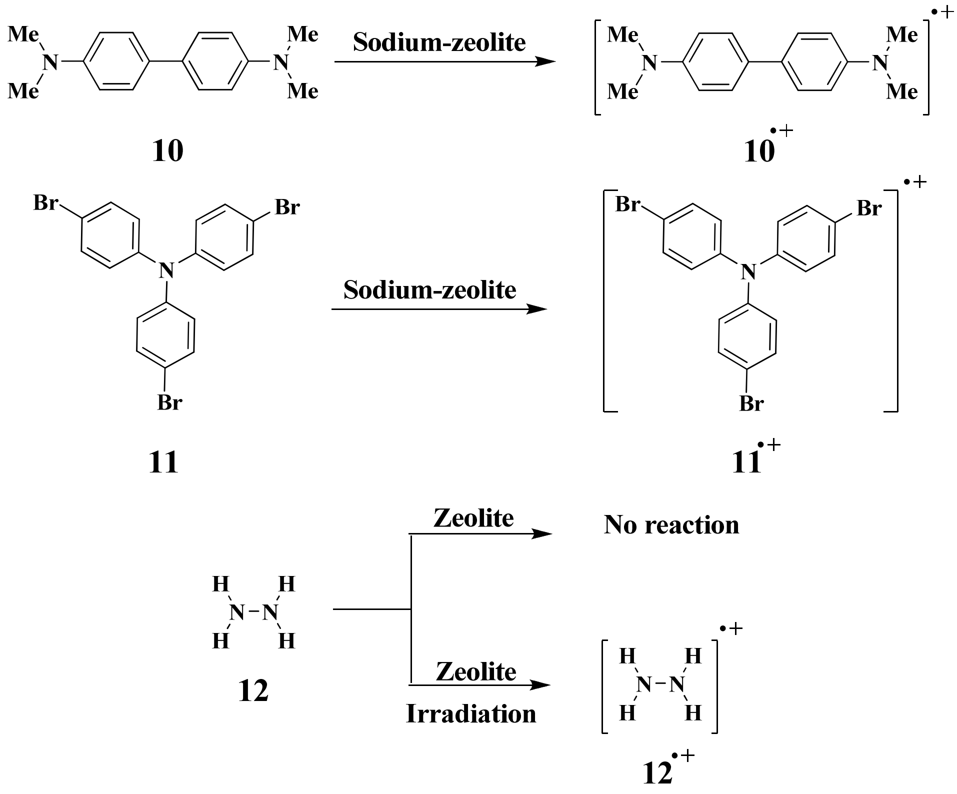

Scheme 1.8

1.2.2. Electrochemical Oxidation

Radical cations can also be generated electrochemically by means of heterogeneous electron transfer between an electrode, namely anode, and a substrate in a solution. An electrode is fundamentally an electron transfer agent so that, given the proper solvent system, anodic oxidation allows formation of the radical cation without formation of a reduced species in the immediate vicinity of the radical cation. Moreover, because the potential of the electrode can be adjusted precisely, its oxidizing power can be controlled and further oxidation of the radical cation can be avoided. A variety of electrochemical techniques, such as bulk electrolysis and micro-electrode techniques have been employed for the generation and study of organic radical cations.

Electrochemical methods in combination with optical and ESR spectroscopy has been of wide use to analyze radical cations. The electrochemical method, however, suffers from the disadvantage that the radical cations are formed in very high concentrations at the electrode surface, leading to their dimerization. This often hampers the reactions of the radical cations with other substrates.

Anodic oxidations of several aromatic amines have been well studied using trivial electrochemical setups and also in combination with a number of spectroscopic techniques like rapid scan spectrophotometry and ESR. Adams and coworkers have examined anodic oxidation pathways of triphenylamine (**6**) by electrochemical and ESR studies.[25] Since the existence of radical cation on the electrode surface is fleeting, they have carried out controlled potential electrolysis directly in the optical cell and spectrum was recorded during the first few seconds of electrolysis. For example, they detected $\mathbf{6}^{\bullet+}$ with absorption maximum near 640 nm. This assignment was in agreement with the early assignment of triphenylamine radical cation by Lewis and Lipkin, who obtained $\mathbf{6}^{\bullet+}$ via photooxidation in rigid media.[26] Radical cation of *N,N,N',N'*-tetraphenyl-*p*-benzidine ($\mathbf{7}^{\bullet+}$) was generated by external electrolysis of **7** and absorption spectrum exhibiting maximum at 480 nm could be recorded.

1.2.3. Radiolytical Generation of Radical Cations

W. H. Hamill pioneered this method and generated many organic radical cations and characterized them by ESR spectroscopy.[27] In this method ionized matrix materials were utilized as oxidizing agents to abstract electrons from target molecules. Halocarbon solvents, such as carbon tetrachloride, chlorobutane or freon mixtures served as matrix materials. High energy photons such as X-rays or γ- rays are employed to eject electrons from the matrix, which in turn abstracts electrons from the substrates to generate their radical cations.

Shida and coworkers generated radical cations of aromatic amines using γ-irradiated polycrystalline CCl_4 at 77 K.[28] γ-Irradiation of CCl_4 at 77 K resulted in an intermediate which absorbs in the visible and near UV (λ_{max}= 400 nm) regions. When a small amount of aromatic amine was added, a noticeable reduction of these absorption bands with the concomitant appearance of new bands characteristic of the amine radical cations were observed. The results obtained in this work indicated that the charge on CCl_4, generated by irradiation, can migrate to the amine sites to give amine radical cations. Radical cations generated in this way include *N,N'*-dimethyl-*p*-phenylenediamine (**4**), *N,N,N',N'*-tetramethyl-*p*-phenylenediamine (**5**), aniline (**8**), triphenylamine (**6**), diphenylamine (**1**), *N*-methylaniline (**13**) *N,N*-dimethylaniline (**14**), and *N,N*-diethylaniline (**15**).

1.2.4. Photoinduced Electron Transfer

Oxidative photoinduced electron transfer (PET) is a versatile method for the generation of radical cations. Since aromatic amines are good electron donors, excitation of the amines in presence of an acceptor or excitation of an acceptor in presence of an amine would lead to formation of amine radical cation as shown in Scheme 1.9.

$$\mathbf{A}^{*} + \mathbf{Amine} \longrightarrow \mathbf{A}^{\bullet -} + \mathbf{Amine}^{\bullet +}$$

$$\mathbf{A} + \mathbf{Amine}^{*} \longrightarrow \mathbf{A}^{\bullet -} + \mathbf{Amine}^{\bullet +}$$

Scheme 1.9

Generation of aromatic amine radical cation via PET mechanism is well documented in the literature. For example, radical cations of *N*,*N*-dimethylaniline (**14**) *N*,*N*,*N'*,*N'*-tetramethyl-*p*-phenylenediamine (**5**) and *N*-methylphenothiazine (**16**) have been detected by Anderson *et al.* in the flash photolysis of solutions containing the amines and tris(2,2'-bipyridyl)ruthenium(II) ($Ru(bpy)_3^{2+}$).[29]

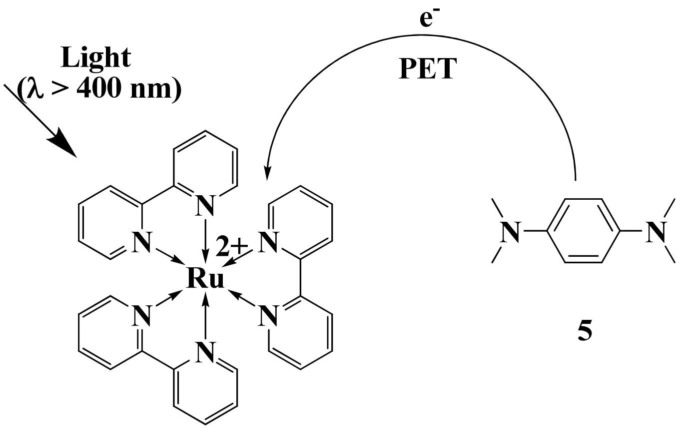

5

$Ru(bpy)_3^{2+}$

Scheme 1.10

For flash photolysis studies an acetonitrile solution containing $Ru(bpy)_3^{2+}$ and the amine was subjected to a visible flash to selectively excite $Ru(bpy)_3^{2+}$ and transient spectral changes were recorded by scanning the solution in the UV-Visible region. As a result of PET reaction, $Ru(bpy)_3^{2+}$ was reduced to $Ru(bpy)_3^{+}$ and amine was oxidized to its radical cation. In the case of amines **5** and **16**, radical cations $\mathbf{5}^{\bullet+}$ (λ_{max} = 564 and 612 nm) and $\mathbf{16}^{\bullet+}$ (λ_{max} = 514 and 753 nm), respectively, were observed. The authors also studied the rate of decay of radical cation and correlated it with the rate of return to ground-state reactants.

1.2.5. Electron Impact Ionization

The method employed here is similar to radiolytical generation of radical cations. In electron impact ionization, high energy electrons, ejected from a heated filament, is allowed to hit on substrate molecules at a very low pressure, nearly 10^{-6} torr. In the collision, energy is transferred to the substrate causing ionization. Low energy electrons produce molecular ions and larger fragments, whereas high energy electrons produce many smaller fragments and possibly no molecular ions. The process is a relatively harsh form of ionization, producing a wide range of molecular fragments. Electron impact ionization is used in mass spectroscopy to ionize and fragment sample molecules before mass analysis.

1.2.6. Chemical Ionization

Chemical ionization (CI) is an ionization technique used in mass spectrometry. CI is a low energy process compared to electron ionization. Low energy results in less fragmentation. In a CI experiment, ions are produced through collision of the analytes with ions of a reagent gas that are present in the ion source in large excess. Common reagent gases include methane, ammonia, and isobutane. Electrons entering the source will preferentially ionize the reagent gas. The resultant collisions with other reagent gas molecules will create an ionization plasma. Positive ions of the analytes will be formed by reaction with this plasma.

1.3. Detection of Radical Cations

Few instrumental techniques are available to detect and identify radical cations. These include optical spectroscopy, electron spin resonance and fluorescence detected magnetic resonance (FDMR).

1.3.1. Optical Spectroscopy

Optical spectroscopy is one of the most useful methods to identify radical cations. Radical cations generally exhibit good absorption in the Vis-NIR region of the spectrum. Changes in the absorption spectrum can be utilized to follow the reaction pathways of radical cations. Because of this, absorption spectroscopy is the preferred detection technique in laser flash photolysis and pulse radiolysis experiments, where radical ions are routinely studied.

1.3.2. Electron Spin Resonance

Electron spin resonance (ESR) spectroscopy is a very powerful and sensitive method for the characterization of the electronic structures of materials with unpaired electrons. A brief description of the ESR technique is given below.

Every electron has a magnetic moment and spin quantum number s= 1/2, with magnetic components $m_s = +1/2$ or $m_s = -1/2$. In the presence of an external magnetic field with strength B_0, the electron's magnetic moment aligns itself either parallel ($m_s = -1/2$) or antiparallel ($m_s = +1/2$) to the field, each alignment having a specific energy. The parallel alignment corresponds to the lower energy state, and the separation between the two states is $\Delta E = g_e \mu_B B_0$, where g_e is the g-factor and μ_B is the Bohr magneton. This equation implies that splitting of the energy levels is directly proportional to the magnetic field strength, as shown in Figure 1.2.

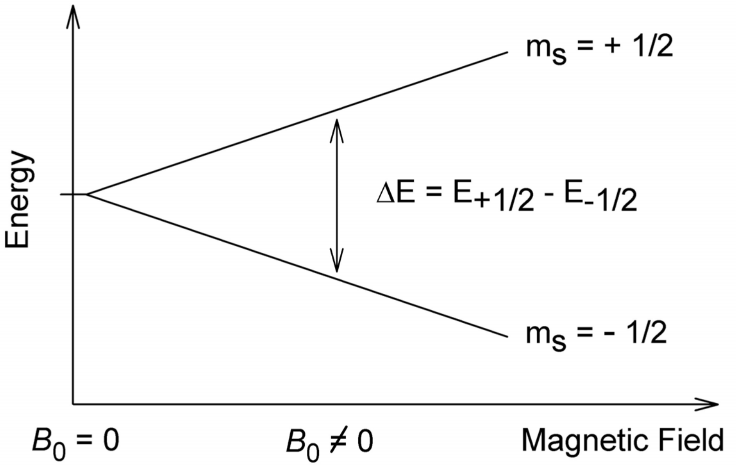

Figure 1.2

An unpaired electron can move between the two energy levels by either absorbing or emitting electromagnetic radiation of energy $\varepsilon = h\nu$ such that the resonance condition, $\varepsilon = \Delta E$, is obeyed. Experimentally, this equation permits a large combination of frequency and magnetic field values, but the great majority of ESR measurements are made with microwaves in the 9–10 GHz region, with fields corresponding to about 3500 G (0.35 T). Experimentally, resonance is approached by sweeping the field in the range near 3500 G and holding the frequency constant, typically at 9.6 GHz.

An important aspect in the identification of the radical or radical ions is the hyperfine interaction, which is the interaction of the unpaired spin with nearby magnetic nuclei. This gives rise to a pattern of signal characteristic of the radical ions. The spacing of the signal and their relative intensities identify the magnitude of interaction between electrons and groups of equivalent nuclei as well as nuclei coupled.

It is possible to detect short lived radical cations generated in flash photolysis experiments using time-resolved electron spin resonance (TR-ESR) techniques. The TR-ESR experiment requires sophisticated instrumentation, as it involves the repetitive generation of radicals by short laser pulses and the subsequent time-resolved recording of the transients.

1.3.3. Fluorescence Detected Magnetic Resonance (FDMR)

Fluorescence detected magnetic resonance **(**FDMR) technique can be used in the study of systems generating geminate ion pairs, where the ion pair produces fluorescence on recombination. It is also useful for examining the ESR spectra of short lived radical ion pairs, if they can form reaction products in electronically excited states that decay by radiative pathways.

Equations 1 to 8, shown in Scheme 1.11, summarize the sequence of processes that leads to a FDMR observation, in a photolytic generation of geminate ion pairs.

$$\mathbf{A} \xrightarrow{\mathbf{h\nu}} {}^{1}\mathbf{A}^{*} \qquad (1)$$

$$ {}^{1}\mathbf{A}^{*} + \mathbf{A} \xrightarrow{\mathbf{h\nu}} {}^{1}\left[\mathbf{A}^{\bullet +}\text{---}\mathbf{A}^{\bullet -}\right] \qquad (2)$$

$$ {}^{1}\mathbf{A}^{*} \xrightarrow{\mathbf{ISC}} {}^{3}\mathbf{A}^{*} \qquad (3)$$

$$ {}^{3}\mathbf{A}^{*} + \mathbf{A} \xrightarrow{\mathbf{h\nu}} {}^{3}\left[\mathbf{A}^{\bullet +}\text{---}\mathbf{A}^{\bullet -}\right] \qquad (4)$$

$$ {}^{1}\left[\mathbf{A}^{\bullet +}\text{---}\mathbf{A}^{\bullet -}\right] \longrightarrow {}^{1}\mathbf{A}^{*} + \mathbf{A} \qquad (5)$$

$$ {}^{1}\mathbf{A}^{*} \longrightarrow \mathbf{A} + \mathbf{h\nu} \qquad (6)$$

$$ {}^{3}\left[\mathbf{A}^{\bullet +}\text{---}\mathbf{A}^{\bullet -}\right] \longrightarrow {}^{3}\mathbf{A}^{*} + \mathbf{A} \qquad (7)$$

$$ {}^{3}\mathbf{A}^{*} \longrightarrow \mathbf{A} + \mathbf{h\nu} \qquad (8)$$

Scheme 1.11

Interaction of radiation such as electron beam, X-ray or laser pulse with the target molecule (**A**), leads to the formation of an excited singlet state (${}^{1}\mathbf{A}^{*}$). As shown in equation 2, the second photon can knock out an electron from the excited molecule resulting in the formation of its radical cation ($\mathbf{A}^{\bullet +}$) and the ejected electron may immediately abstract nearby target molecule, **A** and leads to its radical anion ($\mathbf{A}^{\bullet -}$). Since these ions are in the immediate vicinity they act as geminate ion pair in the singlet state (equation 2). The excited molecule, ${}^{1}\mathbf{A}^{*}$, can also undergo intersystem crossing (equation 3) and leads to an excited triplet state (^{3}**A***). The ^{3}**A*** can also follow the same path, as that of ^{1}**A*** and leads to geminate ion pair in the triplet state (equation 4). The recombination processes (equation 5 and 7) and subsequent de-excitation leads to delayed fluorescence (equations 6 and 8). The recombination of geminate ion pairs in singlet state (equation 5) and subsequent de-excitation (equation 6), produce intense fluorescence than that from a triplet geminate ion pair recombination. In the FDMR measurements, intensity of this delayed fluorescence is measured, when resonance condition for ESR measurements is attained. In presence of a magnetic field, geminate radical ion pairs formed in the singlet state will absorb resonant microwave radiation and recombine to produce the triplet state, leading to a decrease in fluorescence intensity. Similarly, initially formed triplet geminate ion pairs will absorb resonant microwave radiation to yield singlet state, resulting an increase in fluorescence intensity. The observation of an FDMR signal, therefore, will indicate whether photoionization occurs predominantly through a triplet or singlet pathway. The usual FDMR spectrum is a plot of the fluorescence intensity integrated over a selected time interval as a function of the applied magnetic field.

Trifunac *et al.* studied the generated ion pair from *N,N,N',N'*-tetramethyl-*p*-phenylenediamine (**5**) in 2-propanol using FDMR technique.[30] The FDMR spectrum consists of two peaks, a single sharp peak and a weaker broad band. They have assigned the broad spectrum to $\mathbf{5}^{\bullet+}$ and narrow peak to solvated electron, based on simulated spectra generated using coupling constants reported for **5**$^{\bullet+}$ and solvated electron. In the FDMR measurement fluorescence intensity decrease was observed, which indicates that photoionization occurred predominantly from singlet excited state in **5**.

1.4. Energy Levels and Charge Distribution in Aromatic Amine Radical Cations

Electronic transitions in amine radical cations are always observed red shifted to those of parent amines. For example, phenothiazine radical cation absorbs at 514 nm whereas the parent amine absorbs at 310 nm. Similarly, triphenylamine absorbs below 300 nm while its radical cation absorbs near 670 nm. In order to explain these low energy transitions, molecular orbital concept is useful. The ground state electronic configuration of an aromatic amine and its radical cation can be represented as shown in Scheme 1.12. The molecular orbital corresponding to the lone pair electrons on nitrogen is shown as the HOMO in Scheme 1.12. When the amine is oxidized, one of the electrons leaves HOMO and as a result the HOMO will be converted to singly occupied molecular orbital (SOMO) as shown in the Scheme 1.12.

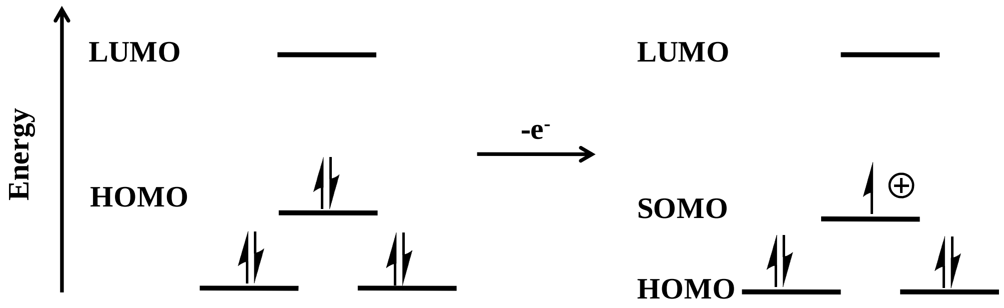

Scheme 1.12

The electronic level just below the SOMO now becomes HOMO. In such a state electronic transition from HOMO to SOMO will be the highest probable transition and which will account for the low energy absorption band in amine radical cations.

Lambert and coworkers studied spectral properties of triarylamine radical cations and correlated the obtained spectra with theoretical results computed using AM1-CISD calculations.[31] They have selected triphenylamine derivatives with all combinations of chloro, methoxy, and methyl substituents in the three *para*-positions and recorded absorption spectra of the radical cations. All the radical cations exhibited an intense absorption at 667-763 nm and a less intense and broader band at 569-653 nm, irrespective of whether the molecule is symmetric or unsymmetric. Actually, for symmetric molecules such as tris(*p*-anisyl)amine and tris(*p*-chlorophenyl)amine only one excitation to a degenerate state ($D_0 \rightarrow D_1$), would be expected as shown in Scheme 1.13.

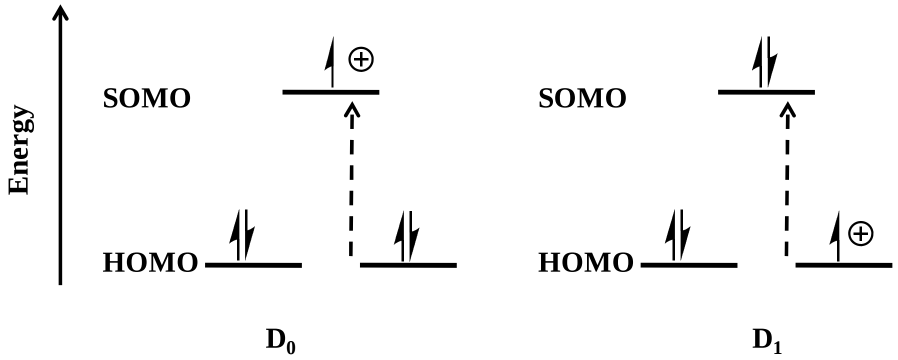

Scheme 1.13

Lambert attributed the dual absorption bands in symmetric molecules to symmetry breaking as a result of interaction with solvent molecules. Tris(*p*-anisyl)amine and tris(*p*-chlorophenyl)amine are propeller shaped, with the phenyl rings twisted out of plane as shown in Figure 1.3.

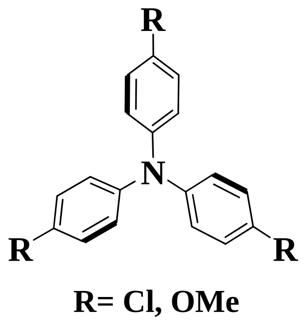

Figure 1.3. Propeller conformation of tris(*p*-anisyl)amine and tris(*p*-chlorophenyl)-amine.

These molecules have C_3 axis of symmetry and belong to C_3 point group. In the radical cation one of the phenyl rings assumes in-plane geometry due to interaction with solvent molecules. As a result it loses its C_3 axis of symmetry and changes to a C_2 point group. This symmetry breaking leads to loss of degeneracy in HOMOs and results in the formation of a low energy HOMO-1 orbital as shown in Scheme 1.14.

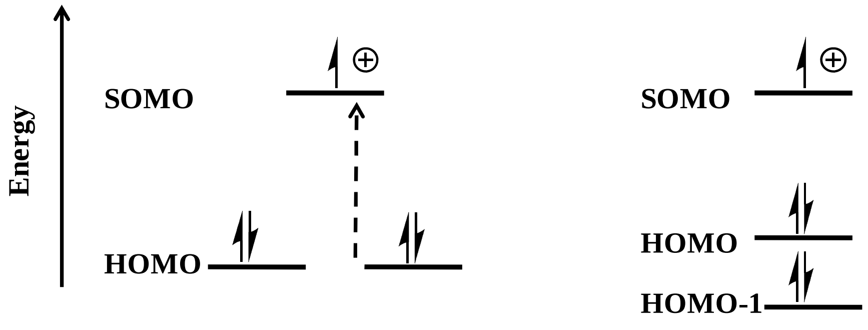

Scheme 1.14

As a result HOMO-1 → SOMO transition (transition from $D_0 \rightarrow D_2$ state) is the second probable excitation. Electronic configurations of D_0, D_1 and D_2 states in these radical cations are shown in Scheme 1.15.

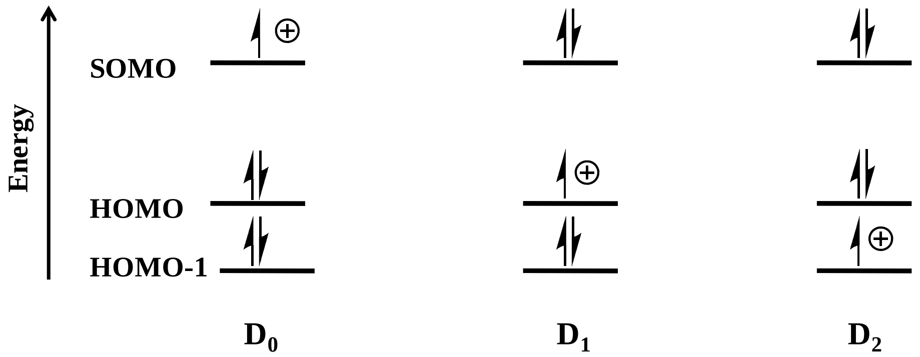

Scheme 1.15

In schematic representation of aromatic amine radical cation, the '•+' sign is usually placed on the nitrogen atom because of the availability of lone pair of electrons on the nitrogen. But recent theoretical studies do not support this representation. Zhang *et al.* made electron density calculations on *N*,*N*-dimethylaniline radical cation using *ab initio* Hartree-Fock molecular orbital methods and observed that nitrogen atom is in fact negatively charged (-0.708) and the two methyl groups bear positive charges of +0.482 each. The positive charge delocalization along benzene ring makes the ring electron deficient with a positive charge of +0.744. The resultant of all these charges is +1.[32] Similarly Nguyen *et al.* have shown by quantum-chemical calculations that nitrogen atom of the triradical-trication of 1,3,5-triaminobenzene bears negative charge and the positive charge is delocalized into the benzene core.[33]

1.5. Reactions of Aromatic Amine Radical Cations

Aromatic amine radical cations undergo a rich variety of reactions, including both unimolecular processes and bimolecular reactions. Bimolecular reactions include dimerization and nucleophilic substitutions. The amine radical cations can also undergo single electron transfer reactions with other substrates and initiate various reactions such as deprotection, isomerization, polymerization and cyclization. Amine radical cations also find important applications as catalyst in Diels-Alder reactions. In the following section, a brief account of these reactions is presented.

1.5.1. Dimerization Reaction of Aromatic Amine Radical Cations

Adams and coworkers generated radical cations of triphenylamine (**6**) and some of its derivatives by anodic oxidation.[25] They observed that radical cations generated at the electrode surface undergo very fast dimerization to yield benzidine derivative. For example, **6** was oxidized to $\mathbf{6}^{\bullet+}$ at +0.92 V vs SCE. The radical cation was found to undergo dimerization to form *N,N,N',N'*-tetraphenyl-*p*-benzidine (**7**). Since **7** is more easily oxidizable than the starting **6,** it undergoes oxidation to $\mathbf{7}^{\bullet+}$ and $\mathbf{7}^{2+}$ at the applied potential. This occurs in two discrete one electron steps. The authors proposed the mechanism shown in Scheme 1.16 for the electrochemical oxidation of **6**.

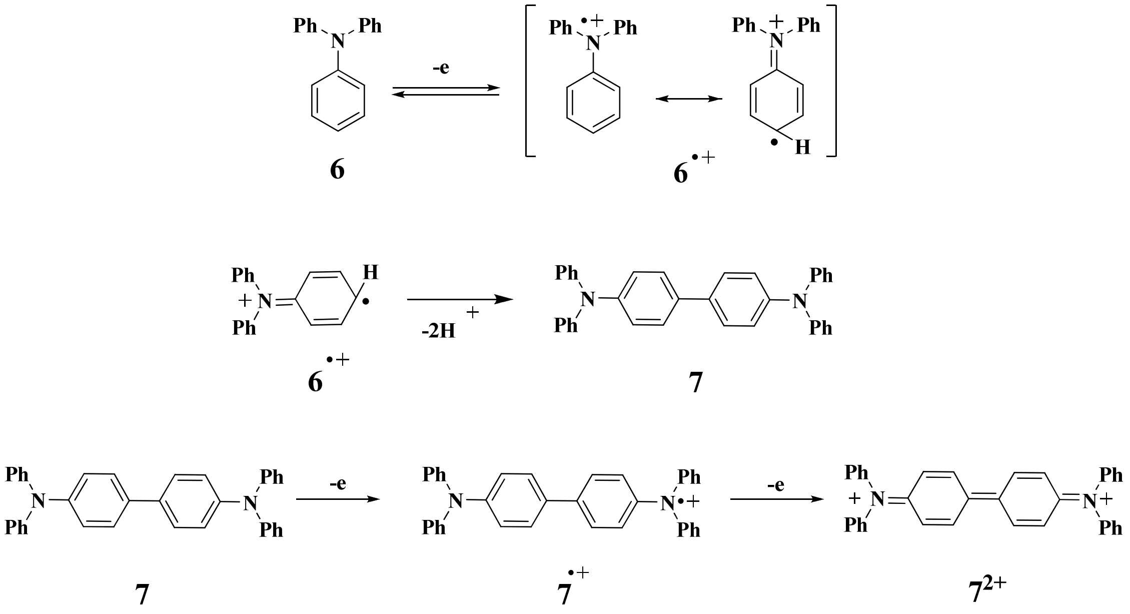

Scheme 1.16

Nelson *et al.* determined coupling rates of mono-*p*-substituted triphenylamine radical cations generated electrochemically in acetonitrile.[34] Quantitative data were obtained for several *p*-substituted triphenylamines in the form of second-order coupling rate constants. In the rate analysis it was found that electron-donating substituents tend to stabilize the cation radicals while electron-withdrawing groups had the opposite effect. The authors tried to correlate substituent effects on coupling rate and established a Hammett-type behaviour. Most of the substituent effects were adequately described by σ^+ values, with the exception of strong electron-donating functional groups.

Oyama and coworkers utilized amine radical cation salts to generate radical cations of various aromatic amines as well as aromatic hydrocarbons, by electron transfer stopped flow (ETSF) method.[35] Radical cations of diphenylamine (**1**), triphenylamine (**6**) and *N*-methyldiphenylamine (**17**) were generated by ETSF method by mixing an acetonitrile solution of tris(*p*-bromophenyl)amine radical cation (**11**$^{\bullet+}$) and these were identified by absorption spectroscopy (Scheme 1.17). Kinetic analysis has shown that decays of the radical cations were second order which confirms that dimerization reaction proceeds through a radical cation - radical cation coupling mechanism.

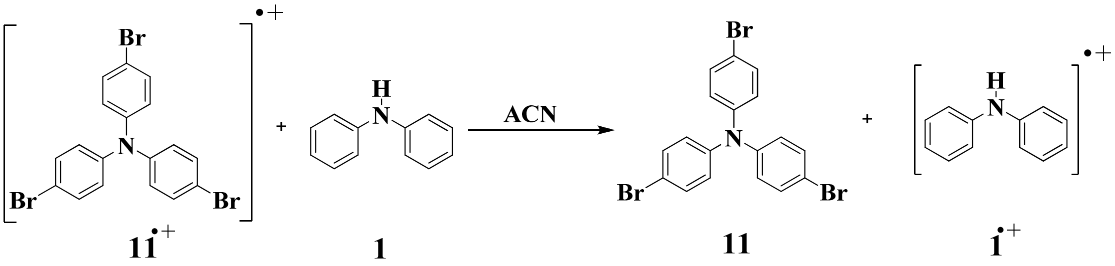

Scheme 1.17

Reaction of *N*,*N*-dimethyl-*p*-toluidine radical cation (**18**$^{\bullet+}$) in the presence of precursor amine (**18**) and pyridine (**19**) were studied in detail.[36] The decay rate of **18**$^{\bullet+}$ was accelerated in the presence of the parent amine and product formed in the reaction was identified as *N,N,N',N'*-tetramethyl-α,α'-bi-*p*-toluidine (**22**) (Scheme 1.18). When **19** was the base, proton is abstracted from one of the *N*-methyl groups leading to the formation of *N,N'*-dimethyl-*N,N'*-di-*p*-tolylethylenediamine (**25)** as shown in Scheme 1.18. Compared to electrochemical methods the ETSF method has permitted straight forward analysis of the decay kinetics of short-lived cation radicals and effect of precursor or other nucleophilic molecules on subsequent reaction.

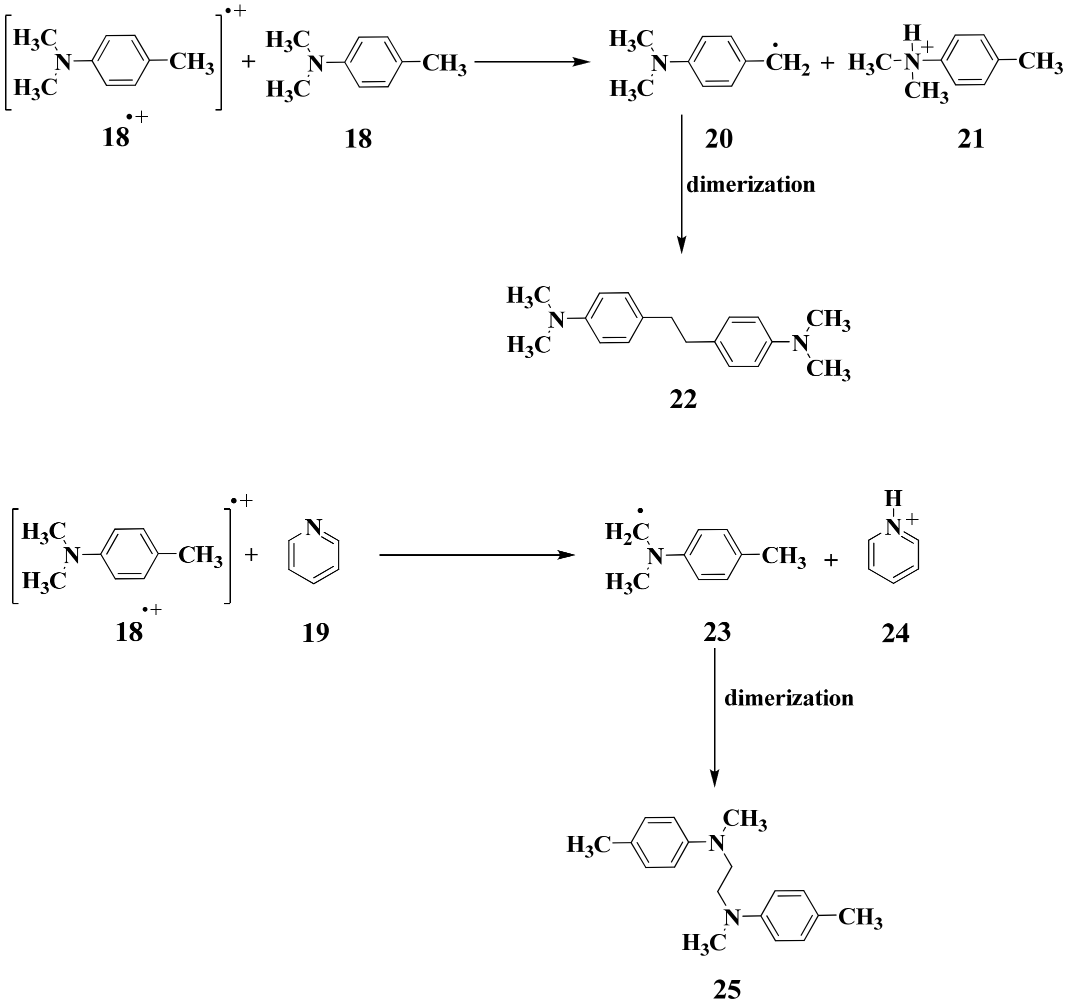

Scheme 1.18

Ichikawa *et al.* have utilized 1,8-bis(diphenylmethylium)naphthalenediyl dication (**26**) for the oxidative coupling reaction of aniline derivatives **27a-f**.[9c] Proposed mechanism for the coupling is shown in Scheme 1.19.

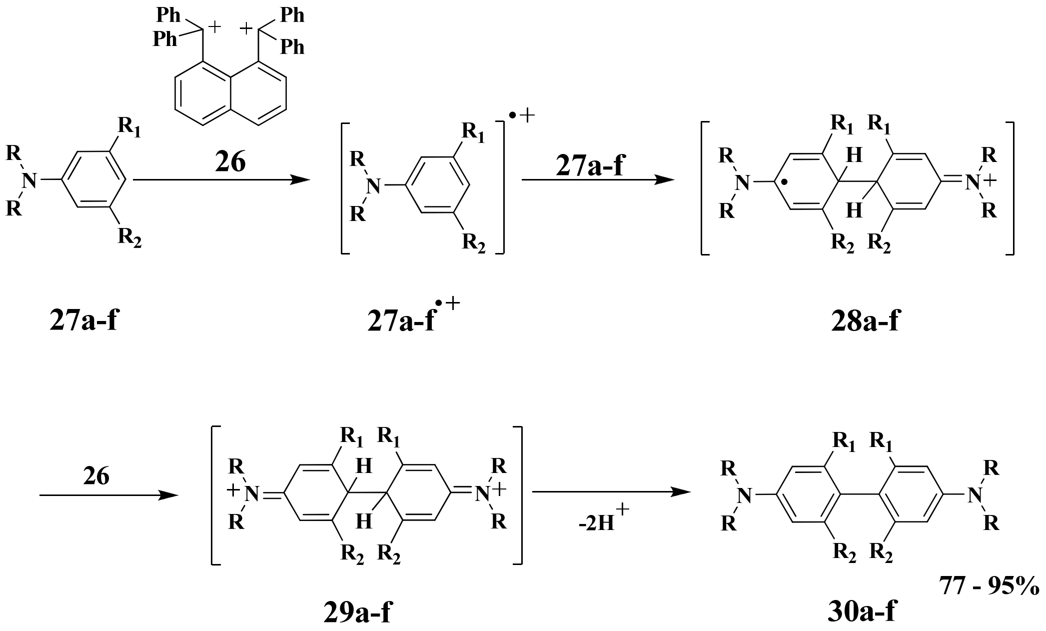

a: R=Me, R_1=R_2=Me
b: R=Et, R_1=R_2=Me
c: R=Et, R_1=R_2=Cl
d: R=Et, R_1=Br, R_2=H
e: R=Allyl, R_1=Me, R_2=Me
f: R=Ph, R_1=Me, R_2=Me

Scheme 1.19

The dication **26** promotes oxidation of dialkylanilines to the radical cation **27a-f** $^{\bullet+}$, which then reacts with the precursor amine to generate intermediate **28a-f**. This is further oxidized by the **26** to give diiminium ions **29a-f**. Deprotonation of **29a-f** gives tetraalkylbenzidine derivatives **30a-f**.

Periasamy and coworkers developed simple method to convert *N,N*-dialkylarylamines to *N,N,N',N'*-tetraalkyl-*p*-benzidines through oxidative coupling using $TiCl_4$ (Scheme 1.20).[9a] The transformation was rationalized by the formation of aryltitanium and radical cation intermediates.

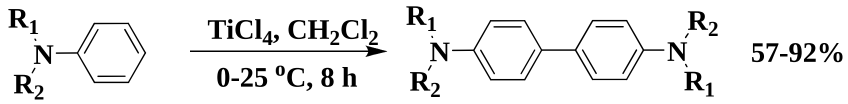

14: R_1=R_2=Me
15: R_1=R_2=Et
31: R_1=Me, R_2=Et

10: R_1=R_2=Me
32a: R_1=R_2=Et
32b: R_1=Me, R_2=Et

Scheme 1.20

Direct oxidative coupling of aniline derivatives (Scheme 1.21), in water was reported by Xi and coworkers.[9d] They have utilized ceric ammonium nitrate (**CAN**) as one electron oxidant. Product yields were very high when the *N*,*N*-dialkylaniline:**CAN** ratio was 1:2. The proposed mechanism is shown in Scheme 1.21. It involved the formation of a coordinated complex **34**, which undergo oxidative electron transfer with a second molecule of **CAN** to afford the radical cation **35**. Dimerization of **35** gave **36**, which undergo deprotonation to give **37**. During the workup **37** is converted to the benzidine product.

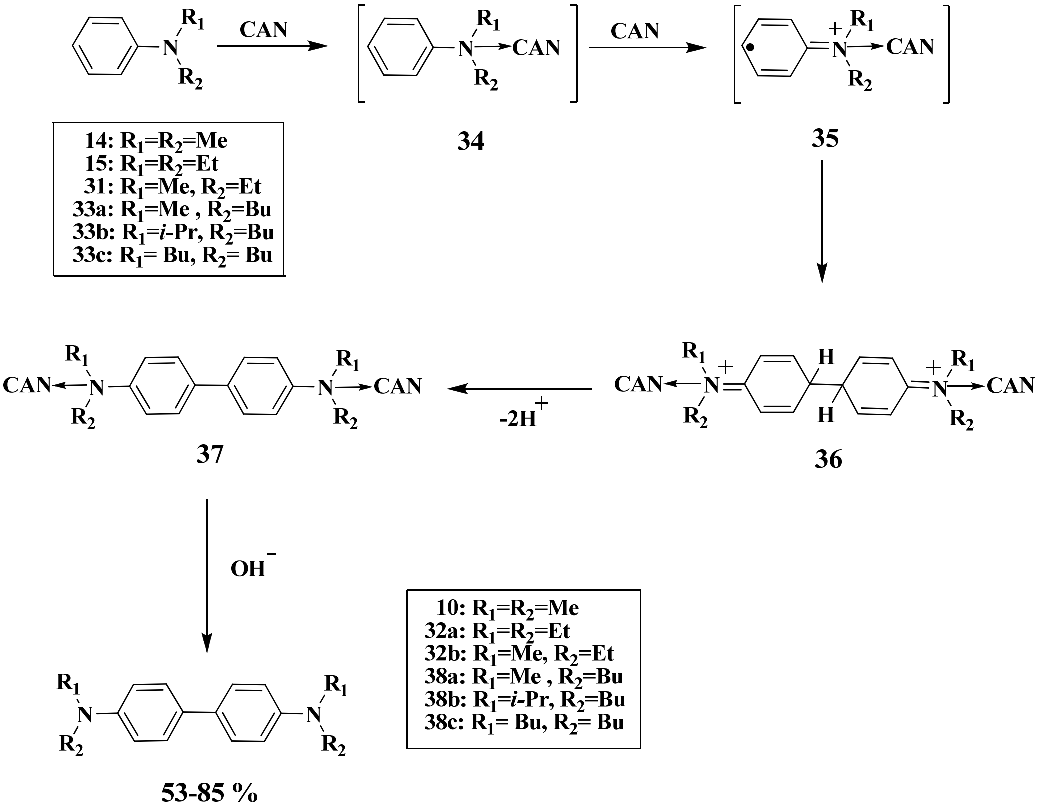

Scheme 1.21

Later the same group reported CuBr/H_2O_2 mediated oxidative coupling of *N*,*N*-dialkylarylamines (Scheme 1.22) in water.[37] The authors studied the effects of copper salts such as $CuCl_2$, $Cu(OAc)_2$, CuCl, CuBr and CuI. Various ratios of *N*,*N*-dialkylaniline, CuBr and H_2O_2 were also checked and reported best yields when the amine/CuBr/H_2O_2 ratio was 1:1:10. The mechanism proposed is shown in Scheme 1.22.

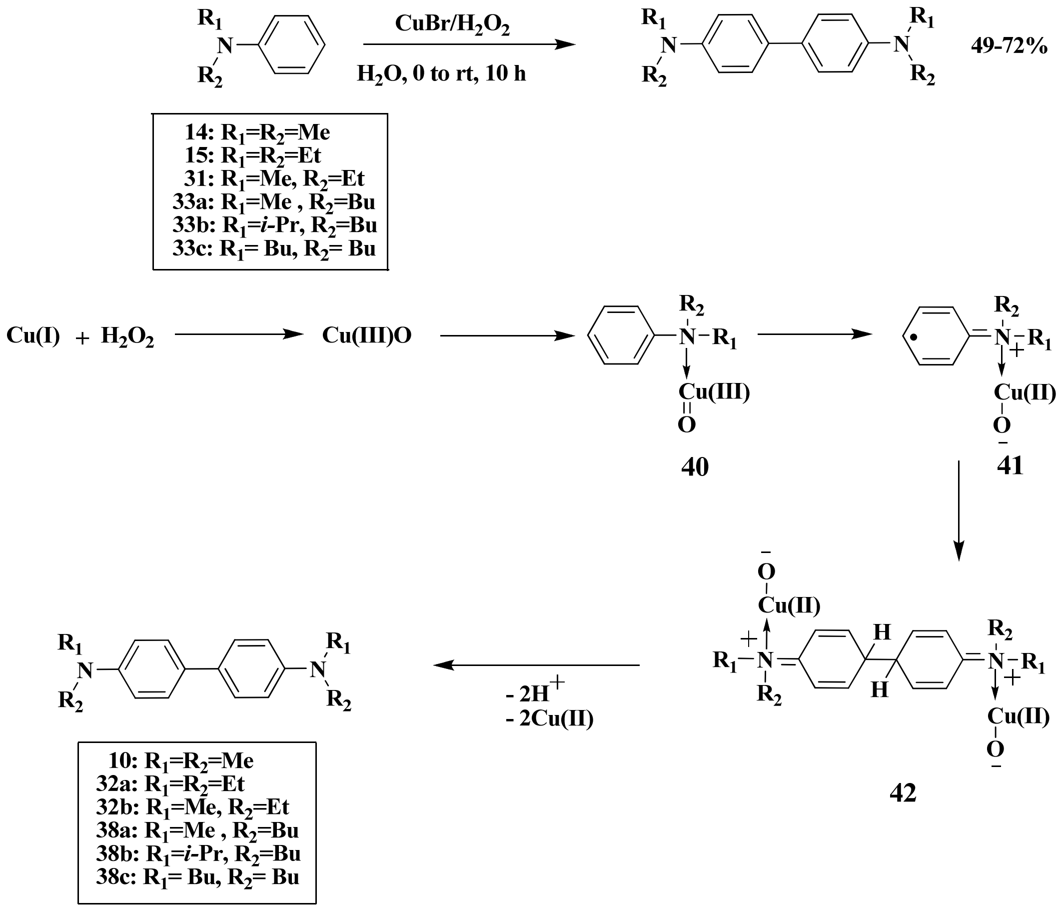

Scheme 1.22

The Cu(I) salt was oxidized by H_2O_2 to give more active Cu(III)O precursor, which coordinated with the tertiary amino group leading to complex **40**. Due to the high electron withdrawing ability of Cu(III) species, an electron transfer occurred from the tertiary amine to copper(III), which resulted in radical cation **41**. Subsequent dimerization to **42** and deprotonation gave the benzidine products.

1.5.2. Reaction of Aromatic Amine Radical Cations with Nucleophiles

Nucleophilic substitution reactions of cyanide and methoxide ions were attempted earlier on electrolytically generated *N,N*-dimethylaniline (**14**) radical cations. Substitution of these ions occurred at the methyl group, and yields were very low. Weinberg and Reddy carried out anodic oxidation of **14** in methanol and observed the formation of substitution products, namely *N*-methoxymethyl-*N*-methylaniline (**43**) and *N,N*-bis(methoxymethyl)aniline (**44**).[38]

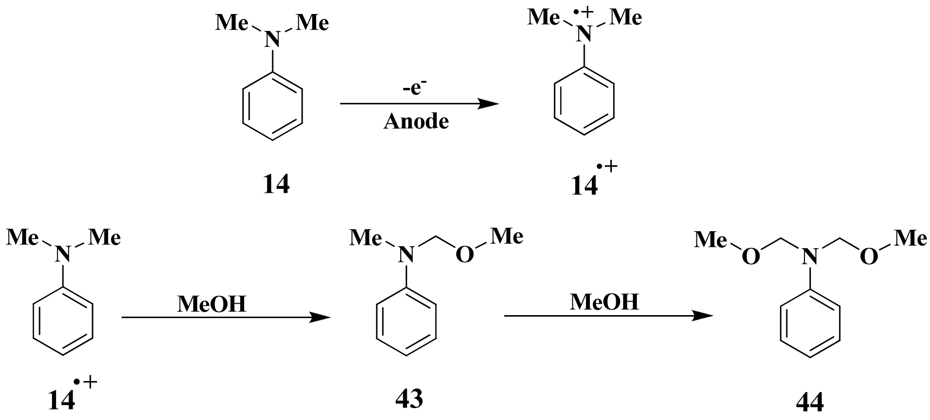

Scheme 1.23

Andreades and Zahnow reported formation of *N*-cyanomethyl-*N*-methylaniline (**45**) by anodic oxidation of **14** in presence of tetraethylammonium cyanide (Et_4NCN) in acetonitrile.[39] (Scheme 1.24)

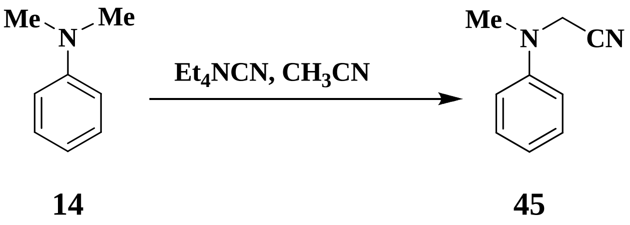

Scheme 1.24

Formation of these products were explained by the mechanism shown in Scheme 1.25, which involved strong adsorption of the amine radical cation on to the positive electrode (**14**$^{\bullet+}$@anode). The basic reaction conditions assist in removing a proton from the radical cation. This is followed by loss of a second electron to the electrode to give Ph-N(CH_3)CH_2^+ (**14**$^+$@anode), which undergoes reaction with cyanide or methoxide ions. Adsorption on to the electrode and basic conditions are required for this mechanism to operate. The amine radical cation is only a transient intermediate in the electrolytic reaction, and the actual species reacting with the nucleophile is a cation.

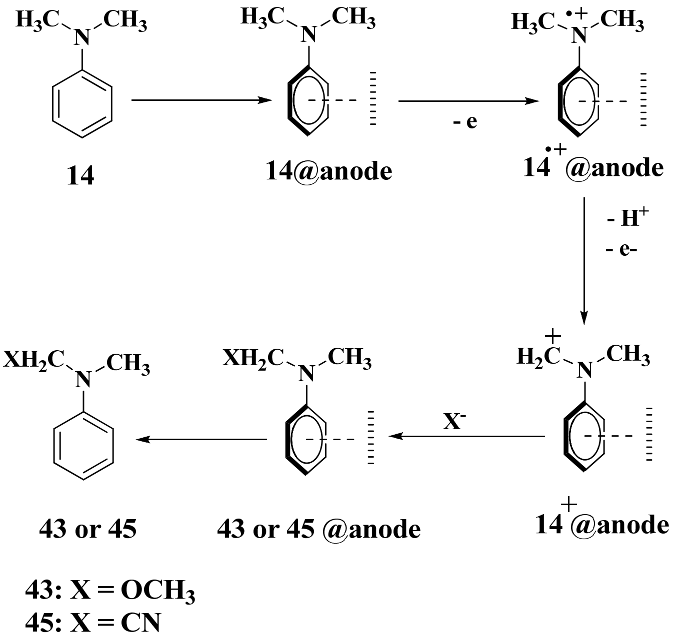

Scheme 1.25

Roy *et al.* published a mild and efficient method for the oxidative chlorinations of **14** and **15,** using acetyl chloride in the presence of catalytic amounts of **CAN** at room temperature, to afford the corresponding chloro substituted products (**46a,b**) in good yields.[9b] Mechanistic details are not discussed in the paper; however, this reaction might have involved radical cations of starting amines.

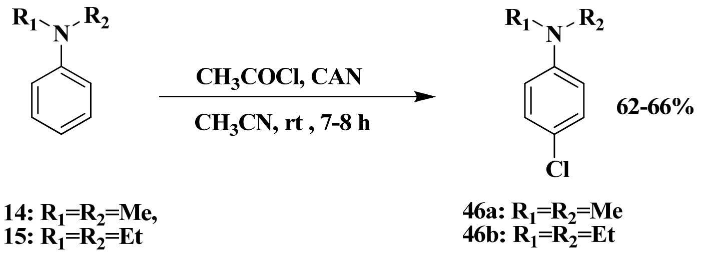

Scheme 1.26

1.5.3. Reaction of Aromatic Amine Radical Cations with Neutral Molecules

Ciminale *et al.* reported formation of 1,4-benzenediamine, **51a-d** by oxidative addition of *N,N*-dimethyl-*p*-anisidine (**47**) on to secondary anilines **48a-d**, in the presence of thallium(III) acetate (**TTA**).[40]

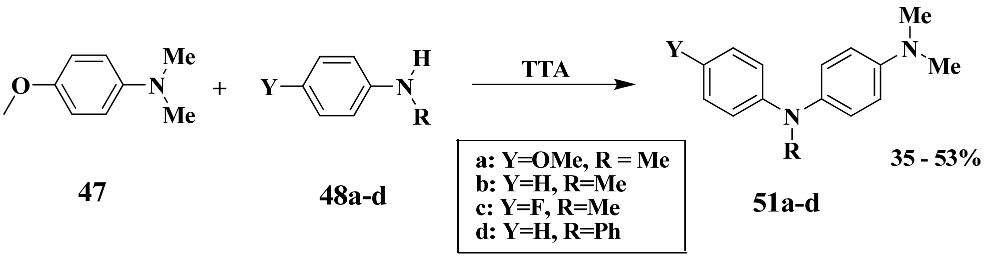

Scheme 1.27

As shown in the Scheme 1.28 the reaction proceeds through formation of an adduct **49** by nucleophilic attack of secondary aniline on radical cation $\mathbf{47}^{\bullet+}$ formed as a result of one electron oxidation of **47**. The adduct **49** eliminates a proton to form the radical **50** and subsequent elimination of methoxy radical results in the formation of **51a-d**.

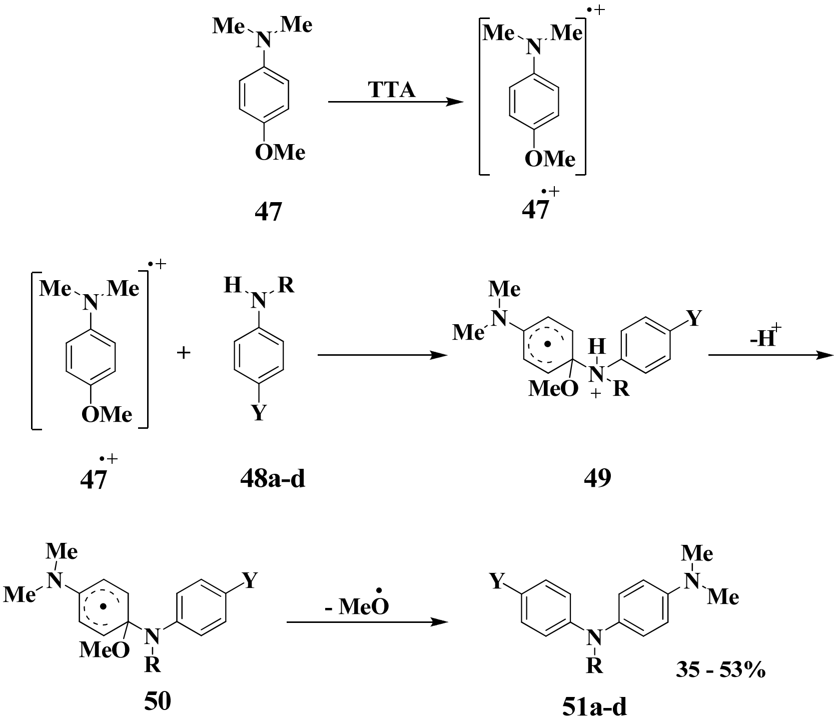

Scheme 1.28

Ichikawa and Saitoh reported an efficient method for diaryl ether (**54**) synthesis via oxidative coupling of *N*,*N*-dialkyl-*p*-phenylthioanilines (**53)** to several phenols (**52**). They have employed **26** as oxidant (Scheme 1.29).[41]

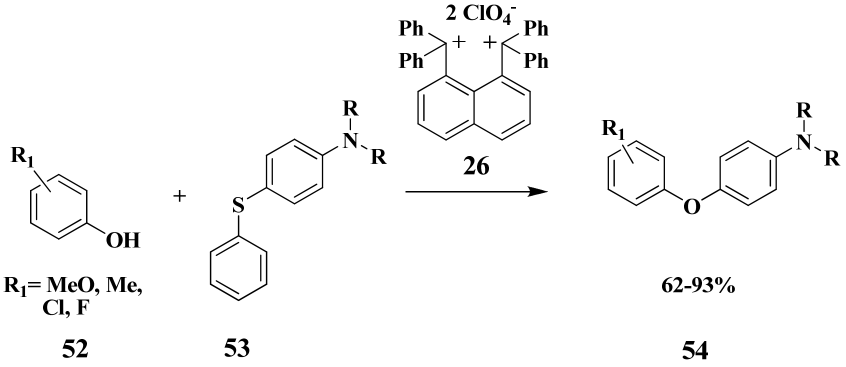

Scheme 1.29

Periasamy and coworkers reported that $TiCl_4$ forms a complex with *N*,*N*-diethylaniline (**15**) and which can add to benzophenone (**56**), benzaldehyde (**57**) and methyl formate (**58**) to provide addition products (**59-61**) as shown in Scheme 1.30.[9a]

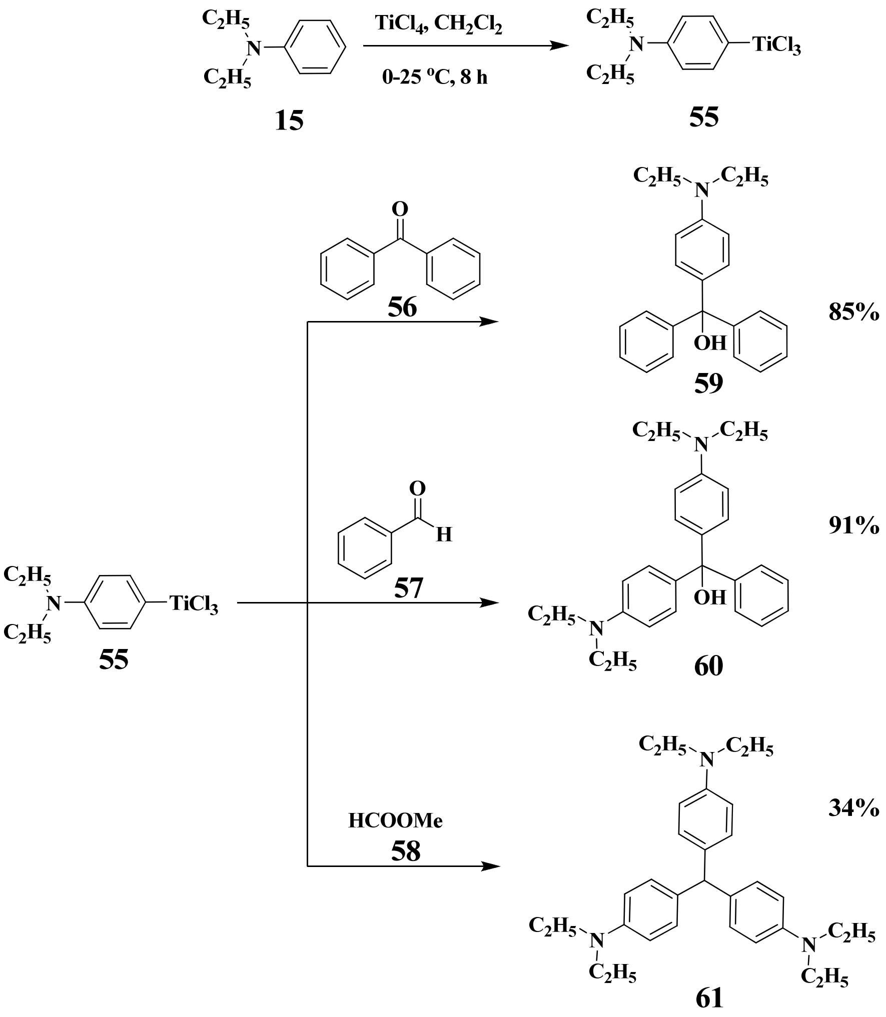

Scheme 1.30

1.5.4. Aromatic Amine Radical Cation as an Electron Transfer Reagent in Deprotection Reaction

Schmidt and Steckhan reported a simple and mild method for the removal of benzyl ether protecting group of alcohols by employing tris(4-bromophenyl)amine (**11**) radical cation or tris(2,4-dibromophenyl)amine (**62**) radical cation.[42] This provided a convenient alternative to usual reductive deprotection, with catalytic hydrogenation or reductive cleavage with sodium in liquid ammonia. In this reaction the stable radical cation acts as electron transfer agent and bond cleavage takes place in moist acetonitrile according to the following reaction scheme (Scheme 1.31). Authors analyzed this reaction in several derivatives and in all cases alcohols were obtained in good to excellent yield in high purity.

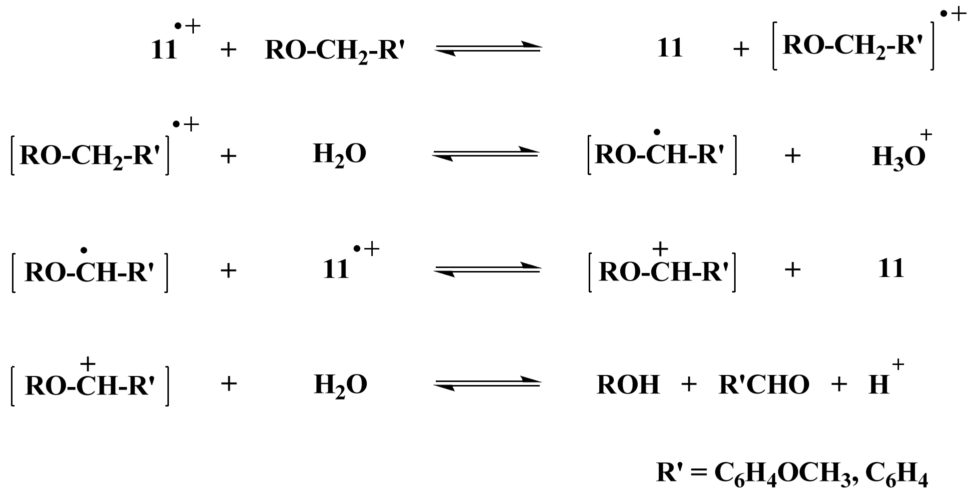

$$\mathbf{11}^{\bullet+} + \mathrm{RO\text{-}CH_2\text{-}R'} \rightleftharpoons \mathbf{11} + \left[\mathrm{RO\text{-}CH_2\text{-}R'}\right]^{\bullet+}$$

$$\left[\mathrm{RO\text{-}CH_2\text{-}R'}\right]^{\bullet+} + \mathrm{H_2O} \rightleftharpoons \left[\mathrm{RO\text{-}\overset{\bullet}{C}H\text{-}R'}\right] + \mathrm{H_3O^+}$$

$$\left[\mathrm{RO\text{-}\overset{\bullet}{C}H\text{-}R'}\right] + \mathbf{11}^{\bullet+} \rightleftharpoons \left[\mathrm{RO\text{-}\overset{+}{C}H\text{-}R'}\right] + \mathbf{11}$$

$$\left[\mathrm{RO\text{-}\overset{+}{C}H\text{-}R'}\right] + \mathrm{H_2O} \rightleftharpoons \mathrm{ROH} + \mathrm{R'CHO} + \mathrm{H^+}$$

$$\mathrm{R'} = \mathrm{C_6H_4OCH_3, C_6H_4}$$

Scheme 1.31

In a similar manner Steckhan and Platen effectively utilized stoichiometric amounts of tris(*p*-tolyl)amine (**63**) radical cation and $\mathbf{11}^{\bullet+}$ as homogeneous electron transfer reagents for removal of 1,3-dithiane and 1,3-dithiolane protecting groups.[43] In both cases deprotected carbonyl compounds (**68**) could be obtained in 70-95% yield. A reaction mechanism similar to deprotection of benzyl ether was proposed (Scheme 1.32).

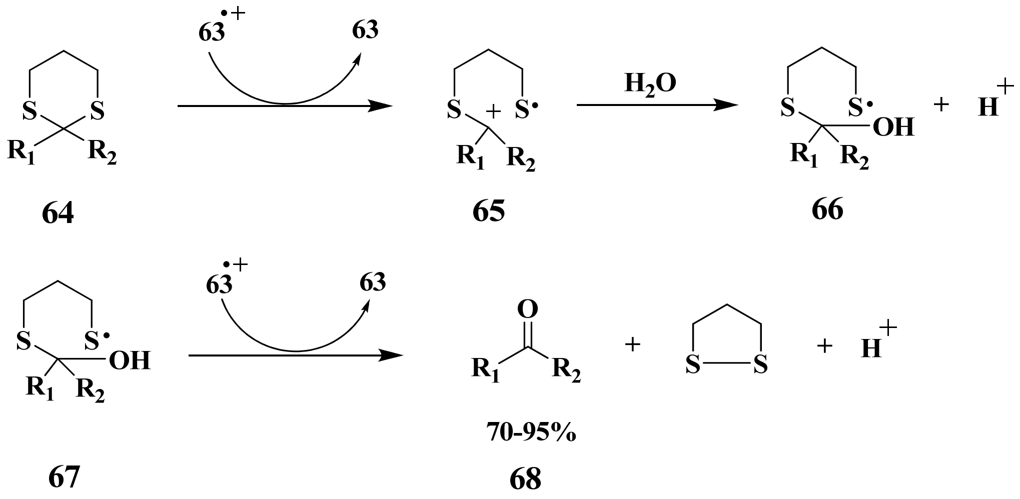

Scheme 1.32

1.5.5. Aromatic Amine Radical Cation as an Electron Transfer Reagent in Isomerization Reactions

Hoffmann and Barth observed rapid isomerization of quadricyclane (**69**) and its 3-substituted derivatives to norbornadiene (**70**) and the corresponding derivatives by the action of catalytic amounts of **11**$^{\bullet+}$.[44]

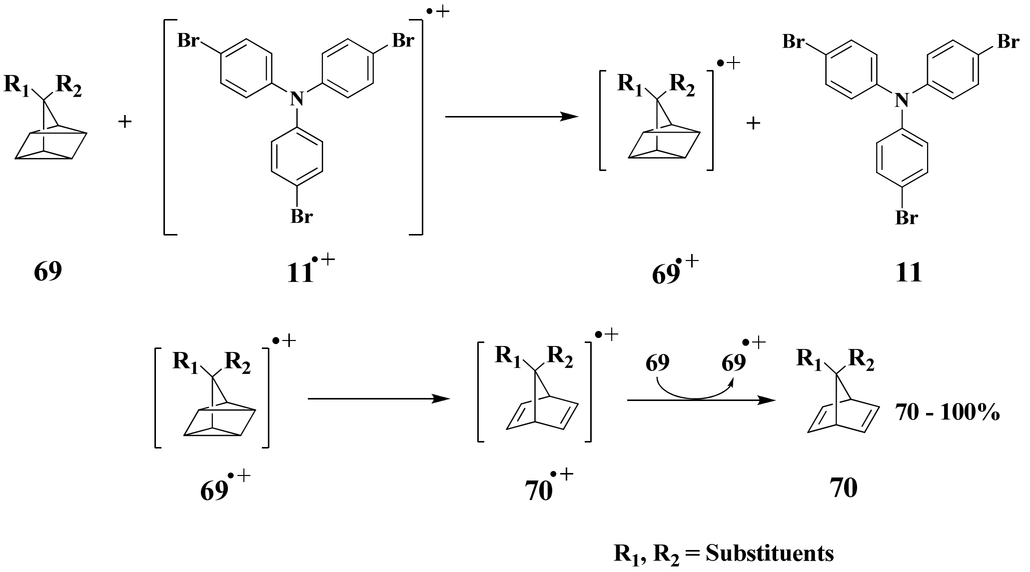

Scheme 1.33

Toshio Mukai and coworkers employed **11**$^{\bullet+}$ to study orientation selective bond cleavage reactions of biphenyl-fused 1,2-diphenylcyclobutanes (**71**) that leads to different conformational isomers (**72**).[45]

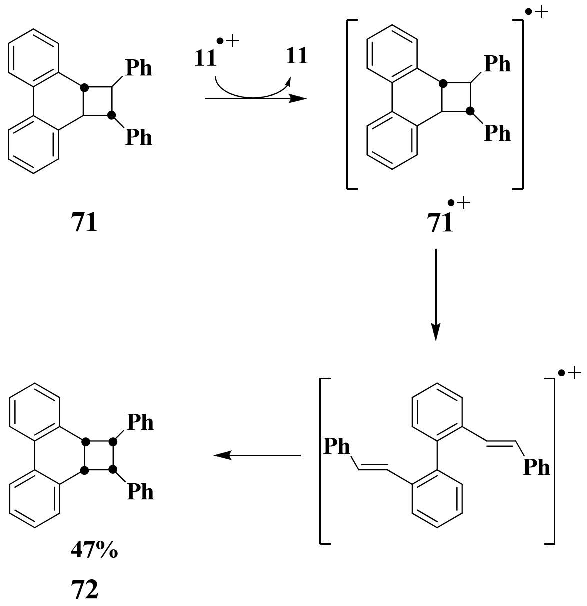

Scheme 1.34

1.5.6. Aromatic Amine Radical Cation as Cyclization Initiator

Liu and coworkers employed **11**$^{\bullet+}$ to initiate cyclization of the monoterpenol geraniol (**73**) and nerol (**74**) to *cis*-*p*-mentha-2,8-dien-1-ol (**75**).[46] (Scheme 1.35)

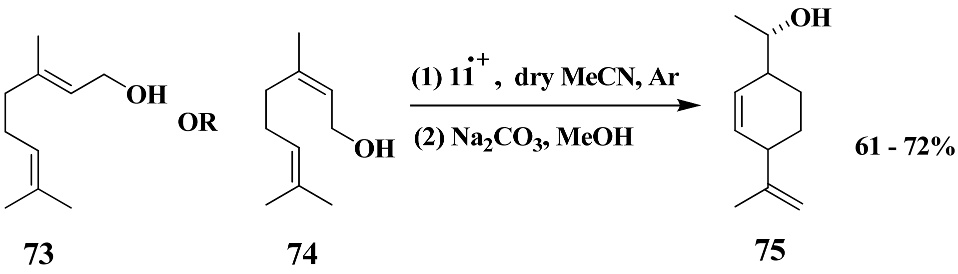

Scheme 1.35

1.5.7. Aromatic Amine Radical Cation as Polymerization Initiator

Ledwith and coworkers generated cation radicals of phenothiazine (**2**), *N*-ethylphenothiazine (**76**) and *N*-ethyl-2-ethyl-phenothiazine (**77**) having SbF_6^- as counter ion and used these as cationic initiators for the polymerization of tetrahydrofuran (**78**), *N*-vinylcarbazole (**80**) and cyclohexene oxide (**82**).[47] They also studied the effect of temperature and light in these reactions.

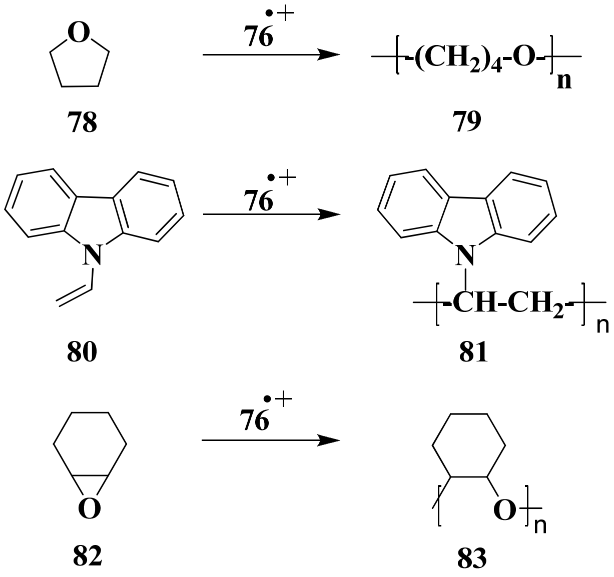

Scheme 1.36

1.5.8. Aromatic Amine Radical Cation as Catalyst in Diels-Alder Reactions

Bauld and Gassman have reported the powerful catalysis of certain Diels-Alder cycloadditions by **11**$^{•+}$.[48] A typical Diels–Alder reaction is not efficient unless the dienophile is substantially electron deficient. For example, the Diels-Alder dimerization of 1,2-cyclohexadiene (**84**) normally requires high temperature and long reaction time to give **85** in an optimum yield of 30%. Bauld *et al.* carried out the same reaction at low temperature and in short time, using **11**$^{\bullet+}$ as catalyst, with higher yield and higher endo-selectivity (Scheme 1.37).

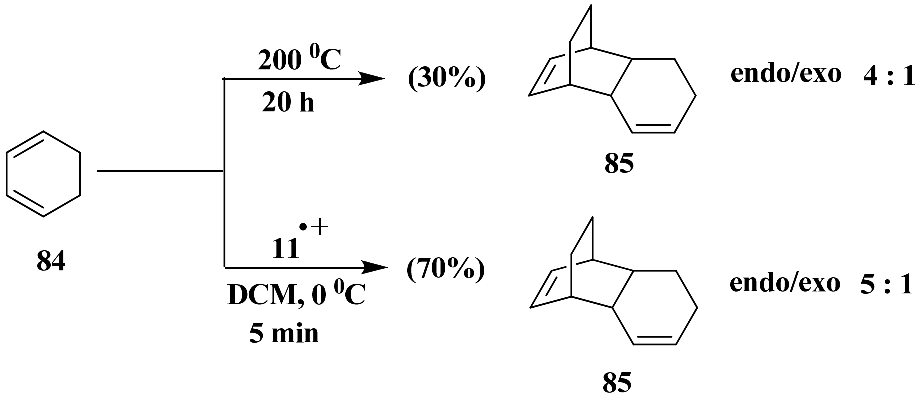

Scheme 1.37

The same catalytic efficiency of **11**$^{\bullet+}$ was observed in the formation of Diels-Alder product **87**. In the absence of **11**$^{\bullet+}$, the reaction did not occur even when heated to 200 ^{0}C for 2 days.

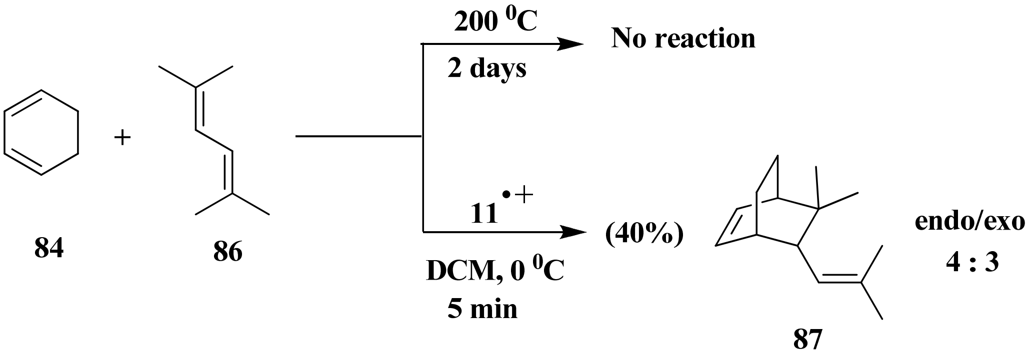

Scheme 1.38

Based on the seminal mechanistic studies, authors proposed the mechanism shown in Scheme 1.39. The reaction is initiated as a result of one electron oxidation of diene (**D**) by **11**$^{\bullet+}$. The diene radical cation, **D**$^{\bullet+}$, thus formed adds to the dienophile (**A**) to form the adduct [**D-A**]$^{\bullet+}$, which serves as an oxidizing agent in the propagation step.

$$\mathbf{D} + \mathbf{11}^{\bullet+} \longrightarrow \mathbf{D}^{\bullet+} + \mathbf{11}$$

$$\mathbf{D}^{\bullet+} + \mathbf{A} \longrightarrow [\mathbf{D\text{-}A}]^{\bullet+}$$

$$[\mathbf{D\text{-}A}]^{\bullet+} + \mathbf{D} \longrightarrow \mathbf{D\text{-}A} + \mathbf{D}^{\bullet+}$$

Scheme 1.39

Thus umpolung of electron rich diene via cation radical formation provides an efficient and direct remedy for the absence of electron deficiency in the dienophile. This type of reactions can lead to a number of Diels-Alder adducts which are otherwise very difficult to make.[49]

1.6. Origin of the Present Work

For the past several years our research group was involved in the study of electron transfer reactions. During the course of these studies we observed that aromatic amines react with Cu^{2+} in acetonitrile to give deeply coloured solutions. A detailed investigation has revealed that the colours are due to radical cations of these amines, formed as a result of electron transfer from the amine to Cu^{2+}. Although electron transfer is unequivocally confirmed in these experiments, the mechanistic details of these reactions were not understood. We anticipated that a spectroscopic and kinetic investigation would provide a better understanding of the mechanistic aspects of this electron-transfer reaction and an attempt in that direction was undertaken and the results are presented in Chapter 2 of this thesis.

We were also interested in finding out if these reactions have any synthetic potential. An exploratory study in that direction is presented in the third Chapter. We further observed that reaction with Cu^{2+} in acetonitrile also provides easy access to dications in the case of easily oxidizable aromatic amines. These studies along with spectroscopic characterization of a few amine dications are presented in last chapter.

1.7. References

1 (a) Isaac, N. S. *Reactive Intermediates in Organic Chemistry*, Wiley-VCH: New York, 1974. (b) McManus, S. P. *Organic Reactive Intermediates*, Academic Press: New York, 1973. (c) Olah, G. A.; *Angew. Chem., Int. Ed.* **1973**, *36*, 2550. (d) Griller, D.; Ingold, K. U. *Acc. Chem. Res.* **1976**, *9*, 13. (e) Chinoporos, E. *Chem. Rev.* **1963**, *63*, 235. (f) Abramovitch, R. A.; Davis, B. A. *Chem. Rev.* **1964**, *64*, 149.

2 Weitz, E. Z. *Electrochem.* **1928**, *34*, 538.

3 Schmittel, M.; Burghart, A. *Angew. Chem., Int. Ed.* **1997**, *36*, 2550.

4. (a) Roth, H. D. *Top. Curr. Chem.* **1992**, *163*, 131. (b) Schmittel, M.; Langels, A. *Angew. Chem., Int. Ed.* **1997**, *36*, 392. (c) Whitted, P. O.; Horner, J. H.; Newcomb, M.; Huang, X.; Crich, D. *Org. Lett.* **1999**, *1*, 153. (d) Newcomb, M.; Miranda, N.; Huang, X.; Crich, D. *J. Am. Chem. Soc.* **2000**, *122*, 6128. (e) Newcomb, M.; Miranda, N.; Sannigrahi, M.; Huang, X.; Crich, D. *J. Am. Chem. Soc.* **2001**, *123*, 6445. (f) Crich, D.;

Neelamkavil, S. *Org. Lett.* **2002**, *4*, 2573. (g) Horner, J. H.; Taxil, E.; Newcomb, M. *J. Am. Chem. Soc.* **2002**, *124*, 5402. (h) Horner, J. H.; Bagnol, L.; Newcomb, M. *J. Am. Chem. Soc.* **2001**, *126*, 14979. (i) Maruyama, T.; Suga, S.; Yoshida, J.-I. *J. Am. Chem. Soc.* **2005**, *127*, 7324. (j) Bally, T.; Matzinger, S.; Bednarek, P. *J. Am. Chem. Soc.* **2006**, *128*, 7828. (k) Jiao, J.; Zhang, Y.; Devery III, J.; Xu, L.; Deng, J.; Flowers II, R. A. *J. Org. Chem.* **2007**, *72*, 5486 (l) Marquez, C. A.; Wang, H.; Fabbretti, F.; Metzger, J. O. *J. Am. Chem. Soc.* **2008**, *24*, 17208.

5 (a) Balzani, V., Ed.; *Electron Transfer in Chemistry*, Wiley–VCH: New York, 2001; Vols. 1–5. (b) Fox, M. A.; Chanon, M.; Eds.; *Photoinduced Electron Transfer;* Elsevier: Amsterdam, The Netherlands, 1988; Parts A-D. (c) Kavarnos, G. J.; Turro, N. J. *Chem. Rev.* **1986**, *86*, 401.

6 (a) Das, S.; Suresh, V. In *Electron Transfer in Chemistry*; Balzani, V.; Ed.; Wiley-VCH: New York, 2001; Vol. 2, pp 379-456. (b) Easton, C. J. *Chem. Rev.* **1997**, *97*, 53.

7 Pullen, G. K.; Allen, N. S.; Edge, M.; Weddel, I.; Swart, R.; Catalina, F.; Navaratnam, S. *Eur. Polym. J.* **1996**, *32*, 943.

8 Theys, R. D.; Sosnovsky, G. *Chem. Rev.* **1997**, *97*, 83.

9 (a) Periasamy, M.; Jayakumar, K. N.; Bharathi, P. *J. Org. Chem.* **2000**, *65*, 3548. (b) Roy, S. C.; Rana, K. K.; Guin, C.; Banerjee, B. *Synlett*

2003, 221. (c) Saitoh, T.; Yoshida, S.; Ichikawa, J. *Org. Lett.* **2004**, *6*, 4563. (d) Xi, C.; Jiang, Y.; Yang, X. *Tetrahedron Lett.* **2005**, *46*, 3909.

10. Laurent, A. *Ann. Chim.* **1835**, *59*, 367.
11. (a) Kehrmann, F.; Speitel, J.; Grandmougin, E. *Ber. Dtsch. Chem. Ges*. **1914**, *47*, 2976. (b) Kehrmann, F.; Diserens L. *Ber. Dtsch. Chem. Ges*. **1915**, *48*, 318.
12. Hilpert, S.; Wolf, L. *Ber. Dtsch. Chem. Ges*. **1913**, *46*, 2215.
13. Kainer, H.; Hausser, K. H. *Chem. Ber.* **1953**, *86*, 1563.
14. (a) Wurster, C. *Ber. Dtsch. Chem. Ges*. **1879**, *12*, 522. (b) Wurster, C.; Schobig, E. *Ber. Dtsch. Chem. Ges*. **1879**, *12*, 1807. (c) Wurster, C. *Ber Dtsch. Chem. Ges*., **1879**, *12*, 2071.
15. (a) Wieland, H. *Ber. Dtsch. Chem. Ges*. **1907**, *40*, 4260. (b) Wieland, H.; Wecker, E. *Ber. Dtsch. Chem. Ges*. **1910**, *43*, 699.
16. Garcia, H.; Roth, H. D. *Chem. Rev.* **2002**, *102*, 3947.
17. Ribeiro, F. R., Ed., *Zeolites; Science and Technology*, Kluwer Academic Publishers: Massachusetts, 1983.
18. (a) Stamires, D. N.; Turkevich, J. *J. Am. Chem. Soc.* **1964**, *86*, 749. (b) Dollish, F. R.; Hall, W. K. *J. Phys. Chem.* **1967**, *71*, 1005.
19. Chen, F. R.; Fripiat, J. J. *J. Phys. Chem*. **1992**, *96*, 819.
20. Flockhart, B. D.; McLoughlin, L.; Pink, R. C. *J. Catal.* **1972**, *25*, 305.
21. Borkowski, R. P.; Doetschman, D. C.; Fox, J. D.; Gargossian, C. *Solid*

Stat. Ion. **1997**, *100*, 95.

22. Khulbe, K, C.; Mann, R. S. *React. Kinet. Catal. Lett.* **1998**, *65*, 87.
23. (a) Werst, D. W.; Han, P. *Catal. Lett.* **1997**, *45*, 253. (b) Vanderveken, D. J.; Baudoux, G.; Durant, F.; Vercatuteren, D. J. *J. Chem. Phys.* **1992**, *88*, 2497.
24. (a) Edlund, O.; Lund, A.; Nilsson, A. *J. Chem. Phys.* **1968**, *49*, 749. (b) Wan, J. K. S. *Ber. Bunsen-Ges. Phys. Chem. Phys.* **1968**, *72*, 245. (c) Smith, P.; Stevens, R. D.; Kaba, R. A. *J. Phys. Chem.* **1971**, *75*, 2048. (d) Nelsen, S. F.; Blackstock, S. C.; Yumibe, N. P.; Frigo, T. B.; Carpenter, J. E.; Weinhold, F. *J. Am. Chem. Soc.* **1985**, *107*, 143. (e) Fantechi, R.; Helcké, G. A. *J. Chem. Soc., Faraday Trans. 2* **1972**, *68*, 924.
25. Seo, E. T.; Nelson, R. F.; Fritsch, J. M.; Marcoux, L. S.; Leedy, D. W.; Adams, R. N. *J. Am. Chem. Soc.* **1966**, *88*, 3498.
26. Lewis, G. N.; Lipkin, E. *J. Am. Chem. Soc*. **1942**, *64*, 2801.
27. (a) Rao, P. S.; Nash, J. R.; Guarino, J. P.; Ronayne, M. R.; Hamill, W. H. *J. Am. Chem. Soc.* **1962**, *84*, 500. (b) Guarino, J. P.; Ronayne, M. R.; Hamill, W. H. *J. Am. Chem. Soc.* **1962**, *84*, 4230. (c) Guarino, J. P.; Hamill, W. H. *Radiation Res.* **1962**, *17*, 379.
28. Shida, T.; Hamill, W. H. *J. Chem. Phys.* **1966**, *44*, 2369.
29. Anderson, C. P.; Salmon, D. J.; Meyer, T. J.; Young, R. C. *J. Am. Chem.*

Soc. **1977**, *99*, 1980.

30. Percy, L. T.; Bakker, M. G.; Trifunac, A. D. *J. Phys. Chem.* **1989**, *93*, 4393.
31. Amthor, S.; Noller, B.; Lambert, C. *Chem. Phys*. **2005**, *316*, 141.
32. Zhang, R.; Zhang, G.; Su, Z.; Qui, Y.; Shen, J. *Macromol. Chem. Phys.* **2000**, *201*, 1774.
33. Nguyen, H. M. T.; Dutta, A.; Morokuma, K.; Nguyen, M. T. *J. Chem. Phys*. **2005**, *122*, 154308.
34. (a) Creason, S. C.; Wheeler, J.; Nelson, R. F. *J. Org. Chem*. **1972**, *37*, 4440. (b) Nelson, R. F.; Feldberg, S. W. *J. Phys. Chem.* **1969**, *73*, 2623.
35. (a) Oyama, M.; Higuchi, T.; Okazaki, S. *Electrochem. Commun.* **2000**, *2*, 675. (b) Oyama, M.; Higuchi, T.; Okazaki, S. *J. Chem. Soc., Perkin Trans*. **2001**, *2*, 1287.
36. Goto, M.; Park, H.; Otsuka, K.; Oyama, M. *J. Phys. Chem. A* **2002**, *106*, 8103.
37. Jiang, Y.; Xi, C.; Yang, X. *Synlett* **2005**, 1381.
38. Weinberg, N. L.; Reddy, T. B. *J. Am. Chem. Soc.* **1968**, *90*, 91.
39. Andreades, S.; Zahnow, E. W. *J. Am. Chem. Soc.* **1969**, *91*, 4181.
40. Ciminale, F.; Ciardo, A.; Francioso, S.; Nacci, A. *J. Org. Chem.* **1999**, *64*, 2459.
41. Saitoh, T.; Ichikawa, J. *J. Am. Chem. Soc.* **2005**, *127*, 9696.

42. (a) Schmidt, W.; Steckhan, E. *Angew. Chem. Int. Ed.* **1978**, *17*, 673. (b) Schmidt, W.; Steckhan, E. *Angew. Chem. Int. Ed.* **1979**, *18*, 801.

43. Platen, M.; Steckhan, E. *Tetrahedron Lett.* **1980**, *21*, 511.

44. Hoffmann, R. W.; Barth, W. *J. Chem. Soc., Chem. Commun.* **1983**, 345.

45 Yamashita, Y.; Yaegashi, H.; Mukai, T. *Tetrahedron Lett.* **1985**, *26*, 3579.

46. Wang, W.; Liu, Y.-C. *J. Chem. Research (S)*, **1998**, 42.

47. (a) Abu-Abdoun, I. I.; Ledwith, A. *Eur. Polym. J.* **1997**, *33*, 1671. (b) Abu-Abdoun, I. I.; Ledwith, A. *J. Macromol. Sci. Pure* **1998**, *35*, 673.

48. (a) Bellville, D. J.; Wirth, D. D.; Bauld, N. L. *J. Am. Chem. Soc.* **1981**, *103*, 718. (b) Bellville, D. J.; Bauld, N. L. *J. Am. Chem. Soc.* **1982**, *104*, 2665. (c) Bauld, N. L.; Pabon, R. *J. Am. Chem. Soc.* **1983**, *105*, 633. (d) Reynolds, D. W.; Lorenz, K. T.; Chiou, H.-S.; Bellville, D. J.; Pabon, R. A.; Bauld, N. L. *J. Am. Chem. Soc.* **1987**, *106*, 4960.

49. Bauld, N. L.; Bellville, D. J.; Harirchian, B.; Lorenz, K. T.; Pabon Jr., R. A.; Reynolds, D. W.; Wirth, D. D.; Chiou, H.-S.; Marsh, B. K. *Acc. Chem. Res.* **1987**, *20*, 371.

Chapter 2

Generation of Aromatic Amine Radical Cations by Reaction with Cu^{2+} in Acetonitrile: Kinetic and Mechanistic Aspects

2.1. Abstract

Kinetic and mechanistic aspects of radical cation formation from a series of triphenylamine derivatives, by reaction with Cu^{2+} *in acetonitrile are reported here. A broad range of triphenylamine derivatives were studied using stopped-flow spectrophotometry. The driving force for the electron transfer reaction was ranged from +3.67 to -8.56 kcal* M^{-1} *and the observed rate constants varied from* 1.09×10^{2} *to* 2.15×10^{5} M^{-1} s^{-1} *for these systems. Activation parameters for the electron transfer reactions were obtained from a study of the temperature dependence of the rate constants and these values were used to estimate the reorganization energy. Fitting of the rate data to the Marcus equation using different values of the electronic coupling matrix element* H_{el} *and estimated reorganization energy, provided a good fit using* $H_{el} = 100$ cm^{-1}*, suggesting that electron transfer in the* ***TPA****/*Cu^{2+} *systems conform to the Marcus type electron transfer. Further-more, the high reorganization energy obtained from these studies is consistent with significant bond cleavage in the transition state and a mechanism consistent with the experimental data is proposed.*

2.2. Introduction

Amine radical cations are important intermediates in electron transfer reactions of amines and these are involved as intermediates in the synthesis of several amino acids, alkaloids and other nitrogen containing compounds of biological and pharmaceutical importance.[1-5] Amine radical cations are also important intermediates in several technological applications such as imaging[6] and photopolymerization.[7] Because of these applications generation of amine radical cations and study of their structural and reactivity aspects are very important. Several methods are now available for generating radical cations of amines in fluid solutions or in solid matrices. These include treatment of the substrates with oxidizing metals, Lewis acids, protic acids, stable radicals and onium salts.[8] Other methods include anodic oxidation,[9-11] photoionization,[12] γ-irradiation,[13,14] photoinduced electron transfer,[3] and inclusion in zeolite cavities.[15,16] Most of these methods, however, require sophisticated experimental setup for preparing and monitoring the follow up reactions of the generated amine radical cations. Amine radical cations generated by photoinduced electron transfer and photoionization, for example, generally have short lifetimes. The electrochemical method suffers from the disadvantage that the radical cations are formed in very high concentrations at the electrode surface, leading to their dimerization. This often hampers the reactions of the radical cations with other substrates. Although long-lived radical cations can be generated within zeolite cavities, monitoring reactions of radical cations inside zeolites are rarely reported and often times difficult to accomplish.

A recent investigation from our laboratory by Sumalekshmy and Gopidas has shown that several aromatic amines react with Cu^{2+} in acetonitrile (ACN) solution to give deeply coloured solutions.[17] A detailed investigation has shown that the colours are due to the radical cations of the amines, which are produced by one electron oxidation of the amines by Cu^{2+}. Aromatic amines which gave radical cations in this way include *N,N*-dimethylaniline (**1**), *N,N,N',N'*-tetramethyl-*p*-phenylenediamine (**2**), *N*-methylphenothiazine (**3**), tris(*p*-bromophenyl)amine (**4**), 2-*N,N*-dimethylaminotetrahydropyrene (**5**) and 2-*N,N*-dimethylamino-7-carboethoxytetrahydropyrene (**6**) (Chart 2.1). $Cu(ClO_4)_2$ was employed as Cu^{2+} source in these studies. For all the aromatic amines studied, formations of the radical cations were monitored by absorption spectroscopy and the results are reproduced in Figure 2.1. The downward arrows in Figure 2.1 indicate the original absorptions due to the aromatic amines and the upward arrows indicate the new absorptions formed upon addition of micro molar amounts of $Cu(ClO_4)_2$.

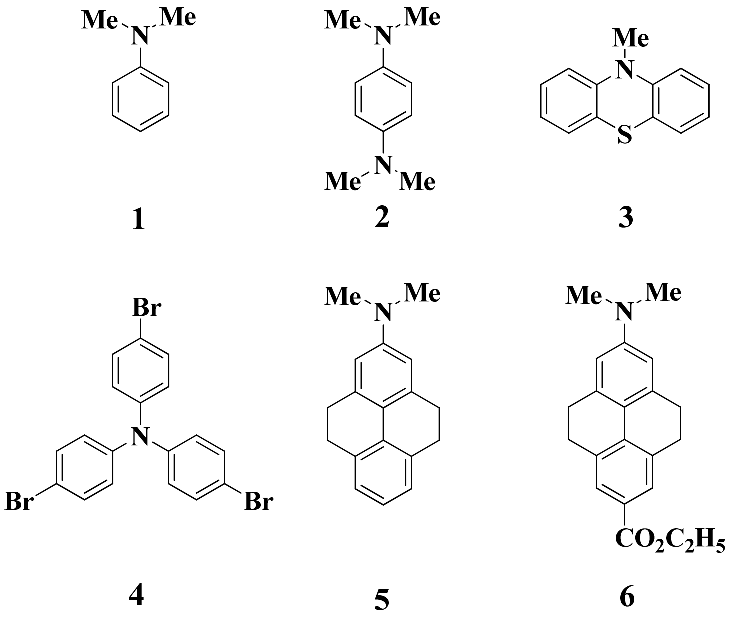

Chart 2.1

1 absorbs below 300 nm. Upon addition of increasing amounts of $Cu(ClO_4)_2$, the absorption due to **1** decreased with concomitant increase in absorption at 470 nm (Figure 2.1A). Complete disappearance of the absorption due to **1** required the addition of nearly two equivalents of $Cu(ClO_4)_2$. On the basis of the literature reports,[18,19] the 470 nm band was unambiguously assigned to the radical cation of **1** ($\mathbf{1}^{\bullet+}$). Figure 2.1B shows the effect of addition of increasing amounts of $Cu(ClO_4)_2$ to **2** in acetonitrile. The absorption due to **2** at < 300 nm decreased with simultaneous formation of a sharp absorption band around 340 nm and a structured absorption around 570 nm (Figure 2.1B). As a result of these absorption changes the solution assumed a deep violet colour. In the case of $\mathbf{2}^{\bullet+}$, the reported absorption spectrum exhibited peaks at 525, 570 and

630 nm.[20] The spectrum obtained upon addition of $Cu(ClO_4)_2$ to **2** in acetonitrile showed all these features.

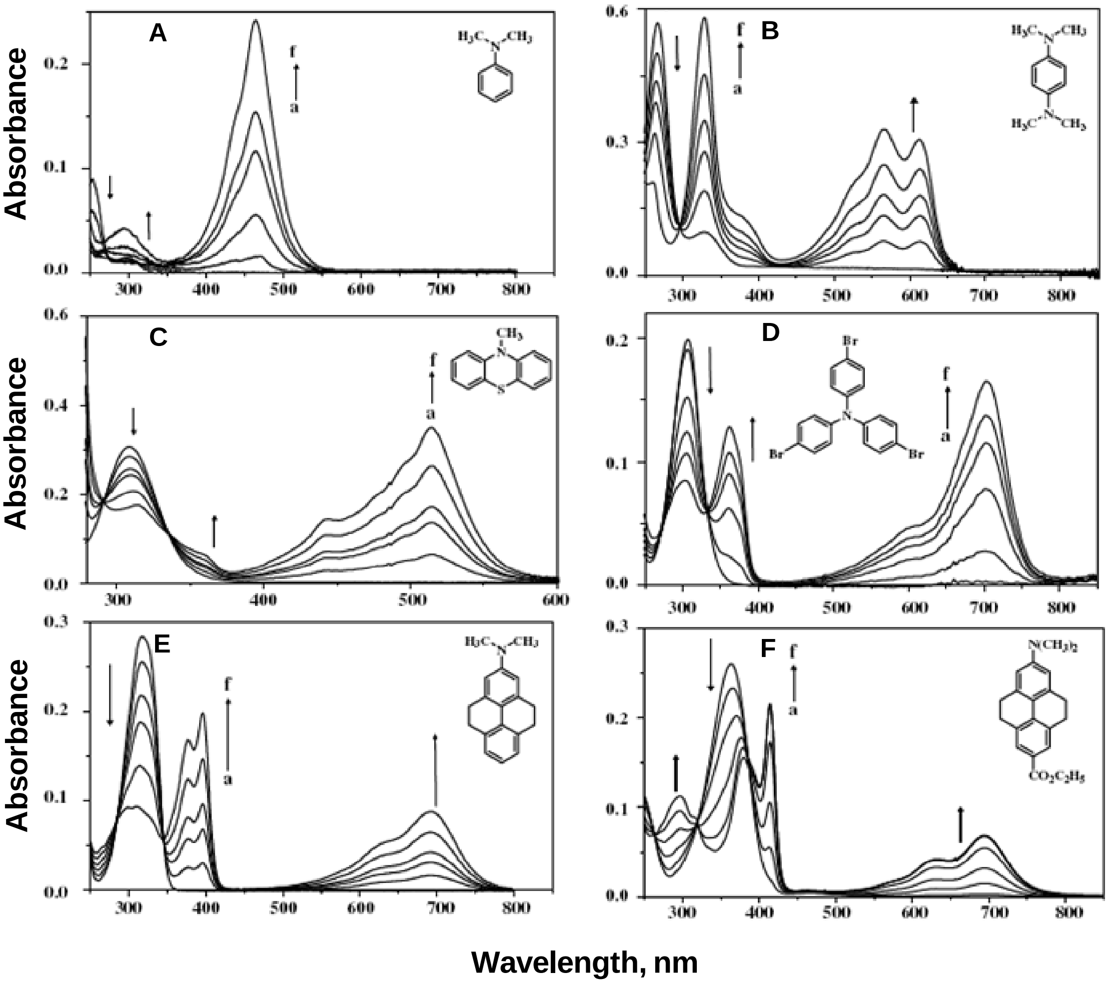

Figure 2.1. Absorption spectra of the various aromatic amines in the absence and presence of $Cu(ClO_4)_2$. [Amines] were 5–10 μM and $[Cu(ClO_4)_2]$ were: (a) 0, (b) 2.2, (c) 4.45, (d) 6.65, (e) 8.84, and (f) 11 μM.

Figure 2.1C shows the effect of addition of $Cu(ClO_4)_2$ to a solution of **3** in acetonitrile. The absorption band due to **3** at 308 nm disappeared leading to the formation of a new band having maximum at 520 nm. **3** is frequently used as a donor in photoinduced electron transfer reactions and the well-known absorption spectrum of **3**$^{\bullet+}$ is identical to the new band formed in Figure 2.1C.[21] Figure 2.1D shows the effect of addition of increasing amounts of $Cu(ClO_4)_2$ to **4**. The absorption due to **4** at 300 nm disappeared leading to the formation of new bands at 370 and 700 nm. The radical cation of **4** is well known[22,23] and its hexachloroantimonate salt is commercially available. The reported absorption spectrum of **4**$^{\bullet+}$ matches very well with the spectrum shown in Figure 2.1D.[24] Figures 2.1E and 2.1F shows the effect of addition of increasing amounts of $Cu(ClO_4)_2$ to acetonitrile solutions of **5** and **6**, respectively. Radical cations of **5** and **6** were unknown previously. Based on the observations from Figures 2.1A – 2.1D, the new absorptions around 700 nm in these cases were assigned to radical cations of these amines. In subsequent experiments the authors generated (vide infra) radical cations of **5** and **6** by way of photoinduced electron transfer and confirmed that the spectra in 2.1E and 2.1F are indeed due to radical cations of these amines. Thus, the experiments shown in Figures 2.1A – 2.1F prompted the authors to suggest that reaction of aromatic amines with Cu^{2+} in acetonitrile is a very facile method for the generation of amine radical cations.

The authors carried out additional experiments to confirm that the species generated from aromatic amines by reaction with Cu^{2+} are actually the radical cations. For example, it was reported in the literature that **3** upon dissolution in conc. sulphuric acid gets oxidized to **3**$^{\bullet+}$. Figure 2.2A shows the absorption spectrum of a solution of **3** in conc. H_2SO_4. This spectrum is identical to the absorption spectrum of the species formed in the **3**/Cu^{2+} reaction (Figure 2.1C).

Formation of $\mathbf{3}^{\bullet+}$ in this experiment was further confirmed by ESR spectroscopy. The ESR spectrum of $\mathbf{3}^{\bullet+}$ is reported to have six peaks with intensities in the ratio 1:4:7:7:4:1.[25] Figure 2.2B shows the ESR spectrum of a solution of **3** (2.0 × 10^{-3} M) in conc. H_2SO_4. This spectrum exhibited the six-line pattern reported in the literature.

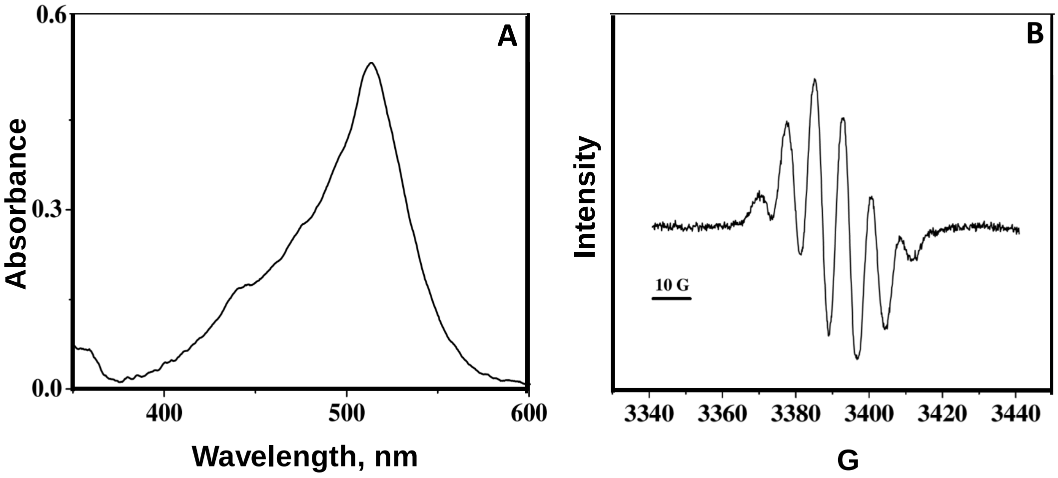

Figure 2.2. Absorption (A) and ESR (B) spectra of **3**/H_2SO_4 system.

Using ESR experiments the authors confirmed that the species generated upon addition of Cu^{2+} to a solution of **3** in acetonitrile was indeed the radical cation of **3**. Figure 2.3A is the ESR spectrum of a solution of $Cu(ClO_4)_2$ (2.0 × 10^{-3} M). Upon addition of one equivalent of **3** to the above solution the ESR spectrum due to Cu^{2+} disappeared and the spectrum shown in Figure 2.3B was obtained. The six-line pattern observed in this case was identical to that observed in the **3**/H_2SO_4 system. This experiment further corroborated the contention that reaction of aromatic amines with Cu^{2+} in acetonitrile is a very good method for the generation of amine radical cations.

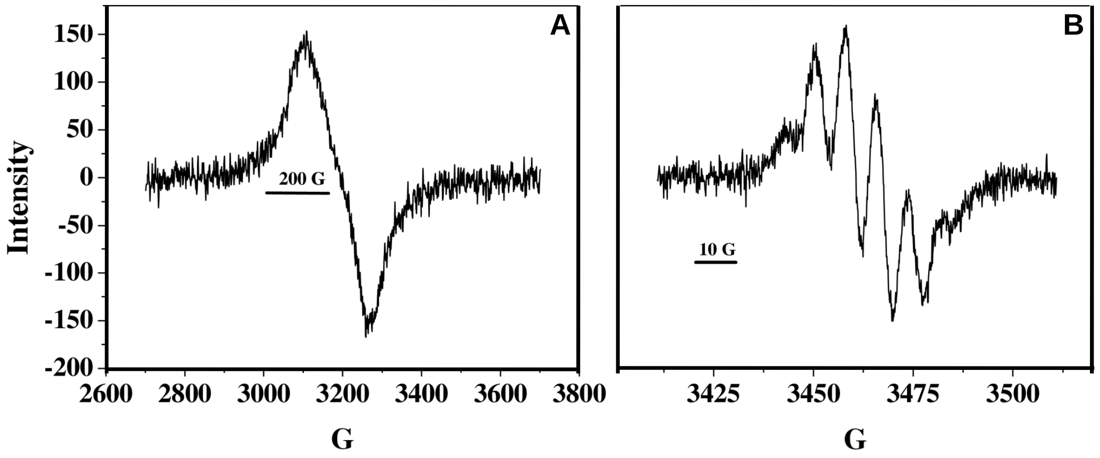

Figure 2.3. (A) ESR spectra of $Cu(ClO_4)_2$ and (B) **3**/Cu^{2+} systems in acetonitrile. (Concentrations of all components were 2.0×10^{-3} M).

Assignment of the species absorbing at 700 nm in Figures 2.1E and 2.1F to radical cations of **5** and **6**, respectively, were confirmed by photoinduced electron transfer experiments. The authors observed that the fluorescence of the electron acceptor azadioxatriangulenium (**7**) cation (Figure 2.4) was quenched by most of the amines shown in Chart 2.1 by an electron transfer mechanism.

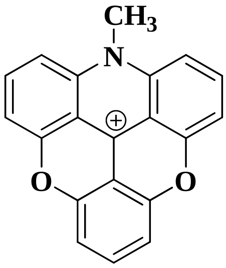

7

Figure 2.4

Figure 2.5A shows the transient absorption spectra obtained for **4** and **6** in these experiments. The transient absorption spectra obtained were very similar to those obtained for the amine/Cu^{2+} systems. These experiments further confirm the formation of radical cations in the reactions of amines with Cu^{2+} in acetonitrile.

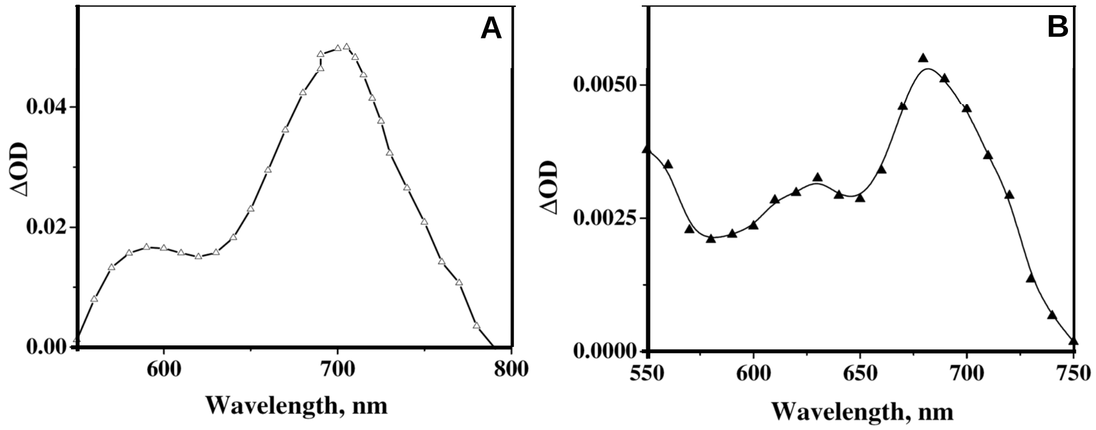

Figure 2.5. Transient absorption spectra of (A) **4/7** and (B) **6/7** systems.

Sumalekshmy and Gopidas also observed that electron donation from aromatic amines to Cu^{2+} leading to the formation of amine radical cations occurred only in acetonitrile solvent.[17] This reaction did not occur in other common solvents. An examination of the literature suggested that the enhanced oxidation ability of Cu^{2+} in acetonitrile could be the reason for this behaviour. For example the redox potential of Cu^{2+}/Cu^{+} system in water, methanol and acetonitrile are -0.09, 0.0 and +0.952 V vs SCE, respectively. The authors observed that the redox potential of the Cu^{2+}/Cu^{+} system in acetonitrile depended on the concentration of water in acetonitrile. Figure 2.6A shows the cyclic voltammogarm of Cu^{2+} in acetonitrile in the presence of increasing concentrations of water. Figure 2.6B is a plot of the redox potential against % of water in acetonitrile. It is very clear from these studies that Cu^{2+} is a much better oxidant in acetonitrile than in water.

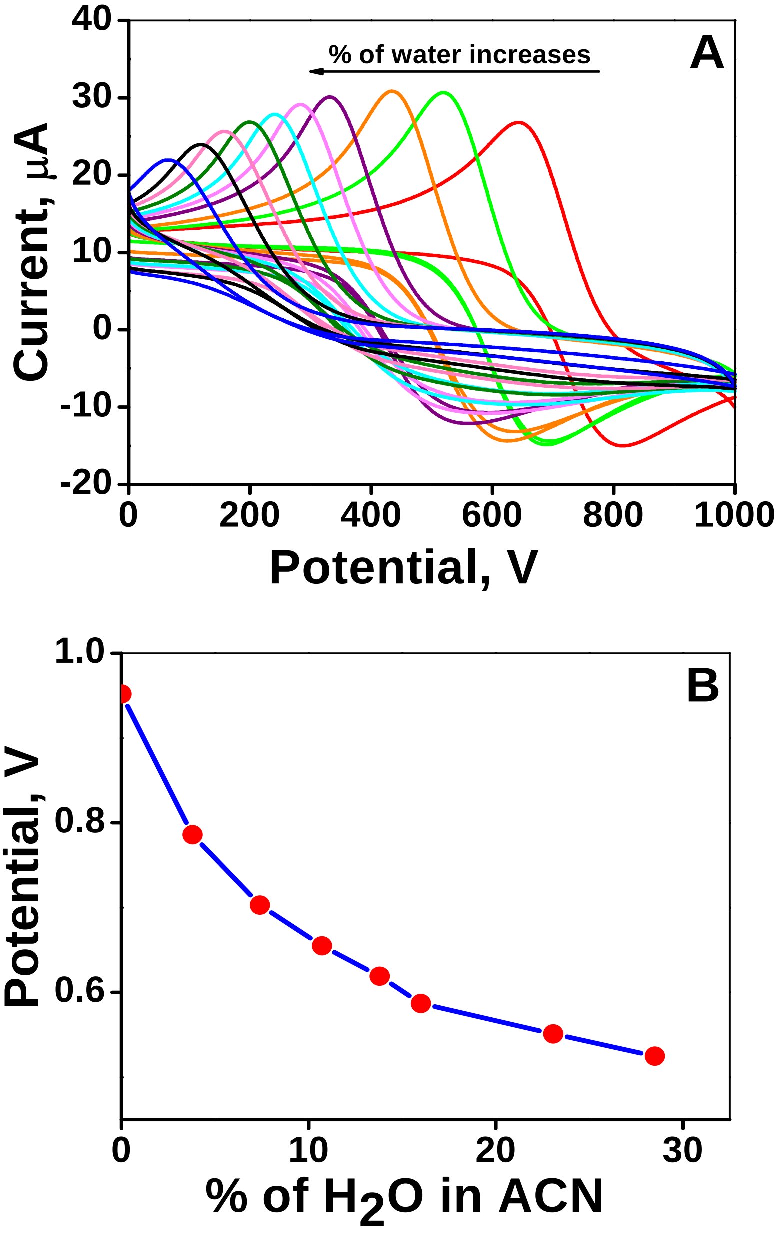

Figure 2.6. (A) Cyclic voltammograms of Cu^{2+} in acetonitrile containing different amounts of H_2O, (B) plot of redox potential vs % of H_2O in ACN for Cu^{2+}/Cu^{+} system.

In the light of all the above experiments the authors concluded that reaction of aromatic amine with Cu^{2+} in acetonitrile is an excellent method for the generation of amine radical cations. An electron transfer mechanism shown in equation 2.1 was proposed for the reaction.

$$\text{Amine} + \text{Cu(II)} \xrightarrow{\text{ACN}} \text{Amine}^{\bullet+} + \text{Cu(I)} \qquad (2.1)$$

In acetonitrile solution the Cu^{+} formed gets converted into the stable tetrakis(acetonitrile)copper(I) complex and this may be one of the important factors contributing to the success of the reaction.

Although electron transfer from aromatic amines to Cu^{2+} is unequivocally confirmed from the experiments described above, the mechanistic details of these reactions were not available. We anticipated that a spectroscopic and kinetic investigation would provide a better understanding of the mechanistic aspects of this electron-transfer reaction and an attempt in that direction was undertaken and the results are presented in this chapter. We observed that for most of the amines reported in Chart 2.1, oxidation by Cu^{2+} in acetonitrile was extremely fast. For a series of triphenylamine (**TPA**) derivatives (**8-15**, Chart 2.2) we observed that the reactions were sufficiently slow and that the rates of radical cation formation could be measured using stopped-flow spectrophotometry. Our interest was to develop an understanding of the measured rate constants and activation parameters in terms of the elementary steps of a model outer-sphere electron-transfer reaction. A major objective of the work presented in this chapter is to correlate the activation parameters obtained from the kinetic studies to the free energy change associated with the reaction and to determine if the reaction conforms to the Marcus theory of electron transfer.[26] We were also interested in proposing a mechanism for the electron transfer reaction. Results of these investigations are presented in this chapter. In the following discussion, the abbreviation **TPA** is used, wherever we refer to this class of compounds as a group, but numbers **8-15** are used while referring to individual members.

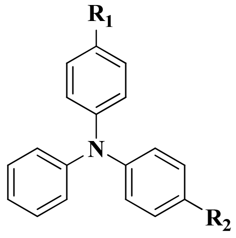

8: (R_1, R_2=OMe)
9: (R_1=H, R_2=OMe)
10: (R_1, R_2=Me)
11: (R_1=H, R_2=Me)
12: (R_1, R_2=H)
13: (R_1=H, R_2=COOMe)
14: (R_1=H, R_2=CHO)
15: (R_1=H, R_2=NO_2)

Chart 2.2

2.3. Results and Discussion

All the **TPA** derivatives were known previously and were prepared by reported procedures.[27] Mixing the **TPA** derivatives with $Cu(ClO_4)_2{\cdot}6H_2O$ in acetonitrile resulted in the formation of a deep blue colour indicative of the formation of **TPA**$^{\bullet+}$. In each of these cases we have recorded the absorption spectra before and after adding Cu^{2+} and these are presented in Figure 2.7. The new peaks formed in the 600-800 nm region were assigned to the radical cations of the **TPA** derivatives. The absorption maxima obtained for all **TPA**$^{\bullet+}$ are presented in Table 2.1.

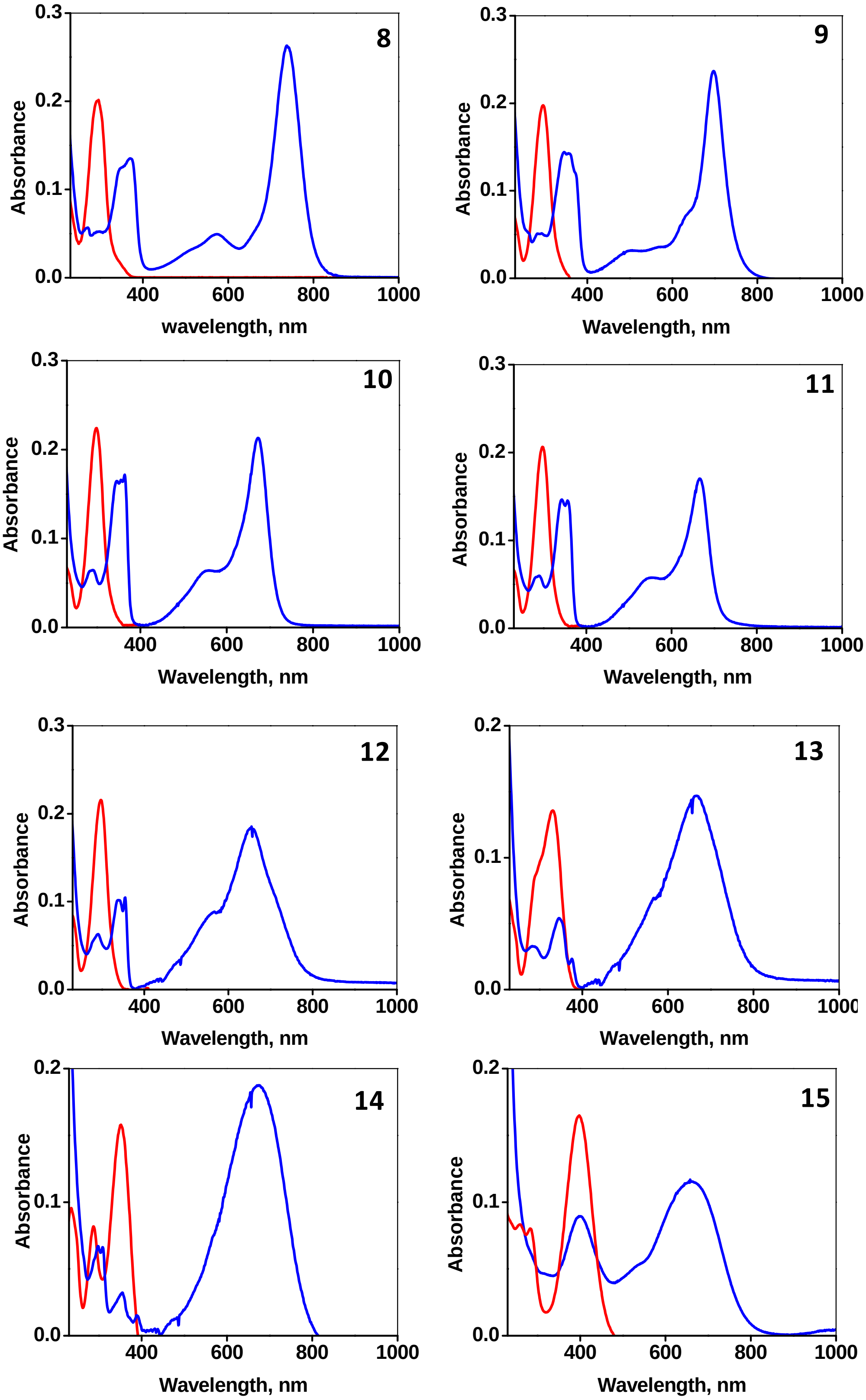

Figure 2.7. Absorption spectra of **TPA**s, **8** to **15** in the absence (–) and presence (–) of $Cu(ClO_4)_2.6H_2O$ in acetonitrile.

Formation of radical cations **8**$^{\bullet+}$ to **15**$^{\bullet+}$ in the reaction of amines with Cu^{2+} was also confirmed by observation of their ESR spectra.[28] We have recorded ESR spectra of all the **TPA** derivatives in the presence of Cu^{2+} (Figure 2.8) . The paramagnetic Cu^{2+} showed an ESR signal around 3000 G. When one equivalent of a **TPA** derivative was added, the ESR signal at 3000 G, completely disappeared and new signals corresponding to radical cations of the **TPA** appeared immediately near 3250 G. This clearly indicates that radical cations of the **TPA**s are formed as a result of electron transfer from the amine to the paramagnetic Cu^{2+}. The ESR signals decayed with time and the spectra presented in Figure 2.8 were collected during the first 3 minutes of mixing. In all cases, we got almost identical single line ESR spectra. Stamires and Turkevich have previously observed unresolved single line ESR spectrum for **TPA**$^{\bullet+}$ at relatively high concentrations.[29] The lack of hyperfine structure was attributed to interactions of the radical cations with each other.

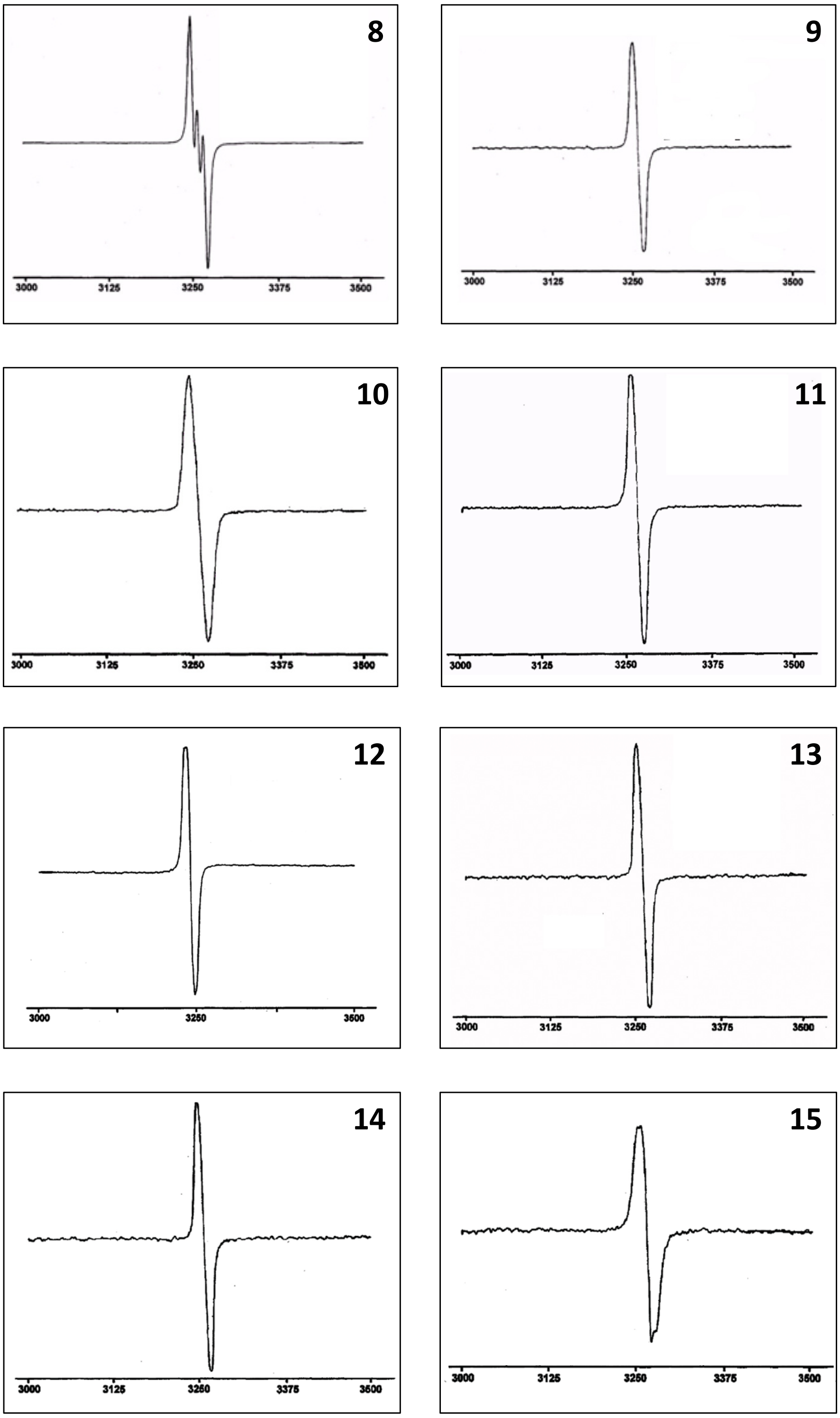

Figure 2.8. ESR Spectra of triarylamines, **8** to **15**, (1 mM) with $Cu(ClO_4)_2$ (1 mM) in ACN.

Data presented in Figures 2.7 and 2.8 clearly confirmed formation of radical cations of **TPA** derivatives as shown in Figure 2.9.

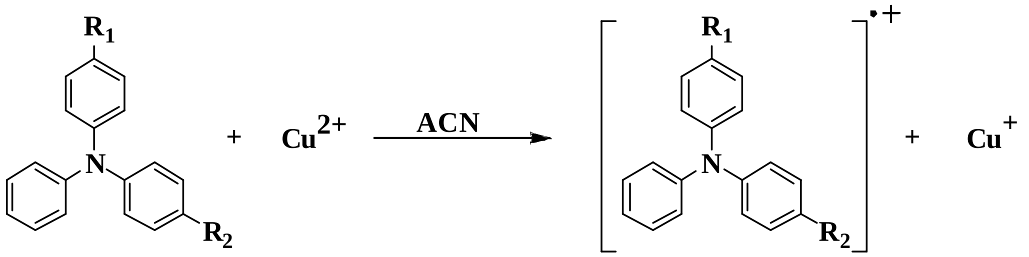

Figure 2.9. Scheme for formation of **TPA**$^{•+}$ from **TPA** and Cu^{2+}.

Reaction shown in Figure 2.9 is an electron transfer reaction, where an electron from the HOMO of **TPA** is transferred to Cu^{2+}. For such electron transfer reactions the free energy change (ΔG^0) can be calculated using the standard expression,

$$\Delta G^0 = E_{\mathrm{ox}} - E_{\mathrm{red}} - e^2/d\varepsilon \qquad (2.2)$$

where E_{ox} is the oxidation potential of the **TPA** derivatives, E_{red} is the reduction potential of Cu^{2+}, d is the center-to-center distance between **TPA** and $Cu(ClO_4)_2$ hexahydrate in the collision complex, and ε is the dielectric constant (= 37) of acetonitrile.[3] We have measured the E_{ox} values for all the **TPA** derivatives in acetonitrile using cyclic voltammetry and the values are presented in Table 2.1. Notice that E_{ox} value ranged from +0.63 V vs SCE for **8** to +1.16 V vs SCE for **15**. Thus, among the **TPA**s studied **8** is the strongest electron donor and **15** is the weakest electron donor. The Coulombic term in equation 2.2 was calculated assuming d = 8 Å. Using these values, the ΔG^0 associated with **TPA**$^{•+}$ formation were calculated for all **TPA** derivatives and the data are presented in Table 2.1.

It can be seen from Table 2.1 that for the series of **TPA** derivatives **8** to**15** studied, ΔG^0 values varied from -8.56 to +3.67 kcal M^{-1}. For **TPA**s **8** to**12,** ΔG^0 values are negative and the reactions are exergonic. For **TPA**s **13** to**15**, where the molecules contain electron withdrawing substituents, ΔG^0 values are positive. Although ΔG^0 values are positive for some of these systems, radical cation formation occurred readily for all **TPA**s as ascertained by absorption and ESR spectroscopies.

Table 2.1. **TPA** derivatives, their oxidation potentials, ΔG^0 values and absorption maxima of **TPA**$^{\bullet+}$.

Compound Number	E_{ox}, V vs SCE	ΔG^0, kcal M^{-1}	$\lambda_{TPA^{\bullet+}}$, nm
8	+ 0.63	- 8.56	737
9	+ 0.76	- 5.56	695
10	+ 0.88	- 2.80	671
11	+ 0.90	- 2.33	669
12	+ 0.92	- 1.87	679
13	+ 1.05	+ 1.13	670
14	+ 1.08	+ 1.82	675
15	+ 1.16	+ 3.67	656

2.3.1. Determination of Electron Transfer Rate Constant (k_{et})

Kinetics of radical cation formation for all **TPA** derivatives were studied under pseudo-first order conditions, using stopped-flow spectrophotometry. **TPA** concentrations employed in these studies were 15 to 20 times larger compared to Cu^{2+} concentrations in order to maintain pseudo-first order condition. An alternate method would be to maintain a low concentration of **TPA** and use excess of Cu^{2+}. This method was not adopted because excess Cu^{2+} led to formation of dications in the case of easily oxidizable **TPA** derivatives. Stopped-flow experiments were carried out by mixing the amine and Cu^{2+} solution using an Applied Photophysics Model SX18 MV spectrophotometer. Formation of the radical cation absorptions for **TPA**s **8** to **15** were monitored at the corresponding absorption maxima.

We observed that at identical concentrations of **TPA** and Cu^{2+}, formation of the radical cations were very fast for **TPA**s with negative ΔG^0 and very slow for **TPA**s with positive ΔG^0 values. Growth profiles for the different **TPA**$^{\bullet+}$ are shown in Figure 2.10A,B

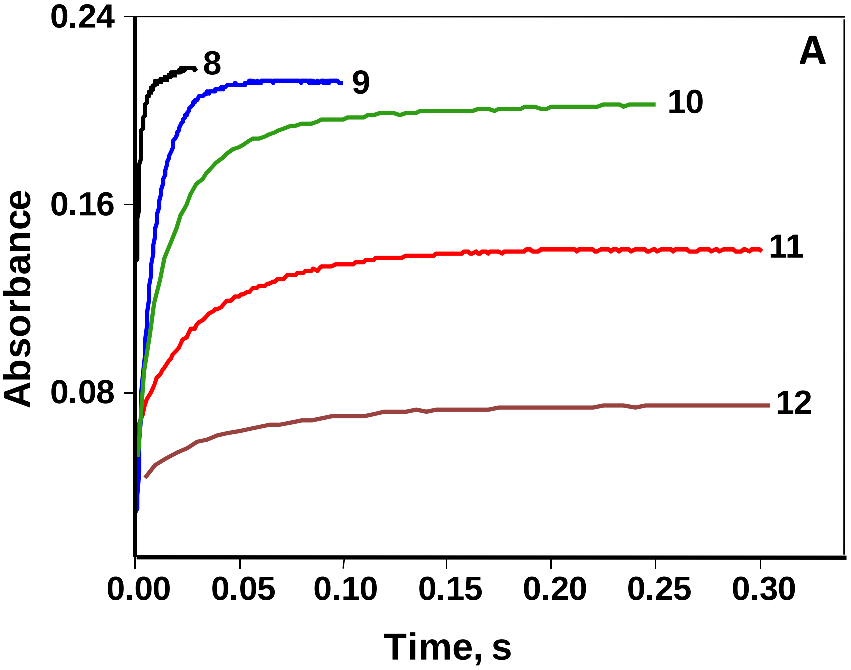

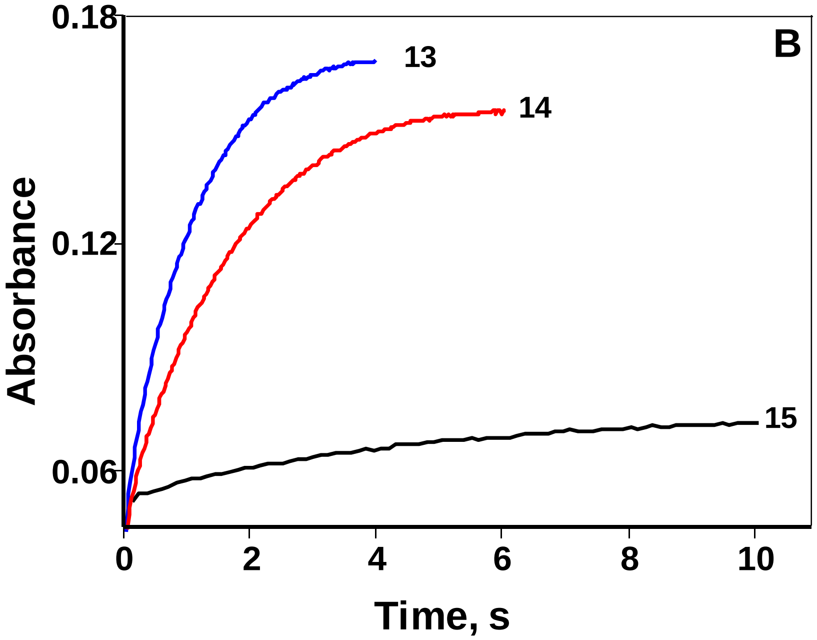

Figure 2.10. Absorbance-time profile for the formation of (A) **TPA$^{\bullet+}$** from **8** to **12** (20 × 10^{-4} M) and $Cu(ClO_4)_2.6H_2O$ (1 × 10^{-4} M) in ACN. (B) **TPA$^{\bullet+}$** from **13 - 15** (20 × 10^{-4} M) and $Cu(ClO_4)_2.6H_2O$ (1 × 10^{-4} M) in ACN.

An examination of Figure 2.10 reveals that for the dimethoxy derivative **8**, radical cation formation was complete within 30 milliseconds, whereas for the nitro derivative **15** radical cation formation was not complete even at 10 s. In addition to TPA systems shown in Chart 2.2, we have also investigated the radical cation formation for tris(4-methoxyphenyl)amine (E_{ox} = + 0.54 V, ΔG^0 = - 11.1 kcal M^{-1}) and di(4-nitrophenyl)phenylamine (E_{ox} = + 1.35 V, ΔG^0 = + 8.05 kcal M^{-1}) under the same conditions. Formation of the radical cation was too fast for the former and too slow for the latter and these systems could not be studied using the stopped-flow technique.

For all systems growth of the $\mathbf{TPA}^{\bullet+}$ absorptions (Figure 2.10) were exponential under pseudo-first order conditions. The growth profiles were fit to a first order kinetic equation (available with the stopped-flow spectrophotometer) to obtain observed rate constants ($k_{obs} = k_{et}$[**TPA**], where k_{et} is the bimolecular electron transfer rate constant). To obtain k_{et} values the k_{obs} values were determined at different concentrations of **TPA** and plotted against [**TPA**]. This is illustrated in Figures 2.11, taking the dimethoxy derivative **8** as an example. Figure 2.11A shows the radical cation growth profiles for the **8**/Cu^{2+}system where [Cu^{2+}] was maintained at 0.1 mM and [**8**] varied from 1.5 to 3.0 mM. The growth profiles obtained were fitted to the first order kinetic equation to get k_{obs} at each of the amine concentrations. Values of k_{obs} were then plotted against concentration of **8** and the straight line plot given in Figure 2.11B was obtained.

The slope of this plot gave the bimolecular rate constant k_{et} for the **8**/Cu^{2+} system.

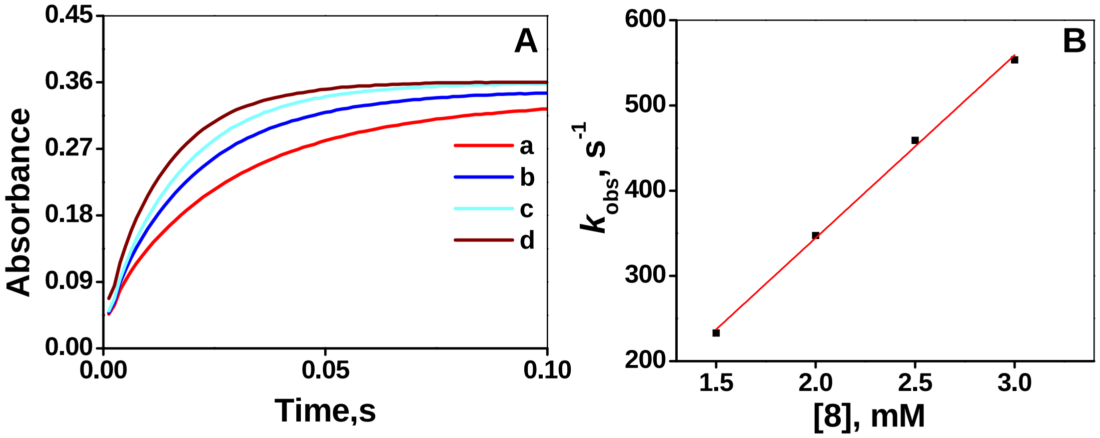

Figure 2.11. (A) Absorbance-time profile for the formation of $\mathbf{8}^{\bullet+}$ at various concentrations of **8**. [**8**] employed were (a) 1.5, (b) 2.0, (c) 2.5 and (d) 3.0 mM and [Cu^{2+}] was 1.0 × 10^{-4} M. (B) Plot of k_{obs} vs [**8**] from Figure 2.11A.

For all the **TPA** derivatives studied, concentration-dependent k_{obs} values were obtained and plotted against **TPA** concentrations. These plots are shown in Figure 2.12. From the slopes of these plots k_{et} values were obtained. The k_{et} values thus obtained were 1.09 × 10^2 M^{-1} s^{-1} for **15**, 3.76 × 10^2 M^{-1} s^{-1} for **14**, 6.08 × 10^2 M^{-1} s^{-1} for **13**, 59.60 × 10^2 M^{-1} s^{-1} for **12**, 92.82 × 10^2 M^{-1} s^{-1} for **11**, 169.34 × 10^2 M^{-1} s^{-1} for **10**, 266.38 × 10^2 M^{-1} s^{-1} for **9**, 2145.60 × 10^{2} M^{-1} s^{-1} for **8** (these values are presented later in Table 2.2). For all these values the error limits were also obtained from the software and these are also reported in Table 2.2.

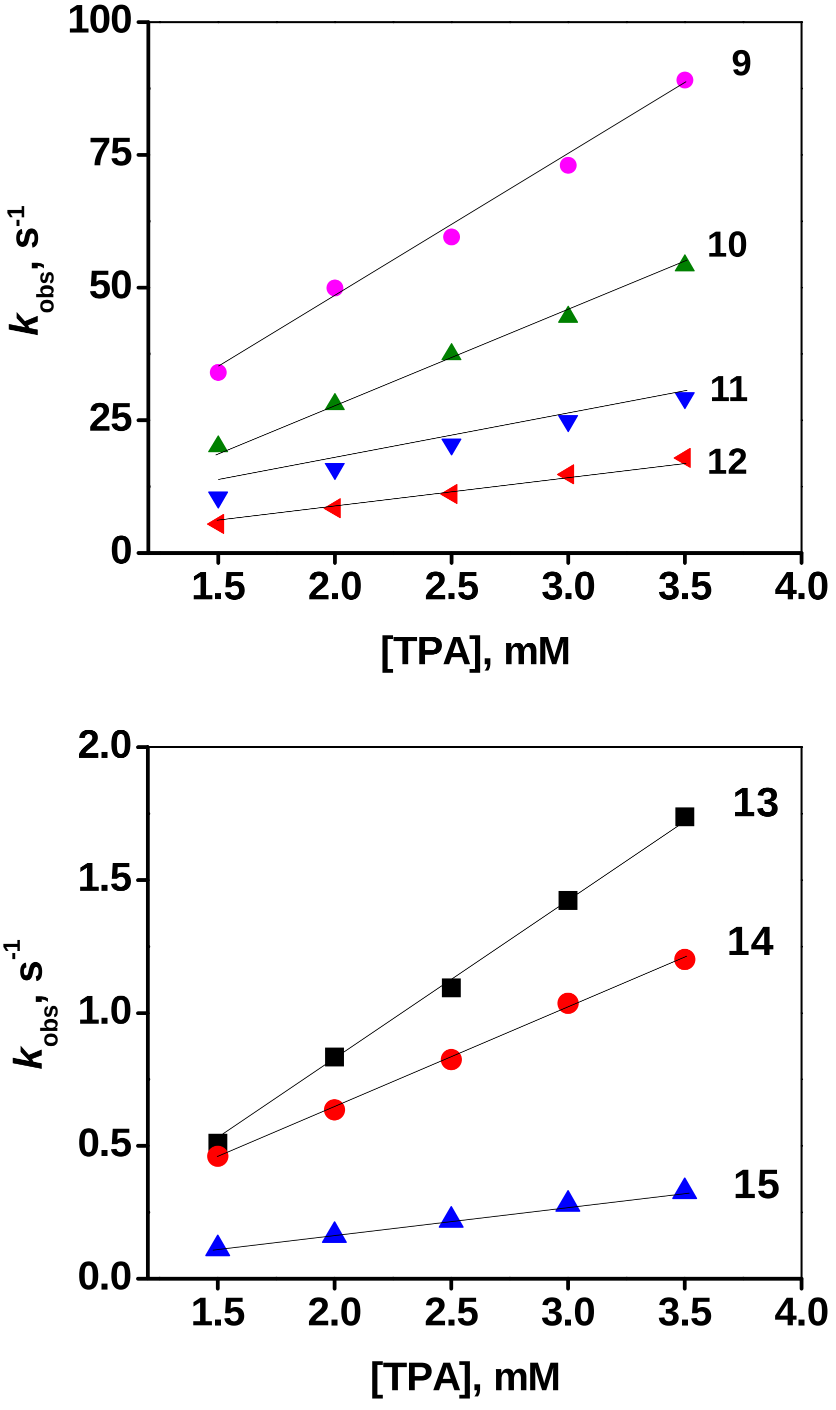

Figure 2.12. Plots of k_{obs} *vs* [**TPA**] for **TPA** derivative **9** to **15**.

Stopped-flow experiments performed as above gave a set of bimolecular rate constants, k_{et}. Since electron transfer between **TPA** and Cu^{2+} is a bimolecular reaction, it would involve steps such as formation of encounter complex, reactant separation, electron transfer within the encounter complex, reverse electron transfer, and product separation as shown in Scheme 2.1. In order to analyze and understand the reaction, all these elementary steps need to be considered.

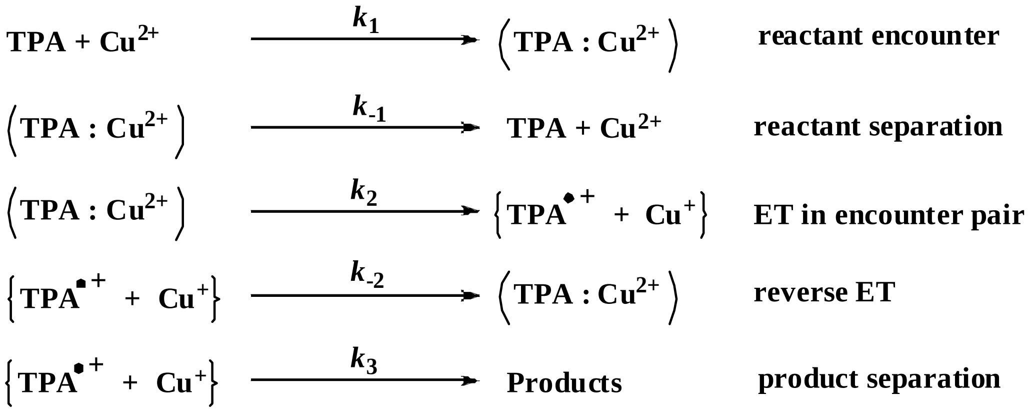

Scheme 2.1

The assumption of steady state conditions for (**TPA** : Cu^{2+}) and {**TPA**$^{\bullet +}$ + Cu^{+}} leads to the following equation.[30,31]

$$-d[\mathbf{TPA}]/dt = k_{et} [\mathbf{TPA}] [Cu^{2+}] \qquad (2.3)$$

where,

$$k_{et} = \{(k_1/k_{-1}) (k_2/k_{-2}) k_3\} / [1 + (k_3/k_{-2}) + (k_2 k_3/k_{-1}k_{-2})] \qquad (2.4)$$

If we assume that $k_3 >> k_{-2}$, then $k_3/k_{-2} >> 1$ and the equation reduces to

$$k_{et} = \{(k_1/k_{-1}) (k_2/k_{-2}) k_3\} / [(k_3/k_{-2}) + (k_2 k_3/k_{-1}k_{-2})] \qquad (2.5)$$

If we further assume that $k_{-1} >> k_2$, the equation further reduces to

$$k_{et} = (k_1/k_{-1}) k_2 \qquad (2.6)$$

It may be noted that (k_1/k_{-1}) = K_d, the equilibrium constant for encounter pair formation. Usually $k_1 \sim k_{-1}$ and hence $K_d \sim 1$ M^{-1} and hence $k_{et} = k_2$ M^{-1}. The conclusion from the above analysis is that the second order rate constant k_{et} obtained from the stopped-flow experiments is the product of the unimolecular electron transfer rate constant k_{et} and the equilibrium constant for encounter pair formation K_d.

In the derivation above we made two assumptions whose validity needs to be examined. The products of electron transfer, namely **TPA**$^{\bullet+}$ and Cu$^+$ are both positively charged and repel each other thereby facilitating product separation leading to a high value for k_3. For **TPA** derivatives **8** to **12**, the free energy change for the reverse electron transfer process will be positive which results in small k_{-2} values. Both factors support our assumption that $k_3 >> k_{-2}$. Since the observed rate constants are well below the diffusion limit, the second assumption is also reasonable.

In general, electron transfer reactions between donors and acceptors are analyzed by the Marcus theory. Our intention was to compare the rate constants k_{et} obtained experimentally for the **TPA**/Cu^{2+} reaction to those calculated using the Marcus theory.

2.3.2. Analysis of Electron Transfer Rate Constant (k_{et}) using Marcus Theory

In the Marcus formalism of electron transfer based on reactive collisions, the rate constant for electron transfer is written as

$$k_{et} = Z \exp(-\Delta G^*/k_BT) \qquad (2.7)$$

where Z is the collision rate and ΔG^* is the Marcus free energy of activation, k_B is the Boltzmann constant and T is the absolute temperature.[32-34] This is the classical form of the Marcus equation and a semi-classical equation is provided later in this chapter. The free energy of activation ΔG^* is given by

$$\Delta G^* = (\Delta G^0 + \lambda)^2/4\lambda \qquad (2.8)$$

where λ is the reorganization energy needed for the electron transfer reaction.[32-34] λ is a combination of (i) internal reorganization energy (λ_i) arising out of changes in bond lengths and bond angles and (ii) solvent reorganization energy (λ_s) arising from the changes in the solvent shell surrounding the redox species. Substituting equation 2.8 in 2.7, we get

$$k_{et} = Z \exp\text{-}(\Delta G^0 + \lambda)^2/4\lambda k_BT \qquad (2.9)$$

Rearrangement of equation 2.9 leads to

$$k_BT\ln k_{et} = \ln Z - (\Delta G^0)^2/4\lambda - \Delta G^0/2 - \lambda/4 \qquad (2.10)$$

If we are considering electron transfer reactions in a series of similar compounds, λ can be considered as a constant for the reaction. For the **TPA**/Cu^{2+} reactions studied here, $|\Delta G^0|$ values are small. If we assume that for a series of similar electron transfer reactions, where $|\Delta G^0/\lambda|$ is small, then equation 2.10 reduces to

$$k_BT\ln k_{et} = \text{Constant} - \Delta G^0/2 \qquad (2.11)$$

In other words, under the conditions stated above, a plot of $k_BT\ln k_{et}$ vs $-\Delta G^0$ is expected to be linear with a slope equal to ½.[35-37] In Figure 2.13, $k_BT\ln k_{et}$ values are plotted against $-\Delta G^0$ along with a theoretical line with slope = ½. The first six experimental points fall on the line indicating that equations 2.7 and 2.8 hold good for the **TPA**/Cu^{2+} reaction. Figure 2.13 can be taken as an indication that these reactions follow the Marcus equation. For the last two systems the assumption $|\Delta G^0/\lambda|$ may not be valid and this may be the reason for the observed deviation.

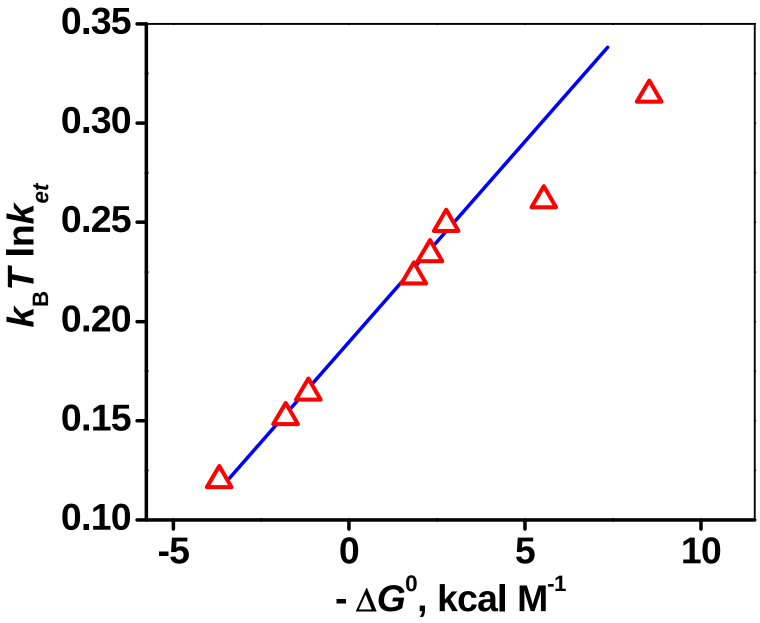

Figure 2.13. Plot of $k_BT\ln k_{et}$ vs $-\Delta G^0$ for the **TPA**/Cu^{2+} systems studied. A theoretical line with slop ½ is also shown.

A preliminary analysis of the rate constant as given by equations 2.7 and 2.8 and Figure 2.13 showed that the **TPA**/Cu^{2+} systems obey the Marcus equation. This has prompted us to undertake a detailed analysis of the reaction in terms of Marcus theory. The semiclassical form of the Marcus equation is given by,

$$k_{et} = (2\pi/\hbar)\,(H_{el})^2\,(4\pi\lambda k_B T)^{-1/2}\,\exp[-(\Delta G^0 + \lambda)^2/4\lambda k_B T] \qquad (2.12)$$

where H_{el} is the donor-acceptor coupling element and $\hbar$ is Planck's constant divided by 2π. H_{el}, is identified with the probability that the reaction proceeds from the initial to the final state. Depending on the magnitude of H_{el} electron transfers can be regarded as taking place in adiabatic, non-adiabatic or intermediate regions. In the adiabatic region electronic interaction between the donor and acceptor are very strong. In the non-adiabatic case the electronic interaction between the donor and acceptor is very weak and the electron tunnels through an energy barrier separating the donor and acceptor. Somewhere between the extremes lies the intermediate region known as weakly adiabatic. This is the region applicable to classical theories where the donor and acceptor is separated by an encounter distance of ≈7 Å and sufficient orbital interaction for electron transfer is possible. It is generally agreed that at H_{el} values below 200 cm^{-1} the reaction becomes increasingly non-adiabatic.

Equations 2.9 and 2.12 predict a parabolic dependence of k_{et} on ΔG^0. The parabolic dependence predicts three kinetic regimes for electron transfer reactions: (1) A "normal" regime for small driving force ($\Delta G^0 > -\lambda$) where the electron transfer is thermally activated and is favoured by an increase in driving force; (2) an "activationless" regime ($\Delta G^0 = -\lambda$) and (3) an "inverted" regime for strongly exergonic reactions ($\Delta G^0 < -\lambda$) where the rate actually decreases with increasing driving force. Although controversial for a long time, the inverted region is well-established now in electron transfer reactions.

2.3.2.1. Determination of Reorganization energy (λ)

We are interested in calculating electron transfer rate constants using the Marcus equation and comparing these values with experimental k_{et} values. For calculating the theoretical values using equation 2.12, H_{el} and λ values are required. These were estimated as follows. The reorganization energy λ is related to the Marcus free energy of activation ΔG^* by equation 2.8. The Marcus free energy of activation in turn is related to the Arrhenius activation energy, E_a through the following equation.

$$\Delta G^* = E_a - RT/2 \qquad (2.13)$$

E_a for these reactions, in turn, could be obtained from a study of temperature dependence of rate constants. Details of the treatment we followed are given below.

According to the activated complex theory the rate constant k_2 is given by,

$$k_2 = (k_B T/h) \exp(-\Delta G^{\#}/RT) \qquad (2.14)$$

where h is the Planck's constant ($k_B T/h$ represents the frequency with which the activated complex crosses over to products) and $\Delta G^{\#}$ is the free energy of activation ($\Delta G^{\#} = \Delta H^{\#}$-T$\Delta S^{\#}$, where $\Delta H^{\#}$ and $\Delta S^{\#}$ are the enthalpy and entropy of activation, respectively. Since the reactants are not charged, work terms can be neglected). Substituting into equation 2.6 provides

$$k_{et} = K_d(k_BT/h)\exp(-\Delta G^{\#}/RT) \qquad (2.15)$$

If we assume that K_d is temperature independent, the activation parameters can be determined by studying the temperature dependence of k_{et}. For all the **TPA**/Cu^{2+} systems k_{obs} values were obtained at different temperatures and the data were plotted using the linear form of the Eyring equation (2.16).

$$\ln(k_{obs}h/k_BT) = -\Delta H^{\#}/RT + \Delta S^{\#}/R \qquad (2.16)$$

Plots of $\ln(k_{obs}h/k_BT)$ vs $1/T$ for all the systems studied are shown in Figure 2.14. For the dimethoxy derivative **8**, radical cation formation was too fast at temperatures above 310 K. Hence this system was studied in the range of 288 to 303 K. Other systems were studied in the range 298 to 323 K. It can be seen from Figure 2.14 that for all the **TPA**s studied, plots of $\ln(k_{obs}h/k_BT)$ vs $1/T$ were linear.

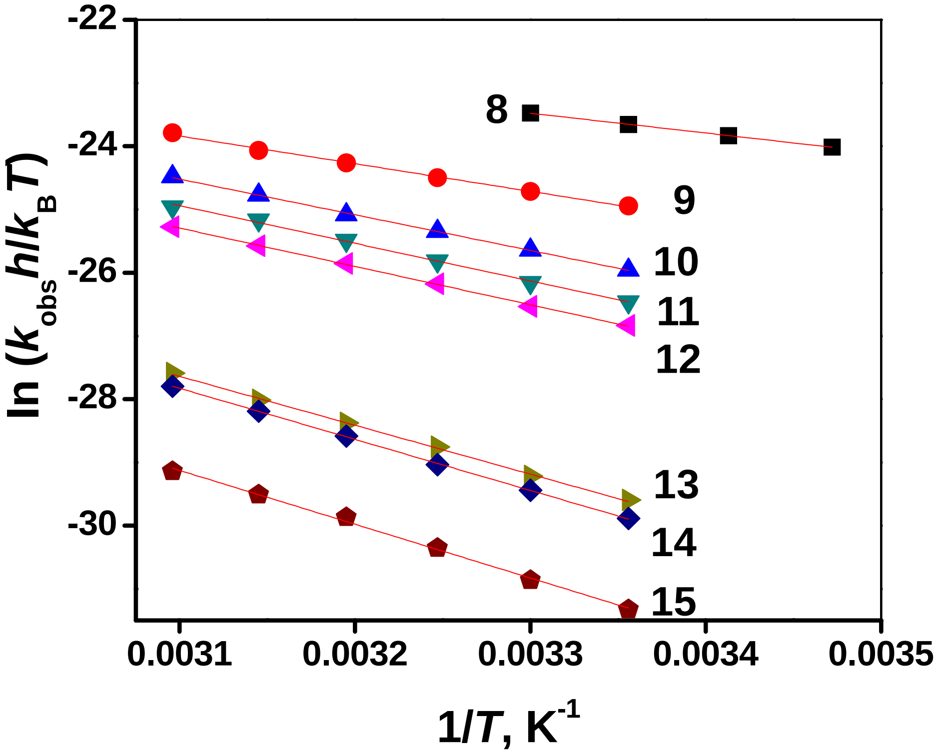

Figure 2.14. Eyring plots for all **TPA**/Cu^{2+} systems in ACN.

From the slopes and intercepts of these plots, $\Delta H^{\#}$ and $\Delta S^{\#}$ values were obtained. Using these values the free energy of activation $\Delta G^{\#}$ (= $\Delta H^{\#}$-T$\Delta S^{\#}$) and Arrhenius energy of activation E_a (= $\Delta H^{\#} + RT$) were also obtained. These values are presented in Table 2.2 along with the observed k_{et} values. Using the E_{a} values thus obtained the Marcus free energy of activation ΔG^{*} were calculated using equation 2.13 and these are also given in Table 2.2.

Table 2.2. Rate constants and activation parameters for the electron transfer between **TPA** and Cu^{2+} in ACN.

TPA	k_{et},[*] $M^{-1}\,s^{-1}$	$\Delta H^{\#}$, kcal M^{-1}	$\Delta S^{\#}$, kcal $M^{-1}\,K^{-1}$	$\Delta G^{\#}$, kcal M^{-1}	E_a, kcal M^{-1}	ΔG^{*}, kcal M^{-1}
8	214,560 ± 6644	6.36	- 0.024	13.98	6.96	6.66
9	26,638 ± 1210	8.90	-0.019	14.61	9.50	9.20
10	16,934 ± 413	11.04	-0.015	15.38	11.63	11.33
11	9,282 ± 241	11.83	-0.013	15.67	12.42	12.12
12	5,960 ± 357	12.63	-0.005	15.90	13.22	12.92
13	608 ± 20	14.55	-0.010	17.47	15.14	14.84
14	376 ± 7	15.64	-0.003	17.68	16.23	15.93
15	109 ± 2	16.90	-0.008	18.47	17.50	17.20

[*] Experimental values are reported as ±σ.

For the **TPA**/Cu^{2+} systems examined, ΔG^{*} varied from 6.66 kcal M^{-1} for **8** (ΔG^{0} = -8.56 kcal M^{-1}) to 17.20 kcal M^{-1} for **15** (ΔG^{0} = +3.67 kcal M^{-1}) as shown in Table 2.2. Figure 2.15, is a plot of ΔG^{*} obtained from the temperature dependence studies, against ΔG^{0}. We have fitted the ΔG^{*} data to equation 2.8 using different λ values. This approach assumes that for the series of **TPA** derivatives **8** to **15** the electron transfer reactions follow the same mechanism and that the reorganization energy λ is relatively constant in the series. The best fit obtained (solid line) using λ = 48.43 kcal M^{-1} is also shown in Figure 2.15. It may be noted that the data points fit very well to equation 2.8.

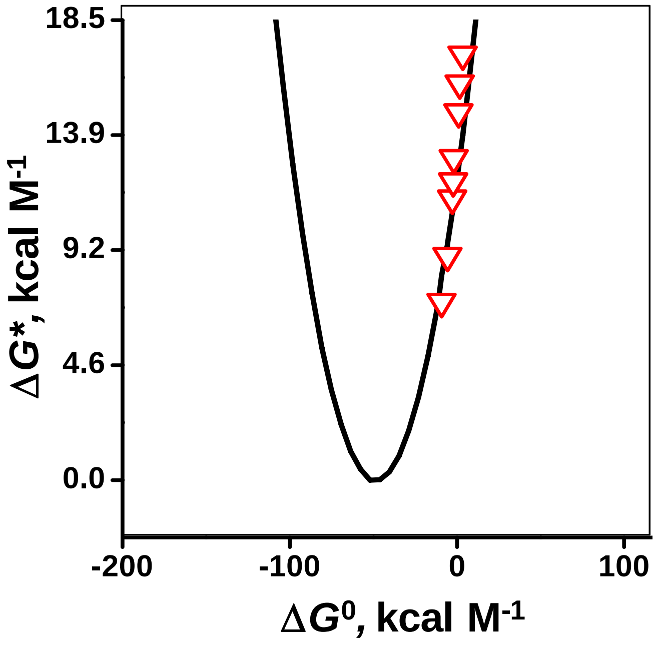

Figure 2.15. Plot of ΔG^* against ΔG^0 and theoretical fit using λ = 48.43 kcal M^{-1}.

2.3.2.2. Determination of Donor-Acceptor Coupling Element (H_{el})

Using the λ value thus obtained, we fitted the experimental k_{et} data using equation 2.12 with different values of H_{el}. The best fit obtained (solid line) using H_{el} = 100 cm^{-1} along with experimental data points is shown in Figure 2.16. It can be seen that the experimental data matches well with values calculated using Marcus equation. The H_{el} value used for the fit is less than k_BT, suggesting that the electron transfer between **TPA** and Cu^{2+} depicted in Figure 2.9 is non-adiabatic and proceeds by an outer-sphere mechanism. Since $\Delta G^0 > -\lambda$ for the cases studied, the data points fall in the “normal” region of the Marcus parabola.

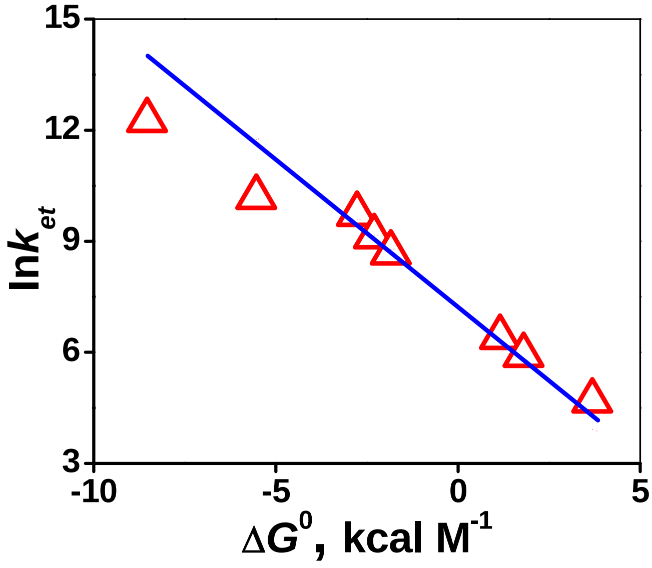

Figure 2.16. Plot of ln k_{et} vs ΔG^0 for **TPA**/Cu^{2+} reaction. The solid line is a fit using H_{el} = 100 cm^{-1} and λ = 48.43 kcal M^{-1}.

2.3.3 Mechanism of Electron Transfer Reaction in TPA/Cu^{2+} Systems

For photoinduced electron transfer reactions between organic donors and acceptors the reorganization energy generally is in the range of 25 to 35 kcal M^{-1} and hence the value of 48.43 kcal M^{-1} obtained for the **TPA**/Cu^{2+} systems seems to be very high.[38] The high λ value is attributed to the high internal reorganization energy associated with the Cu^{2+}/Cu^{+} redox reaction. Cu^{2+} is a d^9 system and adopts a distorted octahedral type six-coordinate geometry or a square pyramidal or trigonal bipyramidal type five-coordinate geometry. Cu^{+} on the other hand is a d^{10} system and adopts a four-coordinate tetrahedral geometry.[39,40] Thus the reduction of Cu^{2+} to Cu^{+} would involve the rupture of one or two coordinate bonds and a change of the remaining bond angles. Equation 2.12 is based on the assumption that no chemical bonds are broken or formed during the electron transfer process. Since bond rupture or formation is involved in the Cu^{2+}/Cu^{+} redox process some researchers have questioned the validity of applying the Marcus equation to Cu^{2+}/Cu^{+} reactions.[41,42] However, the Marcus equation has been successfully applied to a large number of Cu^{2+}/Cu^{+} electron transfer reactions[43] and hence we believe that the same can be done in the case of **TPA**/Cu^{2+} electron transfer reactions also.

In $Cu(ClO_4)_2$ hexahydrate the Cu^{2+} is bonded to six water molecules in a distorted octahedral geometry.[44] Four of the $Cu\text{-}OH_2$ bond lengths are nearly equal (~1.96 Å) while the other two are substantially larger (2.38 Å). When dissolved in ACN the complex most probably exists as $[Cu(OH_2)_n(ACN)_{6-n}]^{2+}$ (n = 0-3) with $[Cu(OH_2)_2(ACN)_4]^{2+}$ as the dominant species in 99% ACN.[45] The Cu-ACN bond length in $[Cu(OH_2)_2(ACN)_4]^{2+}$ is 1.975 Å.[45] Electron transfer from **TPA** leads to formation of $[Cu(ACN)_4]^{+}$, which contains four acetonitrile molecules arranged in a tetrahedral fashion around the Cu^{+} (average bond angle 109.4° and average Cu-N bond length 1.99 Å).[46] Note that the Cu-ACN bond lengths do not change much during the electron transfer process.[45] Based on these factors we suggest the scheme in Figure 2.17 for electron transfer in the **TPA**/Cu^{2+} systems.

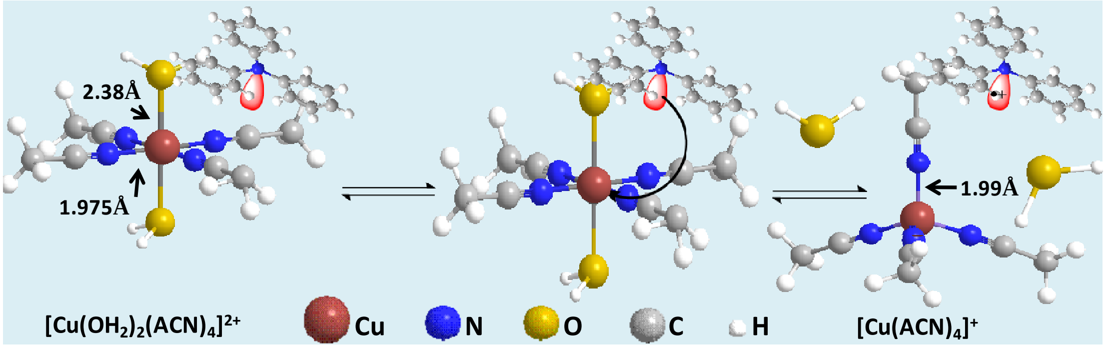

Figure 2.17. Schematic diagram of the electron transfer process in **TPA**/Cu^{2+} system.

The precursor complex is shown in the left, the transition state is shown in the middle and the successor complex is shown in the right. Upon proceeding from the precursor complex to the transition state, the Cu-OH$_2$ bonds weaken and the Cu-ACN bond angles change. Following electron transfer the two Cu-OH$_2$ bonds are cleaved and the Cu-ACN bonds assume tetrahedral geometry in the successor complex, which subsequently dissociates into the products; **TPA**$^{\bullet+}$ and Cu(ACN)$_4^+$. Since the electron transfer involves breaking of bonds and changing bond angles the internal reorganization energy would be very large. In an attempt to determine if the λ obtained is reasonable, this value was used to estimate the reorganization energy for the Cu^{2+}/Cu$^+$ self-exchange reaction (λ_{Cu^{2+}/Cu^+}), and we compared the value thus obtained with literature values.

Reorganization energies for self exchange reactions can be obtained using equation 2.7, if rate constants for self exchange reactions are known. Because of the high reorganization energy, aquacopper(II/I) and acetonitrilecopper(II/I) self-exchange reactions are extremely slow and difficult to study directly and indirect techniques are often used to estimate rate constants of these reactions.[43] Irangu *et al.* recently estimated a value of 4.0×10^{-8} M^{-1} s^{-1} for the self-exchange rate constant ($k_{\mathrm{Cu}^{2+}/\mathrm{Cu}^{+}}$) for Cu^{2+}/Cu^{+} in 100% ACN.[45] Substituting this value in equation 2.7 we obtained $\Delta G^{*} = 25$ kcal M^{-1} (assuming Z = 10^{11} M^{-1} s^{-1}). Since $\Delta G^{0} = 0$ for the self exchange reaction $\lambda_{\mathrm{Cu}^{2+}/\mathrm{Cu}^{+}} = 4 \times \Delta G^{*} = 100$ kcal M^{-1}, which is a very high value compared to that of other metal ions.[47] This value can be used to obtain a theoretical estimate of the reorganization energy for the **TPA**/Cu^{2+} reaction using the cross relationship 2.17.

$$\lambda_{\mathrm{TPA/Cu}^{2+}} = \tfrac{1}{2}\left(\lambda_{\mathrm{TPA/TPA}^{\bullet+}} + \lambda_{\mathrm{Cu}^{2+}/\mathrm{Cu}^{+}}\right) \qquad (2.17)$$

where $\lambda_{\mathrm{TPA/TPA}^{\bullet+}}$ is the reorganization energy for the **TPA/TPA$^{\bullet+}$** self-exchange reaction. It is difficult to study intermolecular **TPA/TPA$^{\bullet+}$** self exchange reactions but reorganization energy for the same can be calculated using standard equations. $\lambda_{\mathrm{TPA/TPA}^{\bullet+}}$ has contributions from λ_{i} and λ_{o}. The λ_{i} contribution was calculated previously from the energies of the neutral and radical cation forms of **TPA** using AM1 (UHF) and BPW1-DFT calculations and the value obtained was 3.23 kcal M^{-1}.[48] The small value of λ_{i} indicates that the geometric change associated with radical cation formation is very small. λ_{o} can be calculated using equation 2.18.

$$\lambda_{\mathrm{o}} = \Delta e^{2}\left(2r_{1}^{-1} + 2r_{2}^{-1} - d^{-1}\right)\left(\varepsilon_{\mathrm{op}}^{-1} - \varepsilon_{\mathrm{s}}^{-1}\right) \qquad (2.18)$$

In equation 2.18, r_1 and r_2 refer to the radii of **TPA** and **TPA$^{\bullet+}$**, d is the center-to-center distance, $\varepsilon_{\mathrm{op}}$ and ε_{s} are the optical and static dielectric constants of the solvent, acetonitrile. Since the geometric change associated with radical cation formation is very small, we can assume that $r_1 \approx r_2$. The radius of **TPA** obtained from AM1 is 5.3 Å. Taking $d = r_1 + r_2$, we obtain $\lambda_o = 16.54$ kcal M^{-1}. Thus, these calculations gave $\lambda_{TPA/TPA^{\bullet+}} = 19.77$ kcal M^{-1}. Substituting in equation 2.17 we get $\lambda_{TPA/Cu^{2+}} = 59.89$ kcal M^{-1}, which is about 20% higher than the value we obtained from fitting our kinetic data. It is to be noted that for the aquacopper(II/I) self exchange reaction, estimated $k_{Cu^{2+}/Cu^{+}}$ values varied in the range 1.9×10^{-4} to 5.4×10^{-7} M^{-1} s^{-1}.[49-53] If we use these $k_{Cu^{2+}/Cu^{+}}$ values in equation 2.7, $\lambda_{Cu^{2+}/Cu^{+}}$ values in the range 39.7 to 94.3 kcal M^{-1} are obtained. Based on Born-Oppenheimer molecular dynamic simulation studies, Blumberger has recently suggested that the reorganization free energies for Cu^{+} and Cu^{2+} are asymmetric and differ by 1.0 eV.[54] $\lambda_{Cu^{2+}/Cu^{+}}$ estimated from this study was 3.9 eV (89.9 kcal M^{-1}). While these studies disagree on the actual value of $k_{Cu^{2+}/Cu^{+}}$ they all show that the self exchange rate constant is exceptionally small in the aquacopper(II/I) system due to the large reorganization energy associated with the reaction. It is important to emphasize that our study also shows the involvement of large reorganization energy in the Cu^{2+}/Cu^{+} redox reaction.

2.4. Conclusions

We have studied the kinetic aspects of the electron transfer reaction between **TPA** and Cu^{2+} in acetonitrile as a function of driving force and temperature. The rate of formation of radical cations was measured using stopped-flow spectrometer under pseudo-first order condition. Growths of the **TPA**$^{\bullet+}$ absorptions were monitored at its absorption maxima and the growth profiles were fit to a first order kinetic equation to obtain observed rate constants (k_{obs}). The electron transfer rate constant (k_{et}) was measured by plotting the k_{obs} values at different concentrations of **TPA** against [**TPA**]. Straight lines were obtained for all systems and k_{et} values were obtained from the slopes of these plots. The second order rate constants (k_{et}) exhibited a dependence on the ΔG^0 values and varied in the range 1.02×10^2 to 2.15×10^5 M^{-1} s^{-1}, when ΔG^0 was varied from +3.67 to -8.56 kcal M^{-1}. To gain a more detailed insight of the electron-transfer process and the transition state, rates of electron transfer were measured over a 30-50 °C temperature range to obtain activation enthalpies ($\Delta H^{\#}$) and entropies ($\Delta S^{\#}$) from the linear form of the Eyring equation. Reorganization energy (λ) was then estimated using these experimentally determined activation parameters. The experimental rate constants fit well to the Marcus equation, which confirmed the involvement of an outer sphere electron transfer taking place in this reaction. The high reorganization energy is consistent with the cleavage of Cu-OH_2 bonds in the transition state and a mechanism consistent with these observations is proposed.

2.5. Experimental Section

2.5.1. Materials

TPA derivatives **8** to **15** were synthesized according to literature procedures. $Cu(ClO_4)_2.6H_2O$ was purchased from Aldrich. Acetonitrile, stored in an Innovative Technology, Inc. dry box containing a nitrogen atmosphere and a platinum catalyst for drying, was used for kinetic studies.

2.5.2. Measurements

The electronic absorption spectra were recorded on a Shimadzu 3101PC UV-Vis-NIR scanning spectrophotometer and Agilent-8453 Diode array spectrophotometer. Redox potentials of the **TPA** derivatives were recorded using a BAS CV50W voltammetric analyzer. Solutions of the **TPA** derivatives (1×10^{-3} M) in acetonitrile containing 0.1 M tetra-*n*-butylammonium hexafluorophosphate as supporting electrolyte, were thoroughly deaerated before use. A Pt disc electrode was used as working electrode and a platinum wire was used as counter electrode and the potentials were referred to saturated calomel electrode (SCE).

Kinetic experiments in acetonitrile were performed with a computer controlled, Applied Photophysics SX 18MV Stopped-Flow Spectrophotometer. Temperature dependence studies with the stopped-flow spectrophotometer were carried out over a range between 15 and 50 °C using a Neslab circulator connected to the sample-handling unit of the stopped-flow reaction analyzer. The step size used for the temperature study was 5 °C and each kinetic trace was recorded at a known temperature that was measured by a thermocouple in the reaction cell.

2.6. References

1. Balzani, V., Ed.; *Electron Transfer in Chemistry*, Wiley-VCH: New York, 2001; Vols. 1–5.
2. Fox, M. A.; Chanon, M., Eds.; *Photoinduced Electron Transfer*, Elsevier: Amsterdam, The Netherlands, 1988; Parts A-D.
3. Kavarnos, G. J.; Turro, N. J. *Chem. Rev.* **1986**, *86*, 401.
4. Das, S.; Suresh, V. In *Electron Transfer in Chemistry*, Balzani, V., Ed.; Wiley-VCH: New York, 2001; Vol. 2, pp 379-456.
5. Easton, C. J. *Chem. Rev.* **1997**, *97*, 53.
6. Theys, R. D.; Sosnovsky, G. *Chem. Rev.* **1997**, *97*, 83.
7. Pullen, G. K.; Allen, N. S.; Edge, M. Weddel, I.; Swart, R.; Catalina, F.; Navaratnam, S. *Eur. Polym. J.* **1996**, *32*, 943.
8. For a recent review, see: Davies, A. G. *J. Chem. Res.* (S) **2001**, 253.
9. Fielder, D. A.; Koppenol, M.; Bond, A. M. *J. Electrochem. Soc.* **1995**, *142*, 862.
10. Gerson, F.; Gescheidt, G.; Knöbel, J.; Martin, W. B.; Neumann, L.; Vogel, E. *J. Am. Chem. Soc.* **1992**, *114*, 7107.
11. Gescheidt, G.; Herges, R.; Neumann, H.; Heinze, J.; Wollenweber, M.; Etzkorn, M.; Prinzbach, H. *Angew. Chem., Int. Ed.* **1995**, *34*, 1016.
12. Krishna, R. M.; Chang, Z.; Choo, H.; Ranjit, K. T.; Kevan, L. *Phys. Chem. Chem. Phys.* **2000**, *2*, 3335.

13. Symons, M. C. R. *Chem. Soc. Rev.* **1984**, *13,* 393.

14. Shida, T.; Haselbach, E.; Bally, T. *Acc. Chem. Res.* **1984**, *17*, 180.

15. Garcia, H.; Marti, V.; Casades, I.; Fornes, V.; Roth, H. D. *Phys. Chem. Chem. Phys.* **2001**, *3*, 2955.

16. Folgado, J.-V.; Garcia, H.; Marti, V.; Espla, M. *Tetrahedron* **1997**, *53*, 4947.

17. Sumalekshmy, S.; Gopidas, K. R. *Chem. Phys. Lett.* **2005**, *413*, 294.

18. Shida, T.; Hamill, W. H. *J. Chem. Phys.* **1966**, *44*, 2369.

19. Shida, T. *Electronic Absorption Spectra of Radical Ions,* Elsevier: Amsterdam, 1988; p 209.

20. Shida, T. *Electronic Absorption Spectra of Radical Ions,* Elsevier: Amsterdam, 1988; p 221.

21. Anderson, C. P.; Salmon, D. J.; Meyer, T. J.; Young, R. C. *J. Am. Chem. Soc.* **1977**, *99*, 1980.

22. Breslin, D. T.; Fox, M. A. *J. Org. Chem.* **1994**, *59*, 7557.

23. Oyama, M.; Higuchi, T.; Okazaki, S. *J. Chem. Soc., Perkin Trans. 2* **2001**, 1287.

24. Burrowds, H. D.; Greatorexan, D.; Kemp, T. J. *J. Phys. Chem.* **1972**, *76,* 20.

25. Katritzky, A. R.; Boulton, A. J., Eds.; *Advances in Heterocyclic Chemistry*, Academic Press: New York, 1968; Vol. 9, p 351.

26. Marcus, R. A. *Angew. Chem., Int. Ed.* **1993**, *32,* 1111.

27. (a) Gauthier, S.; Fréchet, J. M. J. *Synthesis* **1987**, *4*, 383. (b) Lai, G.; Bu, X. R.; Santos, J.; Mintz, E. A. *Synlett* **1997**, *11*, 1275.

28. Sreenath, K.; Suneesh, C. V.; Ratheesh Kumar, V. K.; Gopidas, K. R. *J. Org. Chem.* **2008**, *73*, 3245.

29. Stamires, D. N.; Turkevich, J. *J. Am. Chem. Soc*. **1963**, *85*, 2557.

30. Baggott, J. E. In *Photoinduced Electron Transfer*, Fox, M. A.; Channon, M., Eds.; Elsevier: New York, 1988; Part B.

31. Kavarnos, G. J. *Fundamentals of Photoinduced Electron Transfer*, VCH: New York, 1993.

32. Marcus, R. A. *Faraday Discuss. Chem. Soc.* **1982**, *74*, 7.

33. Marcus, R. A.; Sutin, N. *Biochim. Biophys. Acta* **1985**, *811*, 265.

34. Sutin, N. *Acc. Chem. Res.* **1982**, *15*, 275.

35. Marcus, R. A. *Angew. Chem. Int. Ed.* **1993**, *32*, 1111.

36. Bock, C. R.; Connor, J. A.; Gutierrez, A. R.; Meyer, T. J.; Whitten, D. G.; Sullivan, B. P.; Nagle, J. K. *J. Am. Chem. Soc.* **1979**, *101*, 4815.

37. Fukuzumi, S.; Wong, C. L.; Kochi, J. K. *J. Am. Chem. Soc.* **1980**, *102*, 2928.

38. Gould, I.; Farid, S. *Acc. Chem. Res.* **1996**, *29*, 522.

39. Hathaway, B. J.; Billing, D. E. *Coord. Chem. Rev.* **1970**, *5*, 143.

40. Hathaway, B. J. *Coord. Chem. Rev.* **1981**, *35*, 211.

41. Lee, C.-W.; Anson, F. C. *J. Phys. Chem.* **1983**, *87*, 3360.

42. Lee, C.-W.; Shin, D. S.; Chair, T. S.; Kim, K. *Bull. Korean Chem. Soc*. **1991**, *12*, 454.

43. Rorabacher, D. B. *Chem. Rev*. **2004**, *104*, 651.

44. Gullucci, J. C.; Gerkin, R. E. *Acta Cryst.* **1989**, *C45*, 1279.

45. Irangu, J.; Ferguson, M. J.; Jordan, R. B. *Inorg. Chem*. **2005**, *44*, 1619.

46. Csöregh, I.; Kierkegaard, P.; Norrestam, R. *Acta Cryst.* **1975**, *B31*, 314.

47. Marcus, R. A. *Rev. Mod. Phys.* **1993**, *65*, 599.

48. Low, P. J.; Paterson, M. A. J.; Yufit, D. S.; Howard, J. A. K.; Cherryman, J. C.; Tackley, D. R.; Brook, R.; Brown, B. *J. Mater. Chem*. **2005**, *15*, 2304.

49. Hoselton, M. A.; Lin, C.-T.; Schwarz, H. A.; Sutin, N. *J. Am. Chem. Soc*. **1978**, *100*, 2383.

50. Davies, K. M. *Inorg. Chem*. **1983**, *22*, 615.

51. Sisley, M. J.; Jordan, R. B. *Inorg. Chem*. **1992**, *31*, 2880.

52. Gaunder, R. G.; Taube, H. *Inorg. Chem*. **1970**, *9*, 2627.

53. Manahan, S. E. *Can. J. Chem*. **1967**, *45*, 2451.

54. Blumberger, J. *J. Am. Chem. Soc.* **2008**, *130*, 16065.

Chapter 3

Reactivity Patterns of a few Aromatic Amine Radical Cations

3.1. Abstract

We have studied the reactions of a few aromatic amines with Cu^{2+} *in acetonitrile and characterized the amine radical cations formed by absorption spectroscopy. In a few cases the radical cations were also characterized by ESR spectra. Some of these radical cations exhibited remarkable stability whereas a few others undergo reactions. In the case of a few dialkylanilines, diphenylamines and triphenylamines we followed the reactions of the radical cations using absorption spectroscopy. It was observed that in the absence of nucleophiles, the radical cations undergo dimerization reactions to give benzidine derivatives in good yields. In the presence of nucleophiles such as* -Cl^{Θ}, -Br^{Θ}, *or* -SCN^{Θ}, *the radical cations undergo nucleophilic substitution reactions to give para-substituted products. Rational mechanisms were proposed for these reactions based on spectroscopic data. We have also explored the synthetic utility of these reactions using several aromatic amines. Yields of benzidine derivatives were very high and we project that the radical cation route is very useful for the synthesis of tetra substituted benzidines.*

3.2. Introduction

Several methods are available in the literature for the generation of aromatic amine radical cations[1] and these were reviewed in Chapter 1 of this thesis. Radical cations formed can undergo a variety of reactions and hence understanding the reactivity patterns of radical cations is extremely important. Amine radical cations generated in flash photolysis and pulse radiolysis experiments are generally short-lived. Absorption spectra of the radical cations generated by these methods can be obtained easily, but very little information is available about their reactivity aspects. Aromatic amines such as tris(4-bromophenyl)amine (**1**) give radical cations which are very stable. Stable radical cations can be generated electrochemically and their absorption and ESR spectra could be recorded. In the case of reactive amine radical cations spectroelectrochemical observation is extremely difficult. In these cases, reactivity patterns of the radical cations could be deduced from the structure of isolated products. For example, triphenylamine (**TPA**) derivatives upon anodic oxidation give benzidine derivatives and a mechanism involving dimerization of **TPA**$^{\bullet+}$ is generally proposed. In order to follow the course of these dimerization reactions a 'pulse-electrolysis stopped flow' method was developed by Okazaki and coworkers.[2] In this method, the amine solution is pulse electrolysed using a carbon wool working electrode within a few milliseconds and this solution is quickly delivered to an optical cell by a piston drive. In the optical cell spectroscopic measurements could be carried out after stopping the solution.

Since the solution has to be transferred from the electrolysis compartment to an optical cell, very short-lived radical cations could not be studied using this technique.

Oyama and coworkers have recently introduced a ‘Electron transfer stopped flow’ (ETSF) technique to study the reactivity patterns of reactive aromatic amine radical cations.[3] In the ETSF method, unstable radical cations ($R_3\mathbf{N}^{\bullet+}$**)** are generated by charge shift reaction with stable radical cations. Oyama *et al.* have selected tris(4-bromophenyl)amine, $\mathbf{1}^{\bullet+}$ as the stable radical cation in the ETSF method. If the oxidation potential of the $\mathbf{1/1}^{\bullet+}$ couple is positive to that of $\mathbf{R_3N/R_3N}^{\bullet+}$ couple, the charge shift reaction in Scheme 3.1 will be exergonic and hence spontaneous.

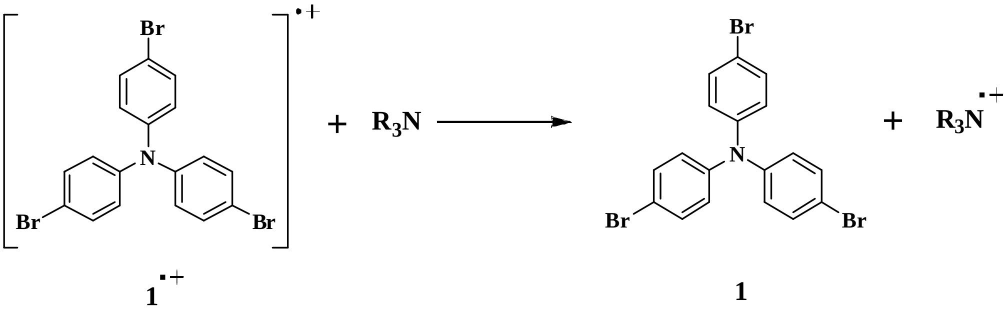

Scheme 3.1

Solutions of $\mathbf{1}^{\bullet+}$ can be obtained by batch electrolysis of **1** in acetonitrile (ACN). $\mathbf{1}^{\bullet+}$ exhibited absorption maximum at 705 nm ($\varepsilon = 32{,}000\ M^{-1}\ cm^{-1}$). In the ETSF technique, $\mathbf{1}^{\bullet+}$ solution of known concentration is prepared. This is then mixed with a solution of $\mathbf{R_3N}$ of appropriate concentration in a stopped flow reactor and absorption spectral changes are monitored during millisecond-to-second time scale. Oyama and co-workers have generated several amine radical cations and studied their dimerization rates using this technique. Most of the aromatic amine radical cations, Oyama *et al.* generated, also exhibited absorption maxima in the 650-750 nm region. Although they claimed that the charge exchange reaction (Scheme 3.1) is complete in the mixing chamber, this claim could not be verified because of the overlapping absorptions of $\mathbf{1}^{\bullet+}$ and $\mathbf{R_3N}^{\bullet+}$.

Since aromatic amines are good electron donors their incorporation into appropriately activated zeolites readily leads to radical cation formation.[4] However, to date only a limited number of amines and diamines have been investigated under these conditions. For example, primary, secondary and tertiary aromatic amines as well as hydrazine and benzidine derivatives undergo one-electron oxidation in zeolites leading to formation of radical cations. Some of these species underwent deprotonation, either spontaneously or after warming the samples, generating free radicals. Although spectroscopic information about products could be obtained using diffuse reflectance spectroscopy, following the courses of these reactions and isolation of products were difficult.

In this thesis we report the oxidation of several aromatic amines with Cu^{2+} in ACN to form radical cations. The radical cations formed underwent dimerization reactions to give benzidine derivatives. In all cases, the dimerization reactions could be followed by absorption spectroscopy and reasonable mechanisms could be proposed. We observed that benzidine formation proceeded with very good yields. Our method compares very well with the methods currently available for the synthesis of benzidine derivatives. In Chapter 1 of this thesis we have reviewed all the methods currently available for benzidine synthesis through the amine radical cation route.[5-7] These methods were not extended for the synthesis of *N,N,N',N'*-tetraphenylbenzidines (**4**), which are most commonly prepared by the Ullmann condensation reaction between diphenylamine (**2**) and an unactivated aryl halide (**3**) in the presence of a copper catalyst (metal, alloy or salt) as shown in Scheme 3.2.[8]

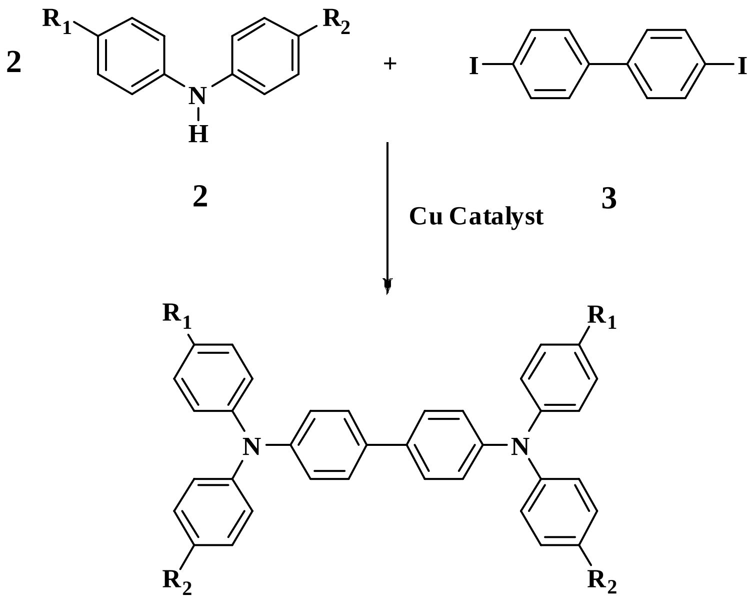

4

Scheme 3.2

High temperatures and extended reaction times are often required and the yields are generally unpredictable because of side reactions such as dehalogenation and homo coupling. Several attempts were made to moderate the Ullmann reaction conditions. For example, Goodbrand *et al.*[8a] and Lu *et al.*[8b] employed a 1,10-phenanthroline ligand along with cuprous chloride and KOH in aromatic hydrocarbon solvents (toluene or xylene) at refluxing temperatures to obtain good yields of tetraphenylbenzidine (**TPB)** derivatives. Ligands such as 1,4-diazabuta-1,3-diene,[8c] 18-crown-6[8d,e] or tri-*tert*-butylphosphine[8f] along with Cu salts and a base (K_2CO_3 or *t*-BuOK) were employed by others. All these modifications could not eliminate the requirements of high reaction temperatures (125 – 150 ^{0}C) and long reaction periods (3 – 45 h). Palladium catalyzed aromatic amination reactions developed by Buchwald and Hartwig appear promising, but these have not been applied for the synthesis of **TPB** derivatives.[9] Thus, new synthetic methodologies, which involve mild reaction conditions and cheap chemicals, are very desirable. In this context the Cu^{2+} mediated dimerization of triarylamine radical cations that we report in this chapter (vide infra) for the synthesis of **TPB** derivatives, appear very promising.

3.3. Results and Discussion

In this chapter we report the reaction of a few aromatic amines with Cu^{2+} in acetonitrile. The amines we have studied are listed in Chart 3.1.

All these aromatic amines give radical cations upon reaction with Cu^{2+}. In the absence of any nucleophiles the radical cations undergo dimerization reactions to give benzidine derivatives. These reactions could be followed by UV-Vis spectroscopy. When nucleophiles are present, the radical cations underwent nucleophilic substitution reactions. Details of our studies are presented below.

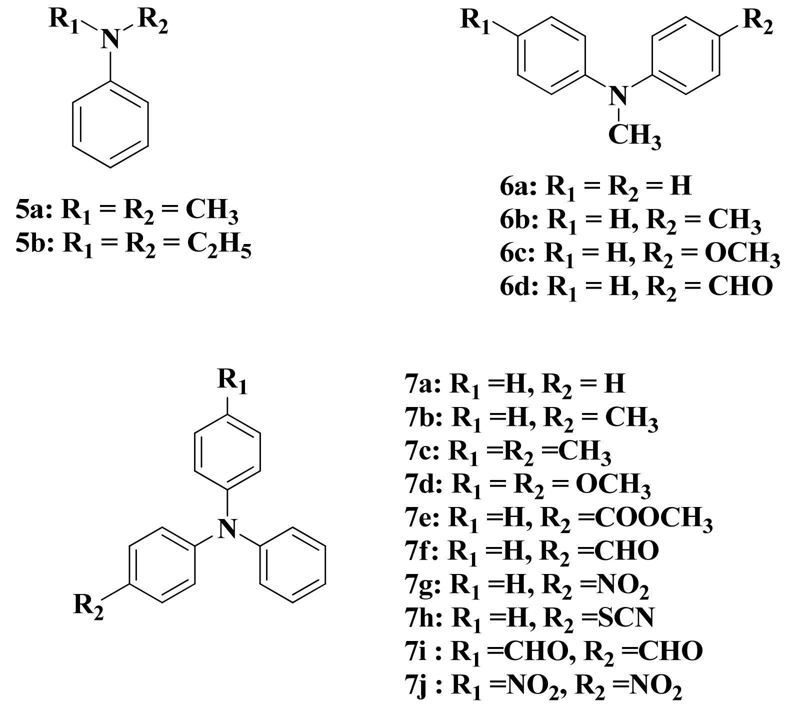

5a: $R_1 = R_2 = CH_3$
5b: $R_1 = R_2 = C_2H_5$

6a: $R_1 = R_2 = H$
6b: $R_1 = H, R_2 = CH_3$
6c: $R_1 = H, R_2 = OCH_3$
6d: $R_1 = H, R_2 = CHO$

7a: $R_1 = H, R_2 = H$
7b: $R_1 = H, R_2 = CH_3$
7c: $R_1 = R_2 = CH_3$
7d: $R_1 = R_2 = OCH_3$
7e: $R_1 = H, R_2 = COOCH_3$
7f: $R_1 = H, R_2 = CHO$
7g: $R_1 = H, R_2 = NO_2$
7h: $R_1 = H, R_2 = SCN$
7i : $R_1 = CHO, R_2 = CHO$
7j : $R_1 = NO_2, R_2 = NO_2$

Chart 3.1

3.3.1. Dimerization Reactions

3.3.1.1. Reactions of Dialkylanilines with Cu^{2+} in Acetonitrile

Aniline and alkylanilines reacted with Cu^{2+} in ACN to give mixtures of products. These reactions were not synthetically useful and hence not included in this work. Reactions of dialkylanilines (**5a,b**) with Cu^{2+} in ACN gave dimerization products in good yields. Spectroscopic investigations of these reactions are presented in this section. Figure 3.1A shows the absorption spectrum of *N,N*-dimethylaniline (**5a**), which is characterized by the strong π-π* absorption at 260 nm and a weak n-π* absorption at 300 nm. When one equivalent of $Cu(ClO_4)_2$ in acetonitrile was added, the absorption band due to **5a** disappeared and a new band at 470 nm appeared as shown in Figure 3.1B.

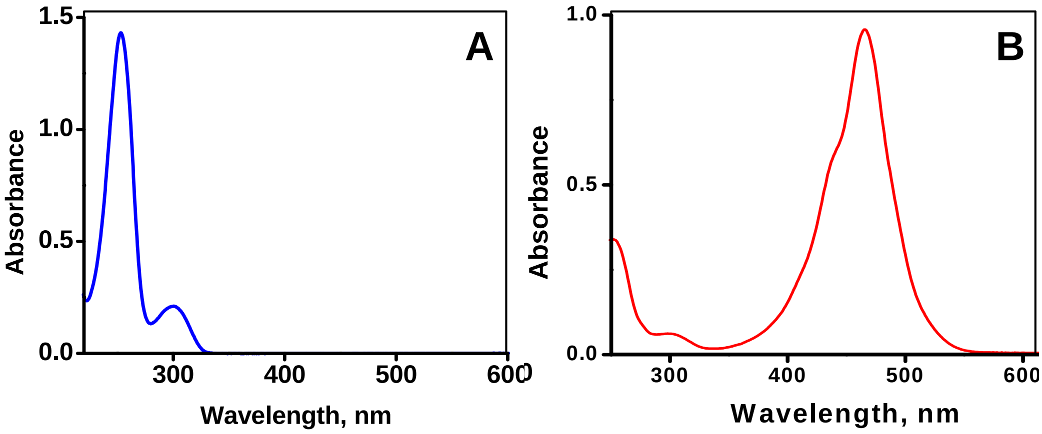

Figure 3.1. Absorption spectrum of a solution of **5a** (5×10^{-5} M) in ACN before (A) and after (B) adding one equivalent of $Cu(ClO_4)_2.6H_2O$

On the basis of literature reports[10] and our own product isolation studies (vide infra) the 470 nm absorption was unambiguously assigned to the *N,N'*-dimethylaniline radical cation (**5a**$^{\bullet+}$). We observed that the absorption at 470 nm is not very stable and gradually decreases in intensity. The absorption spectra were recorded at different time intervals and the results are presented in Figure 3.2. It can be seen from the figure that the radical cation absorption changes into structured absorption bands around 470 and 1000 nm, with a clear isosbestic point at 600 nm, as shown in Figure 3.2.

The new species formed is very stable. The absorption spectrum was monitored for a week and no changes were observed. A literature search has suggested that the 470 and 1000 nm absorptions could be due to tetramethylbenzidine radical cation (**8a**$^{\bullet+}$, Scheme 3.3).[11]

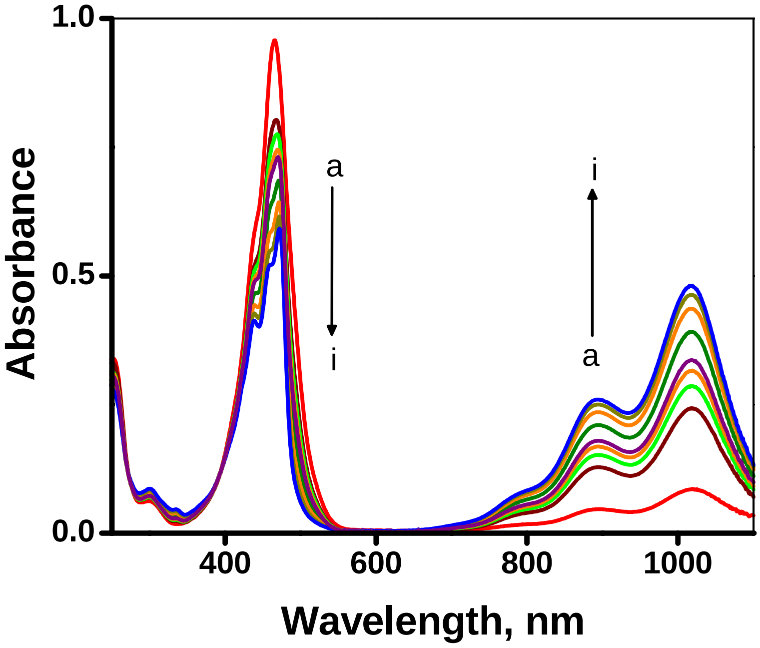

Figure 3.2. Time-dependent changes observed in the absorption spectrum of **5a**/Cu(ClO_4)$_2$ mixture. Spectra a-d were recorded at 1 minute intervals, and e-i were recorded at 5 minutes intervals. Concentrations of **5a** and Cu(ClO_4)$_2$ were as in Figure 3.1.

In order to confirm this assignment, we generated **8a**$^{\bullet+}$ by reacting **8a** with Cu^{2+} in ACN (Scheme 3.3). The absorption spectra of the final products obtained were identical in both cases. In the absorption spectrum of **8a**$^{\bullet+}$ (Figure 3.2i), the 470 nm band can be assigned to the $D_0 \rightarrow D_1$ transition. The long wavelength absorption band in the 700 -1200 nm region can be attributed to the intervalence charge transfer. **8a**$^{\bullet+}$ consists of a neutral **5a** unit and a **5a**$^{\bullet+}$ unit. The intervalence charge transfer band arises as a result of photo-excited electron transfer from the neutral moiety **5a** to the **5a**$^{\bullet+}$.[12]

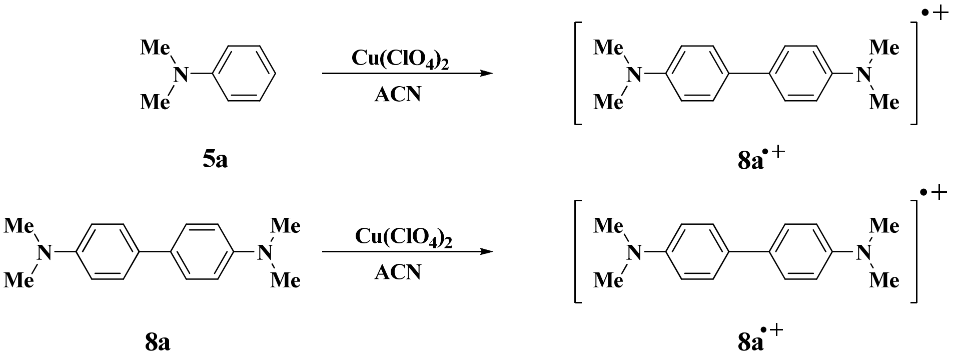

Scheme 3.3

We observed that the absorption due to **8a**$^{•+}$ disappears upon addition of a base such as triethylamine (TEA) or potassium carbonate. The effect of adding TEA is shown in Figure 3.3. When increasing amounts of TEA were added the absorption bands due to the **8a**$^{•+}$ decreased with concomitant formation of a new absorption around 300 nm, which could be assigned to the product of the reaction.

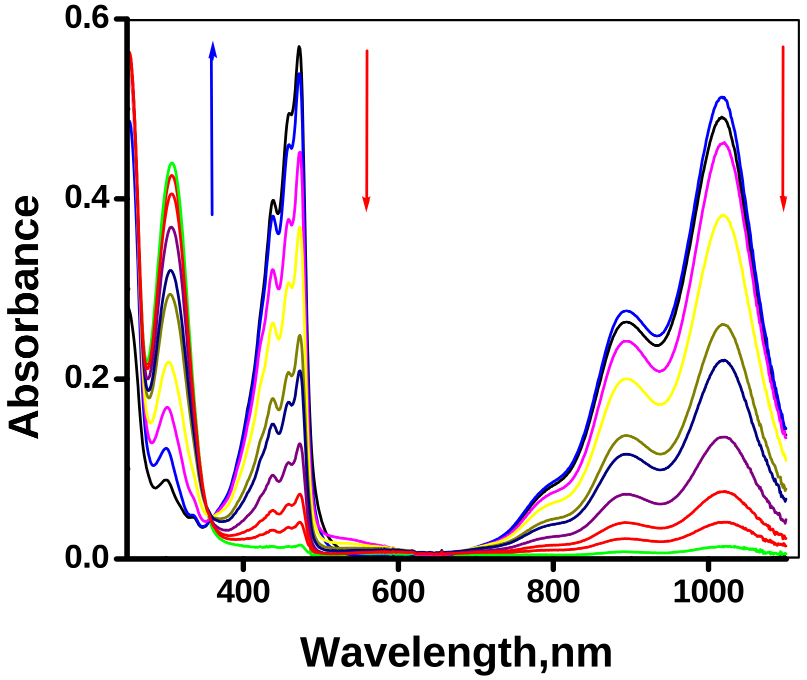

Figure 3.3. Effect of addition of increasing amounts of TEA to solution in spectrum 3.2(i) above.

In order to fully understand the reaction we have scaled up the reaction as described in the experimental section, wherein we used solid K_2CO_3 to neutralize the radical cation. The reaction mixture was filtered through a short pad of alumina and concentrated to give a solid, which was recrystallized from petroleum ether. The product was analyzed by Gas Chromatography Mass Spectrometer (GC-MS). The chromatogram exhibited single peak at retention time (RT) 22.102 corresponding to M^+ peak 240 a.m.u.

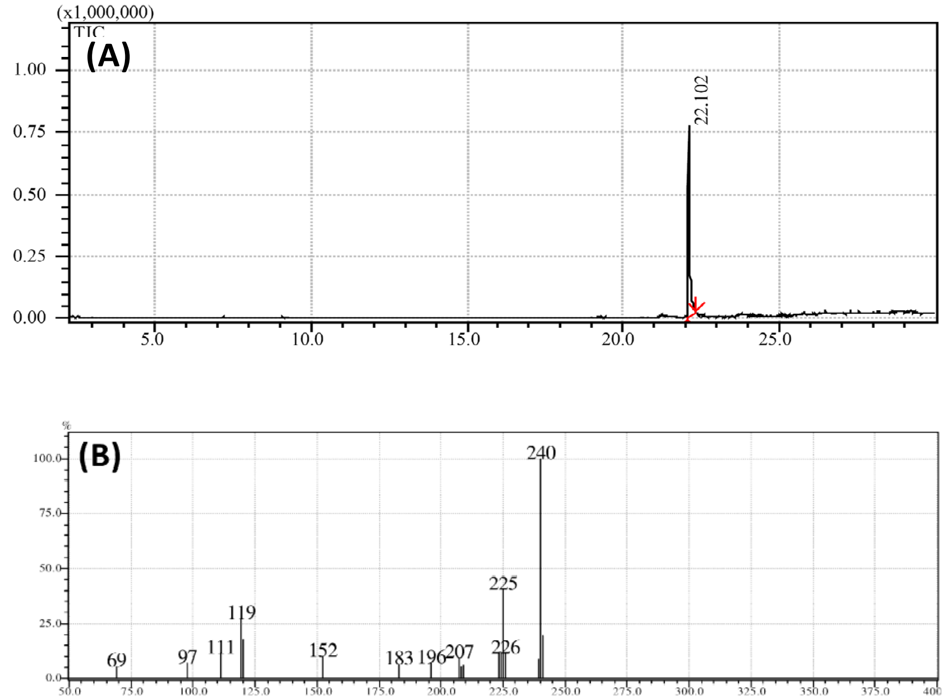

Figure 3.4. (A) Gas chromatogram and, (B) fragmentation pattern of product obtained in **5a**/Cu^{2+} reaction.

The product exhibited ^1H NMR (300 MHz, $CDCl_3$) chemical shifts at δ 7.4 (d, 4 H), 6.7(d, 4 H), and 2.9 (s, 12 H). Based on the above data the product was identified as *N,N,N',N'-tetramethyl-p-benzidine* (**8a**). The ^1H NMR and IR spectra of the product were identical to those of **8a** prepared by previously known methods.[5-7]

We also investigated the reaction of *N*,*N*-diethylaniline (**5b**) with Cu^{2+} in ACN and obtained identical results. **5b**$^{\bullet +}$ (λ_{max} = 470 nm) is formed immediately upon addition of Cu^{2+} to a solution of **5b** in ACN, which underwent time dependent changes as shown in Figure 3.5. These changes are nearly identical to that exhibited by **5a**. We have scaled up the reaction and isolated *N*,*N*,*N'*,*N'*-tetraethylbenzidine (**8b**) as the only product.

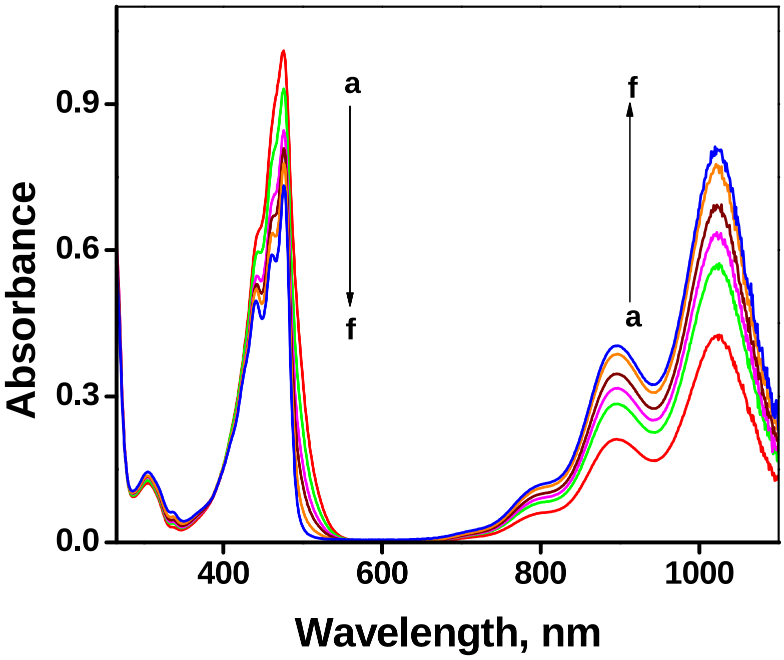

Figure 3.5. Time-dependent changes observed in the absorption spectrum of a **5b**/$Cu(ClO_4)_2$ mixture. Spectra a-c were recorded at 1 minutes intervals, and d-f were recorded at 5 minutes intervals.

Based on data in Figures 3.1-3.5 we propose that reaction of **5a,b** with Cu^{2+} in ACN leads to the sequence of reaction shown in Scheme 3.4.

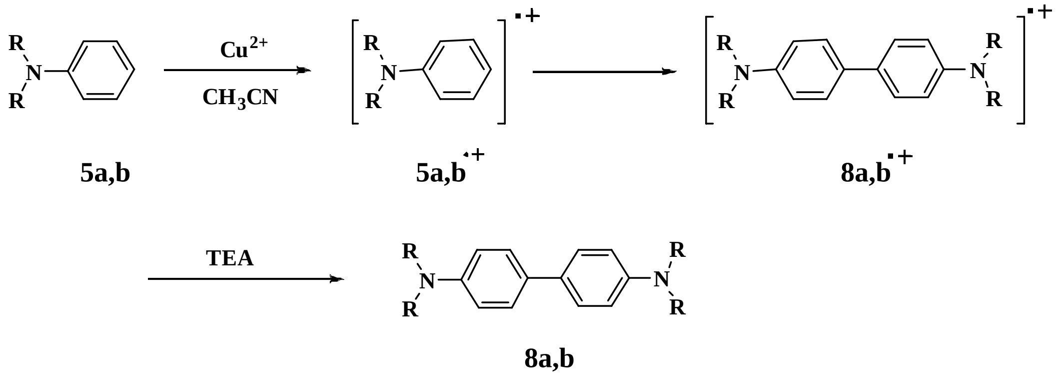

Scheme 3.4

Figure 3.2 suggests that transformation of **5a**$^{\bullet+}$ to **8a**$^{\bullet+}$ does not involve any stable observable intermediates. This transformation, however, has to involve dimerization, deprotonation, and electron donation as shown in Scheme 3.5.

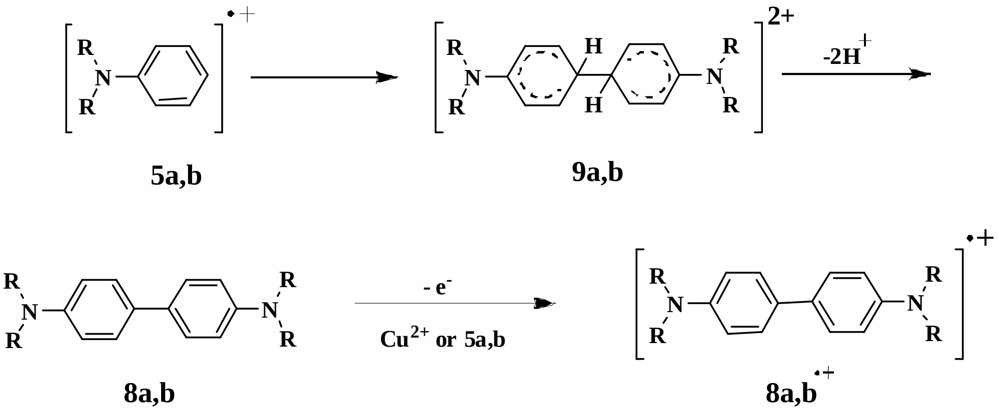

Scheme 3.5

Presence of clear isosbestic points, in Figures 3.2 and 3.5 suggests that the dimerization to form the dihydrotetraalkylbenzidine dications (**9a,b**) is the slowest step in Scheme 3.5. Since dications are highly acidic compared to neutral **5a/b**, the second step in Scheme 3.5 is expected to be very fast. The **8a/b** thus formed are better electron donors (E_{ox} = 0.32 V vs SCE) compared to **8a/b**

(E_{ox} = 0.81 V vs SCE).[13] Hence a very fast electron exchange reaction takes place between **5a**$^{\bullet+}$/**b**$^{\bullet+}$ and **8a/b**, leading to the formation of **8a**$^{\bullet+}$/**b**$^{\bullet+}$. If Cu^{2+} is present in excess, electron transfer from **8a/b** to Cu^{2+} can also occur, leading to the formation of **8a**$^{\bullet+}$/**b**$^{\bullet+}$.

Anodic oxidation of **5a** to **8a** was studied previously in aqueous and non-aqueous solutions.[14,15] In these studies, attempts were made to detect **5a**$^{\bullet+}$ using fast cyclic voltammetry and optical spectrophotometry. These attempts were not successful, and it was concluded that **5a**$^{\bullet+}$ is very unstable and undergoes dimerization by a mechanism similar to that shown in Scheme 3.5. Under our experimental conditions the radical cations **5a**$^{\bullet+}$/**b**$^{\bullet+}$ were reasonably stable and could be characterized by UV-Vis spectroscopy.

According to Scheme 3.5, the product benzidines inhibits the reaction by reducing part of Cu^{2+} to Cu^{+} or converting part of **5a**$^{\bullet+}$/**b**$^{\bullet+}$ back to **5a/b**. This means that more than one equivalent of Cu^{2+} is required to drive the reaction to completion. In order to identify the optimum amount of Cu^{2+}, we have carried out the dimerization of **5a** at different concentrations of Cu^{2+} and it was found that the product yield reached a maximum at 1.5 equivalents of Cu^{2+}.

In an attempt to see if the reactions could be scaled up to preparatively useful quantities, reactions of **5a/b** with Cu^{2+} were carried out using 10 millimolar **5a/b**. Yield of benzidine was 83% for **5a** and 86% for **5b**. These reactions are carried out under very mild conditions and hence superior to other methods available in the literature.[16]

As a continuation of this work we have studied reaction of several diarylamines and triarylamines (Chart 3.1) with Cu^{2+} in ACN and the results are discussing in the coming section.

3.3.1.2. Reactions of Diarylamines 6a-d with Cu^{2+} in Acetonitrile

We have selected a few diarylamines (**6a-d**, Chart 3.1), and studied their reactions with Cu^{2+} in ACN. The absorption spectrum of *N*-methyl-*N*,*N*-diphenylamine (**6a**) is shown in Figure 3.6A. The absorption maximum for the lowest energy band in **6a** is 291 nm in ACN. Figure 3.6B shows the effect of adding 1.5 equivalents of Cu^{2+} to a solution of **6a** in ACN. Disappearance of the absorption due to **6a** at 291 nm and formation of a new species at 512 nm can be seen in Figure 3.6B. Based on the observations made by us for several aromatic amine/Cu^{2+} systems, we assigned the new absorption to *N*-methyl-*N*,*N*-diphenylamine radical cation (**6a**$^{\bullet+}$).

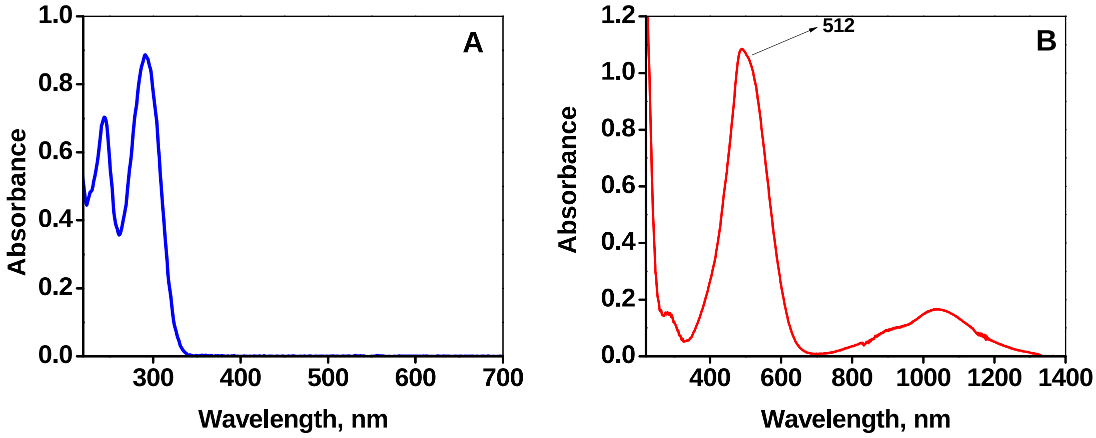

Figure 3.6. (A) Absorption spectrum of **6a** (1×10^{-4} M) in ACN. (B) Absorption spectrum obtained after the addition of 1.5 equivalents of Cu^{2+}.

We observed that the **6a**$^{\bullet+}$ formed undergoes further reactions. We have followed this reaction using absorption spectroscopy and the results are shown in Figure 3.7. The peak at 512 nm gradually shifts to a new band at 475 nm (Figure 3.7(a-i)). This is associated with the formation of a new band in the 700-1400 nm region (Figure 3.7). Isosbestic points are also seen at 420 and 680 nm, indicating the presence of two absorbing species in solution.

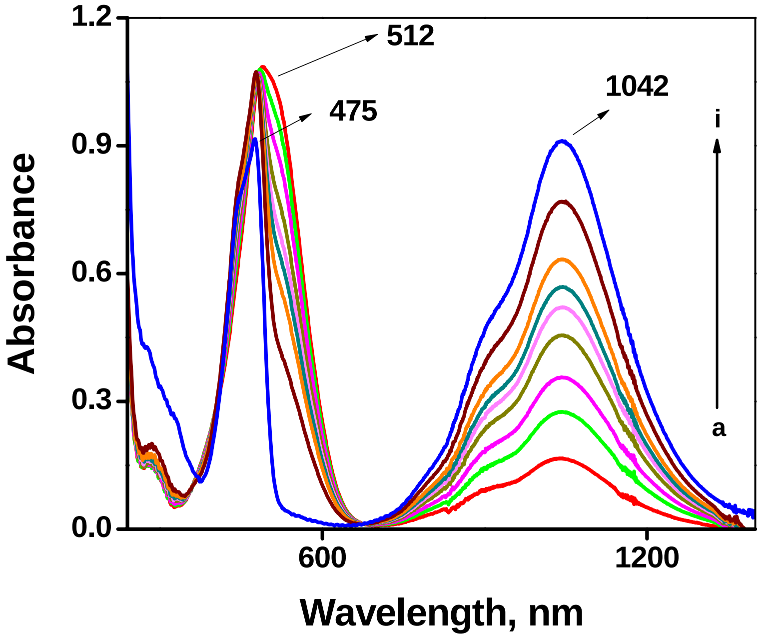

Figure 3.7. Time-dependent changes observed in the absorption spectrum of **6a**/Cu^{2+} in ACN. Spectra a-d were recorded at 1 minute time intervals, and e-g were recorded at 5 minutes time intervals and g-h were recorded at 30 minutes time intervals. The spectrum 'i' was recorded after 15 h.

The species absorbing at 512 nm was found to be stable for several hours, but can be decomposed upon addition of a base such as triethylamine (TEA) or potassium carbonate. Figure 3.8 shows the effect of addition of increasing amount of TEA. Intensity of the peak at 475 and 1042 nm decreased with concomitant formation of a new peak at 325 nm (spectrum 3.8(i-n) in Figure 3.8).

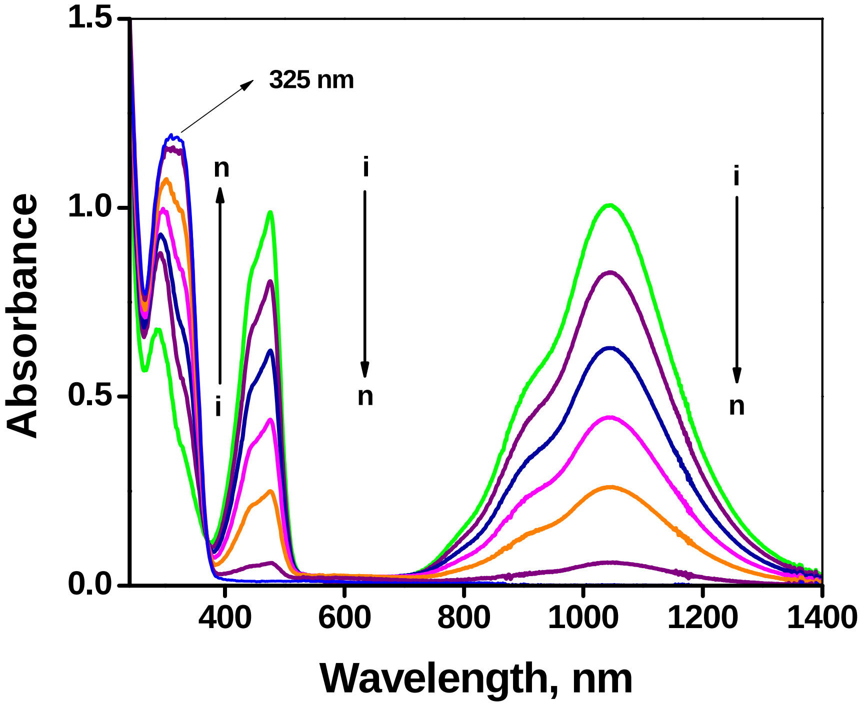

Figure 3.8. Effect of addition of increasing amounts of TEA to the spectrum 3.7(i).

In order to identify the product which absorbs at 325 nm, the reaction was scaled up (see experimental section) and product was isolated. From the NMR and mass data we identified the product as *N*,*N'*-dimethyl-*N*,*N'*-diphenylbenzidine (**10a**). The results obtained here are very similar to those observed for **5a/b** and hence we propose the mechanism in Scheme 3.6 for the formation of **10a**. Based on this mechanism the absorption at 1042 nm in Figure

3.7 was assigned to intervalence charge transfer in **10a**$^{\bullet+}$. We further confirmed this assignment by generating **10a**$^{\bullet+}$ from **10a** using Cu^{2+} in ACN.

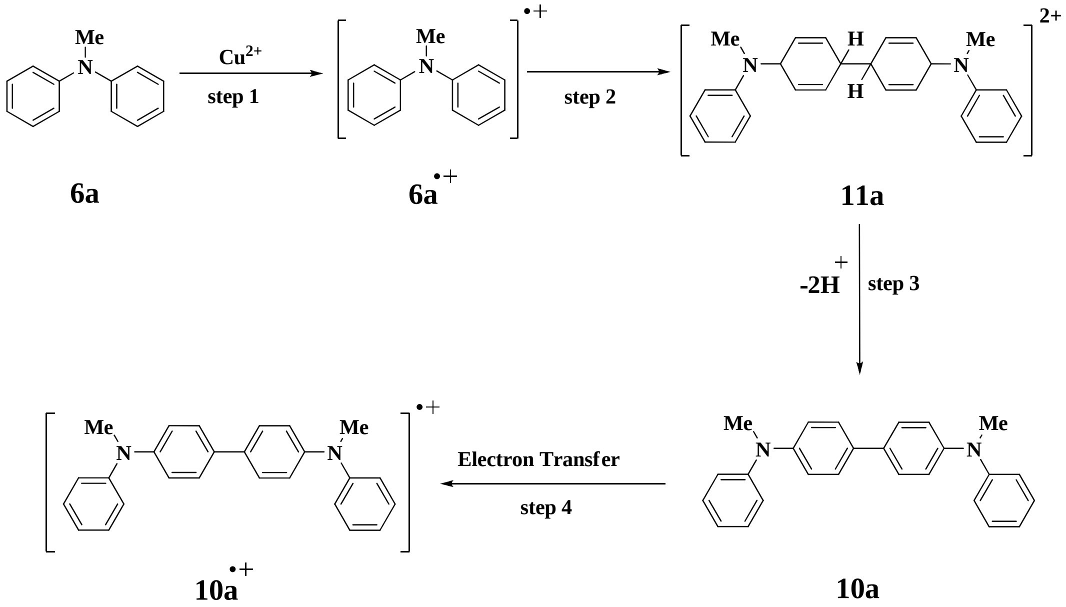

Scheme 3.6

In order to establish the general nature of the reaction, we have treated diphenylamine derivatives **6b-d** also with Cu^{2+} in ACN. Observations similar to those in Figures 3.7 and 3.8 were made in all cases. The reactions were scaled up and product benzidines were isolated and identified using standard spectroscopic techniques. Structures of products and isolated yields are shown in Table 3.1.

Table 3.1. Starting amine, products, and yields of Cu^{2+} - initiated reaction.

Entry	Amine	Product	Yield*(%)
1	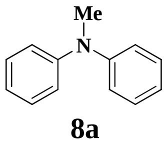 **8a**	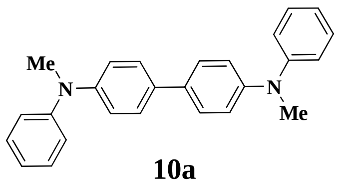 **10a**	68
2	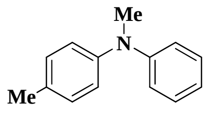 **8b**	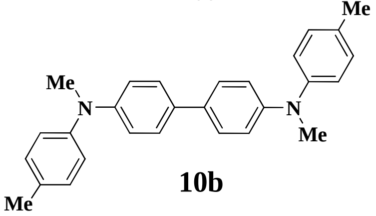 **10b**	82
3	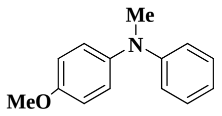 **8c**	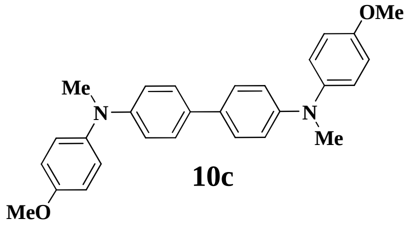 **10c**	76
4	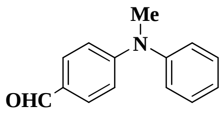 **8d**	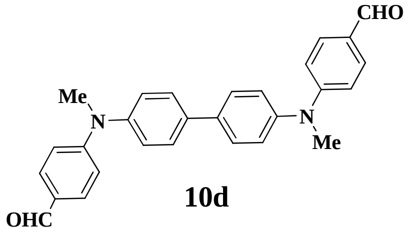 **10d**	66

*** Yield based on recovered starting material**

3.3.1.3. Reaction of Triarylamines (7a-h) with Cu^{2+} in Acetonitrile

Absorption spectrum of **7a** is shown in Figure 3.9A. Upon addition of 1.5 equivalents of $Cu(ClO_4)_2$, an intense absorption band in the 600-800 nm region is formed and as a result the solution turned blue. Absorption spectrum of **7a**/Cu^{2+} system in acetonitrile immediately after mixing is shown in Figure 3.9B. Based on the observations we made for several aromatic amine/Cu^{2+} systems, the band at 600-800 nm region was assigned to $\mathbf{7a}^{\bullet+}$.[1,16]

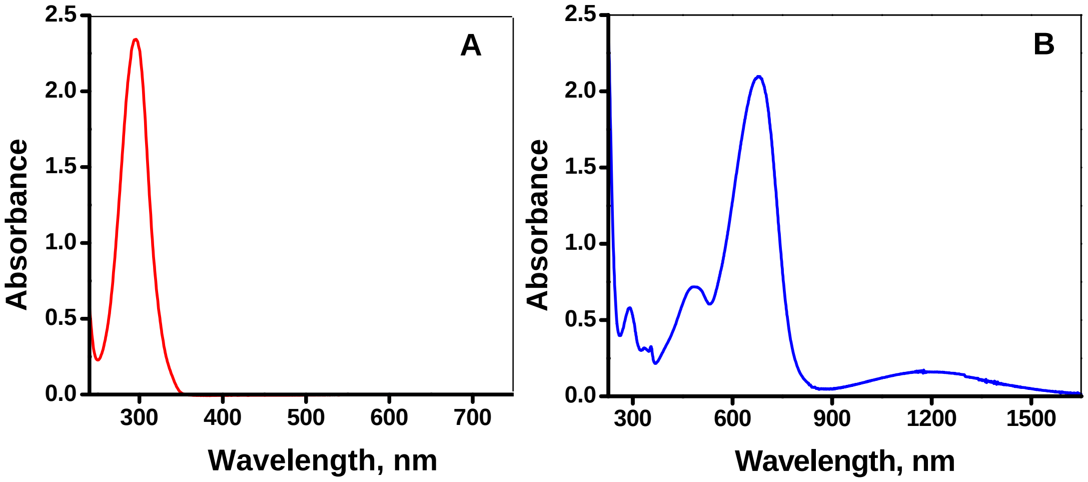

Figure 3.9. (A) Absorption spectrum of **7a** (1×10^{-4} M) in acetonitrile. (B) Absorption spectrum obtained after the addition of 1.5 equivalents of Cu^{2+}.

Lewis and Lipkin had generated **7a**$^{\bullet+}$ by photoionization of **7a** in rigid matrix at low temperature.[17a] **7a**$^{\bullet+}$ thus generated exhibited absorption maximum at 660 nm. Hasegawa had shown that **7a**$^{\bullet+}$ generated by the chemical oxidation of **7a** with acid zeolites absorbed at 678 nm.[17b] Hall obtained **7a**$^{\bullet+}$ by reacting **7a** with silica-alumina catalyst and reported its absorption maximum as 660 nm.[17c] Dollish and Hall generated **7a**$^{\bullet+}$ by reacting **7a** with iodine and showed that this species absorbed around 660 nm.[17d] In the present case the absorption maximum obtained was 680 nm, which is very close to the values reported earlier by others.

The absorption due to **7a**$^{\bullet+}$ was monitored as a function of time and the results are presented in Figure 3.10(a-n). The absorption due to **7a**$^{\bullet+}$ decreased with time along with concomitant increase in the absorptions in the 400-580 nm and 900-1600 nm regions. Presence of the isosbestic points in Figure 3.10 suggest that the species responsible for the new absorptions originate from **7a**$^{\bullet+}$. This is also clear from the decay at 680 nm and the matching growth at 1270 nm (Figure 3.11).

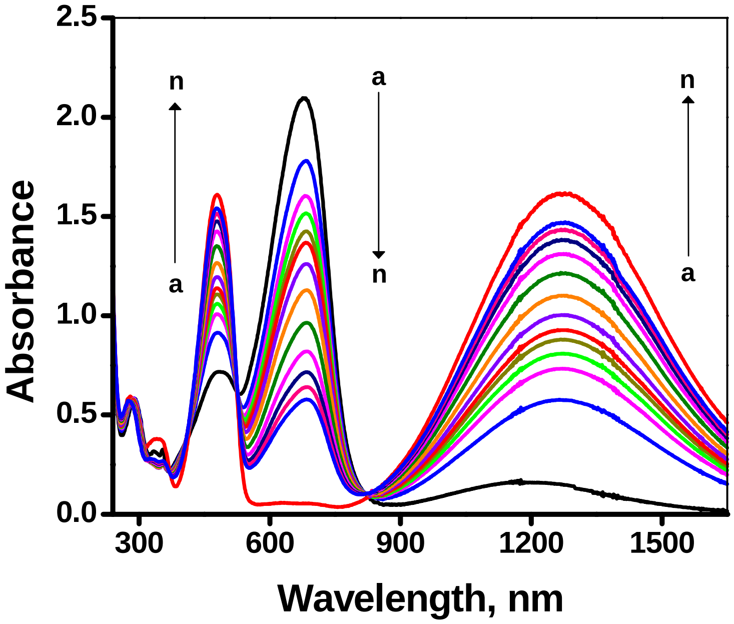

Figure 3.10. Time-dependent changes in the absorption spectrum of a solution containing **7a** (1 x 10^{-4} M) and $Cu(ClO_4)_2$ (1.5 x 10^{-4} M) in ACN. Spectrum "n" was taken after 24 h.

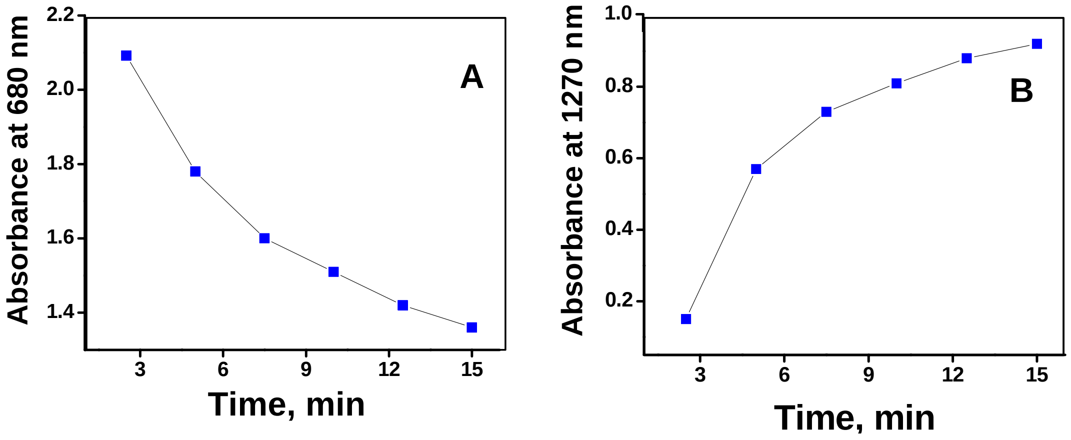

Figure 3.11. Time dependences of absorptions at (A) 680 and (B) 1270 nm of a solution containing **7a** (1 x 10^{-4} M) and $Cu(ClO_4)_2$ (1.5 x 10^{-4} M) in ACN.

The final spectrum (Figure 3.10n) was very stable (more than 24 h) and is assigned to *N*,*N*,*N'*,*N'*-tetraphenylbenzidine radical cation (**4a$^{\bullet+}$**) based on literature reports and our previous results.[1,15-18]For example, Seo *et al.* observed that electrolysis of **7a** or **4a** at +1.15 V gave the same species having absorption at 480 nm, and this was identified as **4a$^{\bullet+}$**.[15] Dollish and Hall generated **7a$^{\bullet+}$** by oxidizing **7a** with silica-alumina catalyst and observed that the initial absorption band at 660 nm assignable to **7a$^{\bullet+}$** decreased with time leading to the formation a new band at 480 nm.[17d] This band was assigned to **4a$^{\bullet+}$**, arising from a π -π* transition. The long wavelength band in the 1000-1600 nm region for **4a$^{\bullet+}$**, is due to the intervalence charge transfer excitation.[12] We observed that **4a$^{\bullet+}$** could also be generated by the reaction of **4a** with Cu^{2+} and the spectrum obtained in this reaction was identical to Figure 3.10(n). The absorptions due to **4a$^{\bullet+}$** at 400-580 nm and at 900 - 1600 nm were very stable for several hours. Upon addition of excess TEA these bands disappeared leading to the formation of a new absorption below 400 nm (Figure 3.12). Based on a comparison with authentic sample, the product was identified as **4a**.

The isosbestic points in Figure 3.10 suggest that **7a$^{\bullet+}$** is converted smoothly into **4a$^{\bullet+}$**, and there are no observable intermediates in this transformation. As in the case of **5a,b**/Cu^{2+} and **6a**/Cu^{2+} systems, the **4a** also was formed as a result of dimerization of **7a$^{\bullet+}$**, followed by deprotonation (Scheme 3.7).

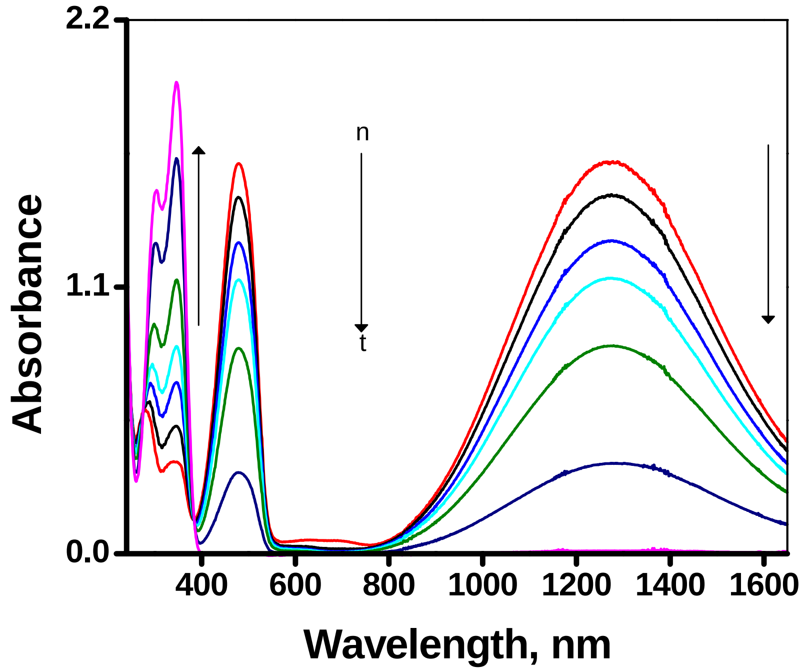

Figure 3.12. Effect of addition of increasing amounts of TEA to solution of spectrum 'n' in Figure 3.10.

Since oxidation potential of **4a** (0.68 V vs SCE) is much lower than that of **7a** (0.92 V vs SCE), very fast electron exchange between **7a**$^{\bullet+}$ and **4a** takes place and leads to **4a**$^{\bullet+}$. Because of these very fast deprotonation and electron exchange **12** and **4a** are not observable in spectroscopic analysis.

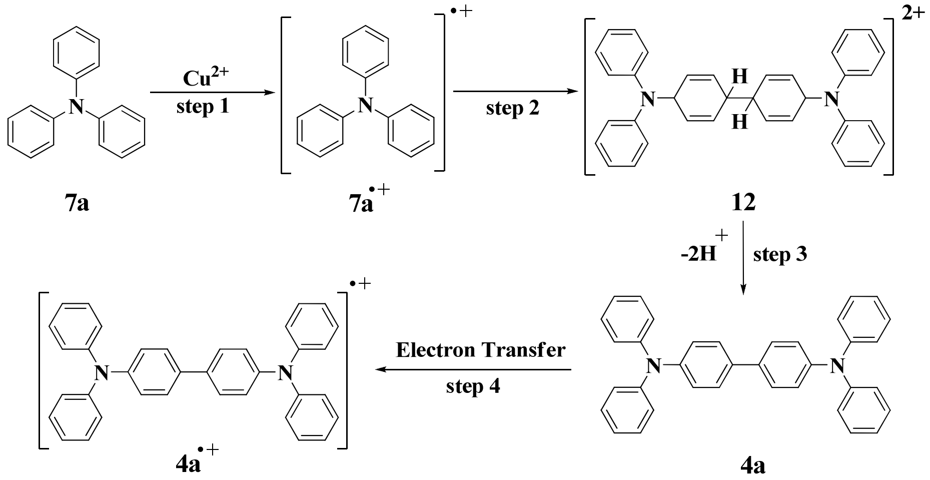

Scheme 3.7

Dimerization of electrochemically generated **7a**$^{\bullet+}$ was studied in detail and a mechanism for the dimerization was proposed previously.[15,19] Using cyclic voltammetry and spectroelectrochemical measurements (ESR, UV-Vis-NIR), Dunsch and co-workers have clearly established the reaction pathways of several closely related, electrochemically generated triarylamine radical cations.[20a,b] Electrochemical behaviors of several amino substituted **TPA** derivatives were recently studied by Chiu *et al.*[20c] The mechanism we proposed in Scheme 3.7 is in line with those proposed in the electrochemical work.

In order to explore synthetic utility of this reaction we have treated triphenylamine derivatives **7a-h** with Cu^{2+} in ACN and isolated the benzidine products in each case (Table 3.2, see experimental section for details). It can be seen from Table 3.2 that the reaction gives good yields even when sensitive groups such as -CHO, -$COOCH_3$, or -SCN are present in the substrate. Tetraphenylbenzidine derivatives of the type shown in Table 3.2 are generally prepared by Ullmann reaction, which generally fails with sensitive substrates. The method presented here is obviously better than the above approaches.[29] It may, however, be noted that electron-withdrawing substituents such as -CHO and -NO_2 exert a negative effect on this reaction. When the triphenylamine contains one -CHO or -NO_2 group the reactions did not go to completion. Nearly 30% of the starting materials were recovered. The yields reported in Table 3.2 are based on the amount of starting materials reacted. When two -CHO or -NO_2

groups were present, benzidine formation did not take place, and most of the starting materials were recovered unchanged

Table 3.2. Starting amines, products and yields of Cu^{2+}- initiated reactions.

Entry	Amine	Product	Yield*(%)
1	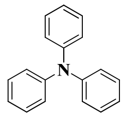 7a	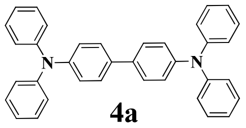 4a	81
2	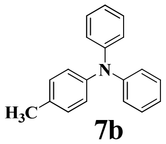 7b	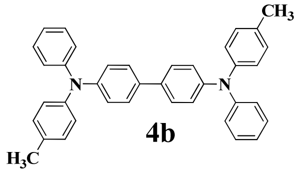 4b	86
3	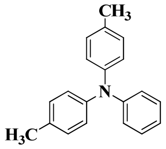 7c	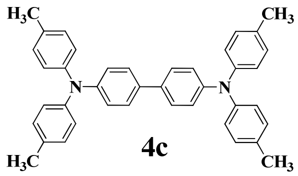 4c	94
4	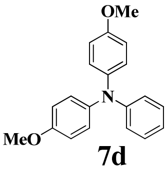 7d	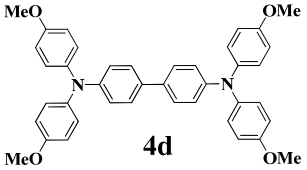 4d	87
5	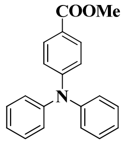 7e	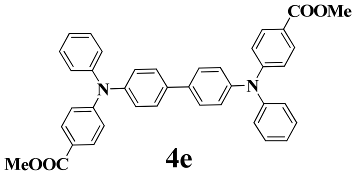 4e	83
6	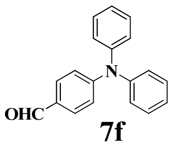 7f	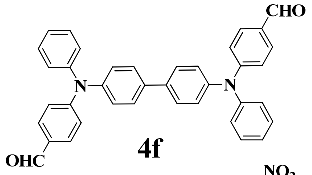 4f	85
7	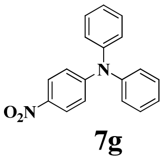 7g	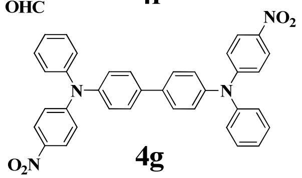 4g	81
8	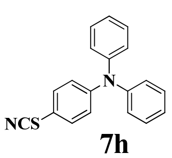 7h	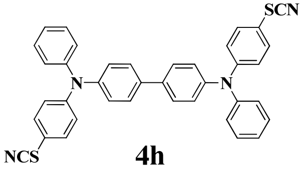 4h	82

*** Yield based on recovered starting material**

3.3.2. Nucleophilic Substitution Reactions

Aromatic amines and many of their derivatives in combination with other functional molecules find application in organic light emitting devices, field effect transistors and photovoltaic devices.[21] Thus there is a general need to develop new methodologies for easy functionalization of aryl amines. Reactions involving electrophilic substitution find widespread applications in introducing various functional groups in aromatic amines. Reagents for electrophilic halogenation are available in various forms. For example, bromo substituted aromatic amines have occasionally been prepared by direct substitution with molecular bromine in an appropriate solvent such as acetic acid or carbon tetrachloride.[22] Liquid bromine, however, is corrosive and its transportation and handling are difficult. Reagents such as *N*-bromosuccinimide,[23] and alkylammonium tribromide[24] are promising and are widely using for electrophilic bromination in aromatic amines. Similarly *N*-chlorosuccinimide[25] *tert*-butyl hypochlorite,[26] benzyltrimethylammonium tetrachloroiodate[27] etc have been used for electrophilic chlorination. Even though product distribution is generally predictable in these methods, special efforts and care are required for the generation of these reagents. In this context, development of new methodologies which utilize mild conditions and easily available reagents are very desirable.

We reasoned that if amine radical cations are generated in the presence of nucleophiles, these ions might be able to react with the radical cations before they undergo dimerization reactions and this could be used as a simple alternative to usual electrophilic substitution reactions. In order to verify this possibility we have generated radical cations of few aromatic amines in the presence of nucleophiles, such as Br^{Θ}, Cl^{Θ}, and SCN^{Θ} and analyzed the reaction products using different analytical techniques. In all cases we could observe formation of substitution products in good yields. Details of these studies are presented below.

3.3.2.1. Reaction of *N*,*N*-Dialkylaniline (5a,b) with Cu^{2+} in Presence of Nucleophiles in Acetonitrile

Reaction of *N*,*N*-dialkylanilines (**5a,b**) with nucleophiles such as Br^{Θ}, Cl^{Θ}, and SCN^{Θ} in the presence of Cu^{2+} were studied and products were isolated and characterized using GC-MS and NMR analysis. Tetrabutylammonium bromide (TBAB) was used as Br^{Θ} source (see experimental section for reaction procedure) and after work up the reaction mixture was analyzed using GC-MS. The gas chromatogram of the crude extract is shown in Figure 3.13. Only one peak was seen in the chromatogram at RT 8.031 and this is was assigned to 4-bromo-*N*,*N*-dimethylaniline (**15b**).

The solvent was removed and the residue was taken in petroleum ether. This was filtered through a small alumina column and crystallized from the same solvent. Melting point and ^1H NMR data of the compound were taken, which also supported the GC-MS analysis. (See experimental section for details).

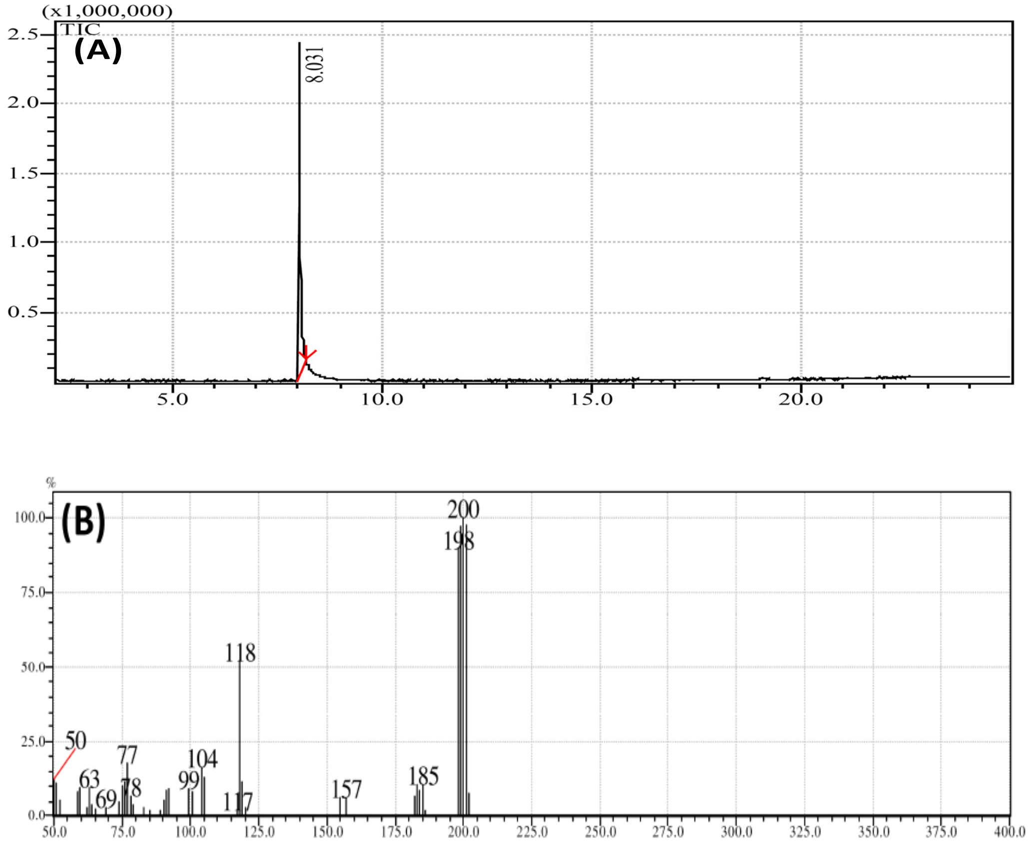

Figure 3.13. (A) Gas chromatogram and, (B) MS fragmentation pattern of product obtained in **5a**/Cu^{2+} reaction in presence of TBAB.

In order to check synthetic utility of these reactions, we have extended this reaction to *N*,*N*-diethylaniline (**5b**) and also to nucleophiles such as Cl$^{\ominus}$ and SCN$^{\ominus}$. In all these cases, the *N*,*N*-dialkylaniline radical cations underwent nucleophilic substitution reactions and gave the *para*-substituted products in good yields. The derivatives studied and isolated yields of products are given in Table 3.3.

Table 3.3. Product and yields in Cu^{2+} - initiated nucleophilic substitution reaction.

Entry	Substrate	Reagents	Product	Yield (%)
1	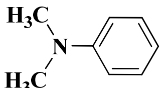 **5a**	$CuCl_2$	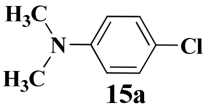 **15a**	52
2	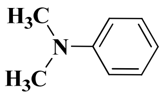	$n(Bu)_4NBr, Cu(ClO_4)_2$	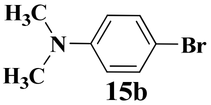 **15b**	86
3	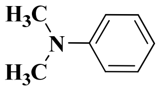	$NaSCN, Cu(ClO_4)_2$	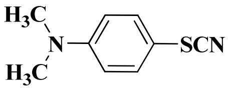 **15c**	82
4	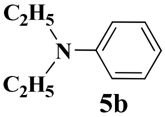 **5b**	$CuCl_2$	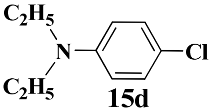 **15d**	58
5	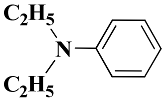	$n(Bu)_4NBr, Cu(ClO_4)_2$	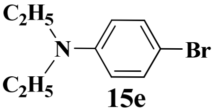 **15e**	88
6	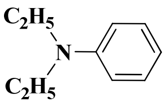	$NaSCN, Cu(ClO_4)_2$	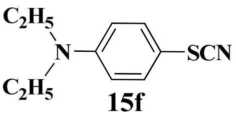 **15f**	85

A possible mechanism for the formation of the substitution products is given in Scheme 3.8.

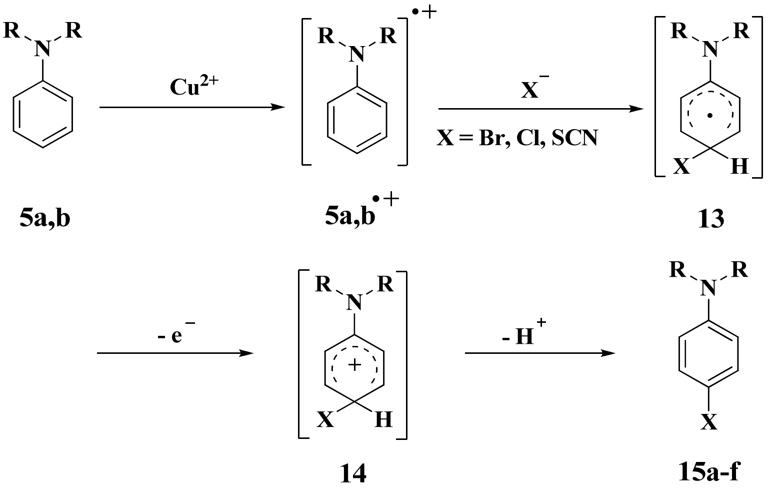

Scheme 3.8

The **5a**$^{\bullet+}$/**b**$^{\bullet+}$ formed as a result of electron transfer to Cu^{2+} is immediately trapped by the nucleophile to form the radical (**13**), which gives away an electron to form a cationic species (**14**). The electron can be transferred to **1a**$^{\bullet+}$ or to Cu^{2+} (if present in excess). The cationic species subsequently undergoes deprotonation to give the product, **15a-f**.

Although *N*,*N*-dialkylaniline radical cations are well-known, nucleophilic substitution reactions involving these species have attracted little attention. Chlorination of **5a** using acetyl chloride in presence of ceric ammonium nitrate was reported recently,[28] and this reaction might have involved **5a**$^{\bullet+}$. Mechanistic details, however, were not discussed in the paper.

We have examined the scope of the above substitution reactions in the case of few diphenylamine and triphenylamine derivatives. In the case of triphenylamines multiple substitutions occurred and the reactions were of little synthetic value because of the difficulties associated with the separation of the products. In the case of some diarylamine systems we observed that the reaction conditions can be tuned to favour certain products over the others. An account of this study is given in the following section.

3.3.2.2. Reaction of Diarylamines 6a-d with Cu^{2+} in Presence of Nucleophiles in Acetonitrile

In the presence of Br^{Θ} and Cu^{2+}, **6a** gave mono- and di-substitution products in larger amounts along with trace amounts of a tri-substitution product. Relative amounts of the substituted products depended on the amount of Cu^{2+}

and nucleophile employed and the reaction conditions could be tuned to obtain high amounts of single products as shown in Table 3.4 (see experimental section for details). When one of the phenyl rings is substituted at the *para* position, mono substitution occurred in very good yields as shown in Table 3.4.

Table 3.4. Starting material, reagents, products and yields, of Cu(II) mediated nucleophilic substitution reactions.

Entry	Amine	Reagents	Product	Yield* (%)
1	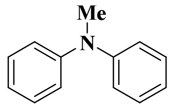 **6a**	$Cu(ClO_4)_2$, $(nBu)_4NBr$	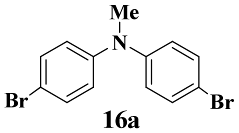 **16a**	67
2	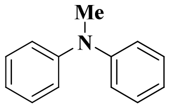 **6a**	$CuCl_2$	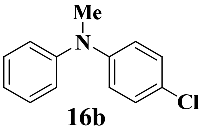 **16b**	58
3	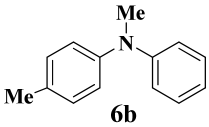 **6b**	$Cu(ClO_4)_2$, $(nBu)_4NBr$	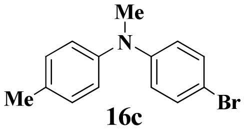 **16c**	83
4	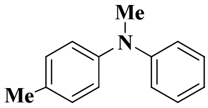 **6b**	$CuCl_2$	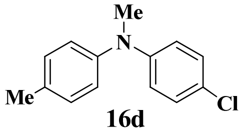 **16d**	68
5	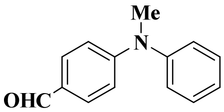 **6d**	$Cu(ClO_4)_2$, $(nBu)_4NBr$	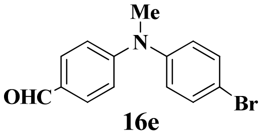 **16e**	85
6	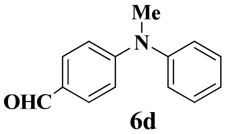 **6d**	$Cu(ClO_4)_2$, NaSCN	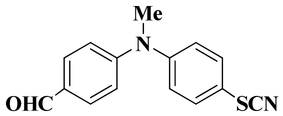 **16f**	79
7	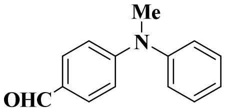 **6d**	$CuCl_2$	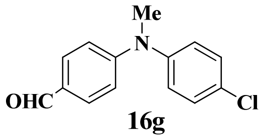 **16g**	65

* 1-4 yield obatined from GC-MS and 5-7 are isolated yields

3.4. Conclusions

We have investigated the electron transfer reaction between Cu^{2+} and aromatic amines. When *N*,*N*-dialkylaniline was reacted with one molar equivalent of Cu^{2+}, its radical cation was formed very readily which was characterized by its absorption near 450 nm. *N*-methyldiphenylamine in the presence of Cu^{2+} has shown a characteristic absorption band at 512 nm and triphenylamine under the same condition has shown an absorption band at 700 nm. In the case of triphenylamine derivatives the existence of radical cations were further confirmed by ESR spectroscopy. The radical cations generated in the electron transfer reaction underwent very fast dimerization to yield benzidine radical cations. These intermediates were also characterized by its structured absorption around 400-600 nm and 800-1600 nm regions. Upon addition of a base, benzidine radical cations transformed the benzidine product. A mechanism in line with previously reported electrochemical oxidation, is proposed for benzidine formation. Yields of benzidine were very high and the reaction is of high synthetic value. When the aromatic amine was treated with two molar equivalents of Cu^{2+} in the presence of nucleophiles such as $-Cl^{\Theta}$, $-Br^{\Theta}$ and $-SCN^{\Theta}$, substitution products were obtained. *N*,*N*-dialkylanilines yielded *para*-substituted products exclusively and reaction is synthetically very useful. In the case of diarylamines multiple substitution occurred. The reaction conditions could be tuned to obtain high yields of mono or di-substituted products in some cases. When one of the phenyl rings in the diphenylamine is substituted at the *para* position, mono-substitution products were obtained in good yields.

3.5. Experimental Section

3.5.1. Materials

$Cu(ClO_4)_2.6H_2O$, aromatic amines **5a,b** and **7a** were commercial samples. **5a-d** and **7b-j** were prepared as per reported procedures. Spectroscopic grade solvents were used for kinetic, photophysical and electrochemical measurements.

3.5.2. Measurements

Absorption spectra were recorded on a Shimadzu 3101PC UV-Vis-NIR scanning spectrophotometer. ^1H and ^{13}C NMR spectra were recorded on a Bruker Avance DPX Spectrometer. The chemical shifts, δ, are referred to TMS. GC-MS analyses were performed using a Shimadzu GC-MS-QP2010 gas chromatograph mass spectrometer. The FAB mass spectra were recorded on a JEOL spectrometer. Redox potentials of Cu(II) and all amine derivatives were measured using a BAS CV50W cyclic voltammetric analyser, with a conventional three-electrode system. Solutions of the amine derivatives (1×10^{-3} M) in acetonitrile containing 0.1 M tetra-*n*-butylammonium hexafluorophosphate as supporting electrolyte were thoroughly deaerated before use. A Pt disc electrode was used as the working electrode, a platinum wire was used as counter electrode, and the potentials were referenced to a saturated calomel electrode (SCE). The ESR spectra were recorded at room temperature on a JEOL

JES-TE100 ESR spectrometer operating at X-band frequencies and having a 100 kHz field modulation. All experiments were carried out at room temperature (25±1 °C), unless otherwise mentioned.

3.5.3. Synthesis

3.5.3.1. General Procedure for Dimerization Reaction

A solution of $Cu(ClO_4)_2.6H_2O$ (222 mg, 0.6 mmol) in ACN (10 mL) was added to a solution of the arylamine (0.4 mmol) in ACN (20 mL) at room temperature, and the mixture was stirred for 12 h. Solid K_2CO_3 (500 mg) and water (1 mL) were added, and stirring was continued for 0.5 h. Filtered and the solids were washed twice with chloroform. The combined organic extracts were filtered through a short pad of alumina. The solvent was removed and the residue so obtained was recrystallized form dichloromethane-hexane mixture to give pure products.

***N,N,N’,N’*-Tetramethylbenzidine (8a)**

Yield 83%; ^{1}H NMR (300 MHz, $CDCl_3$): δ 7.6 (d, 4 H), 6.9 (d, 4H), 3.1 (s, 12 H); ^{13}C NMR (75 MHz, $CDCl_3$) δ 149.29, 130.20, 127.03, 113.25, 40.58; Mass Spectrometric analysis (EI) m/z 240 (M^+).

***N,N,N’,N’*-Tetraethylbenzidine (8b)**

Yield 86%; ^{1}H NMR ($CDCl_3$, 300 MHz) δ: 7.4 (d, 4 H), 6.7 (d, 4 H), 3.4 (q, 8 H), 1.2 (t, 12 H); ^{13}C NMR (75 MHz, $CDCl_3$) δ 146.25, 128.90, 127.05, 112.3, 44.52, 12.62; Mass Spectrometric analysis (EI) m/z 296 (M^+).

_N,N'_-Dimethyl-_N,N'_-diphenylbiphenyl-4,4'-diamine (10a)

Yield 68%; ^{1}H NMR (500 MHz, CDCl$_3$) δ 3.37 (s, 6H), 6.97-7.09 (t, 2H), 7.03(d, 8H), 7.28-7.31 (t, 4H), 7.46-7.48 (m, 4H); ^{13}C NMR (125 MHz, CDCl$_3$) δ 40.29, 120.36, 120.83, 121.55, 127.28, 129.27, 133.59, 147.77, 148.85; Mass Spectrometric analysis (FAB) m/z 364 (M$^+$).

_N,N'_-Dimethyl-_N, N'_-di(_p_-tolyl)biphenyl-4,4'-diamine (10b)

Yield 82%; ^{1}H NMR (500 MHz, CDCl$_3$) δ 2.33 (s, 6H), 3.33 (s, 6H), 7.04 (d, 8H), 7.12 (d, 4H), 7.42 (d, 4H); ^{13}C NMR (125 MHz, CDCl$_3$) δ 20.81, 40.41, 118.41, 122.59, 127.06, 129.96, 132.09, 132.51, 146.52, 148.01; Mass Spectrometric analysis (FAB) *m/z* 392 (M$^+$).

_N,N'_-Bis(4-methoxyphenyl)-_N,N'_-dimethylbiphenyl-4,4'-diamine (10c)

Yield 76%; ^{1}H NMR (500 MHz, CDCl$_3$) δ 3.28 (s, 6H), 3.81 (s, 6H), 6.82 (d, 4H), 6.88 (d, 4H), 7.11 (d, 4H), 7.38 (d, 4H); ^{13}C NMR (125 MHz, CDCl$_3$) δ 39.52, 54.48, 111.73, 112.76, 113.71, 115.06, 124.80, 125.84, 147.14, 151.29. Mass Spectrometric analysis (FAB) *m/z* 424 (M$^+$).

_N,N'_-Bis(_p_-formylphenyl)-_N,N'_-dimethylbiphenyl-4,4'-diamine (10d)

Yield 66%; ^{1}H NMR (500 MHz, CDCl$_3$) δ 3.45 (s, 6H), 6.87-6.89 (d, 4H), 7.26-7.33 (d, 4H), 7.65-7.72(d, 4H), 7.723-7.73 (d, 4H), 9.78 (s, 2H); ^{13}C NMR (125 MHz, CDCl$_3$) δ 40.36, 113.98, 126.52, 127.09, 128.39, 131.69, 137.78, 146.27, 153.59, 190.41; Mass Spectrometric analysis (FAB) *m/z* 421 (M+1).

N,N,N',N'-Tetraphenylbiphenyl-4,4'-diamine (4a)

Yield 81%; ^{1}H NMR (300 MHz, $CDCl_3$) δ 6.99-7.45 (m, 28H); ^{13}C NMR (75 MHz, $CDCl_3$) δ 122.76, 124.04, 124.24, 127.25, 129.21, 134.66, 146.66, 147.65; Mass Spectrometric analysis (FAB) *m/z* 488 (M^+).

N,N'-Diphenyl-N,N'-di(p-tolyl)biphenyl-4,4'-diamine (4b)

Yield 86%; ^{1}H NMR (300 MHz, $CDCl_3$) δ 2.32 (s, 6H), 7.07-7.42 (m, 26H); ^{13}C NMR (75 MHz, $CDCl_3$) δ 20.82, 122.33, 123.52, 123.72, 125.00, 127.15, 129.12, 129.93, 132.83, 134.36, 145.11, 146.82, 147.87; Mass Spectrometric analysis (FAB) *m/z* 516 (M^+).

N,N,N',N'-Tetra(p-tolyl)biphenyl-4,4'-diamine (4c)

Yield 94%; ^{1}H NMR (300 MHz, $CDCl_3$) δ 2.15 (s, 12H), 6.83-6.94 (m, 20H), 7.25 (d, 4H); ^{13}C NMR (75 MHz, $CDCl_3$) δ 21.01, 123.15, 124.68, 127.24, 130.05, 132.48, 134.15, 145.51, 147.17; Mass Spectrometric analysis (FAB) *m/z* 544 (M^+).

N,N,N',N'-Tetrakis(4-methoxyphenyl)biphenyl-4,4'-diamine (4d)

Yield 87%; ^{1}H NMR (300 MHz, $CDCl_3$) δ 3.78 (s, 12H), 6.81 (d, 8H), 6.96 (m, 4H), 7.05 (d, 8H), 7.34 (d, 4 H); ^{13}C NMR (75 MHz, $CDCl_3$) δ 55.45, 114.62, 121.08, 126.37, 126.84, 132.99, 140.92, 147.35, 155.67; Mass Spectrometric analysis (FAB) *m/z* 608 (M^+).

N,N'-Bis(p-carbomethoxyphenyl)-N,N'-di(phenyl)biphenyl-4,4'-diamine (4e)

Yield 83%; ^{1}H NMR (300 MHz, $CDCl_3$) δ 3.88 (s, 6H), 7.03 (d, 4H), 7.14-7.19

(m, 10H), 7.30-7.35 (m, 4H), 7.50 (d, 4H), 7.86 (d, 4H); ^{13}C NMR (75 MHz, $CDCl_3$) δ 52.71, 119.34, 121.39, 122.35, 124.81, 126.71, 128.75, 130.71, 131.94, 136.24, 146.54, 145.77, 151.77, 166.86; Mass Spectrometric analysis (FAB) *m*/*z* 605 (M+1).

***N*,*N*’-Bis(*p*-formylphenyl)-*N*,*N*’-diphenylbiphenyl-4,4’-diamine (4f)**

Yield 85%; ^{1}H NMR (300 MHz, $CDCl_3$) δ 7.07 (d, 4H), 7.16-7.25 (m,10H), 7.33-7.38 (m, 4H), 7.53 (d, 4H), 7.69 (d, 4H), 9.81(s, 2H); ^{13}C NMR (75 MHz, $CDCl_3$) δ 119.75, 125.23, 126.16, 126.34, 127.92, 129.34, 129.77, 131.29, 136.62, 145.39, 146.02, 153.11, 190.38; Mass Spectrometric analysis (FAB) *m*/*z* 545 (M+1).

***N*,*N*’-Bis(4-nitrophenyl)-*N*,*N*’-diphenylbiphenyl-4,4’-diamine (4g)**

Yield 81%; ^{1}H NMR (300 MHz, $CDCl_3$) δ 6.90 (d, 4H), 7.12-7.17 (m, 10H), 7.28- 7.33 (m, 4H), 7.48 (d, 4H), 7.97 (d, 4H); ^{13}C NMR (75 MHz, $CDCl_3$) δ 118.57, 125.45, 125.86, 126.41, 126.55, 128.16, 129.98, 137.10, 140.35, 144.98, 145.50, 153.23; Mass Spectrometric analysis (FAB) *m*/*z* 578 (M^+).

***N*,*N*’-Diphenyl-*N*,*N*’-bis(4-thiocyanatophenyl)biphenyl-4,4’-diamine (4h)**

Yield 82%; ^{1}H NMR (300 MHz, $CDCl_3$) δ 7.01 (d, 4H), 7.08 (d, 10H), 7.23-7.33 (m, 8H), 7.42 (d, 4H); ^{13}C NMR (75 MHz, $CDCl_3$) δ 113.73, 121.96, 122.91, 123.41, 125.50, 126.71, 128.64, 130.63, 134.02, 135.90, 145.67, 146.39, 149.65; Mass Spectrometric analysis (FAB) *m*/*z* 602 (M^+).

3.5.3.2. General Procedure for Substitution Reaction

Aromatic amine (1 mmol) and tetrabutylammonium bromide (640 mg, 2 mmol) were dissolved in acetonitrile (30 mL). A solution of $Cu(ClO_4)_2.6H_2O$ (740 mg, 2 mmol) in acetonitrile (10 mL) was added, and the mixture was stirred for 0.5 h at room temperature. Solid K_2CO_3 (1.0 g) was added, and stirring continued for 10 minutes. The reaction mixture was filtered, and the solids were washed twice with $CHCl_3$. The organic fractions were combined and dried over anhydrous Na_2SO_4. The solvent was removed, and the residue was taken in hexane. This was filtered through a small alumina column and crystallized from the same solvent.

4-Chloro-*N,N*-dimethylaniline (15a)

Yield 52 %; ^{1}H NMR (300 MHz, $CDCl_3$) δ 7.0 (d, 2 H), 6.5 (d, 2H), 2.8 (s, 6 H); Mass Spectrometric analysis (EI) m/z 155(M^+).

4-Bromo-*N,N*-dimethylaniline (15b)

Yield 86%; ^{1}H NMR (300 MHz, $CDCl_3$) δ 7.2 (d, 2 H), 6.5 (d, 2 H), 2.9 (s, 6 H); Mass Spectrometric analysis (EI) m/z 200 (M^+).

4-Thiocyanato-*N,N*-dimethylaniline (15c)

Yield 82%; IR (KBr) 2953, 2920, 2860, 2142, 1589, 1512, 1371, 1232, 1082, 968, 949, 808 cm^{-1}; ^{1}H NMR (300 MHz, $CDCl_3$) δ 7.3 (d, 2 H), 6.5 (d, 2 H), 2.9 (s, 6 H); Mass Spectrometric analysis (EI) m/z 178 (M^+).

4-Chloro-*N,N*-diethylaniline (15d)

Yield 58%; ^{1}H NMR (300 MHz, $CDCl_3$) δ 7.0 (d, 2 H), 6.5 (d, 2 H), 3.4 (q, 4 H), 1.2 (t, 6 H); Mass Spectrometric analysis (EI) m/z 183 (M^+).

4-Bromo-*N,N*-diethylaniline (15e)

Yield 88%; ^{1}H NMR (300 MHz, $CDCl_3$) δ 7.2 (d, 2H), 6.5 (d, 2 H), 3.4 (q, 4 H), 1.2 (t, 6 H); Mass Spectrometric analysis (EI) m/z 228 (M^+).

4-Thiocyanato-*N,N*-diethylaniline (15f)

Yield 85%; ^{1}H NMR (300 MHz, $CDCl_3$) δ 7.3 (d, 2 H), 6.6 (d, 2 H), 3.4 (q, 4 H), 1.2 (t, 6 H); Mass Spectrometric analysis (EI) m/z 206 (M^+).

***N*-(*p*-Bromophenyl)-*N*-methyl-*p*-aminobenzaldehye (16e)**

Yield 85%; ^{1}H NMR (500 MHz, $CDCl_3$) δ 3.37 (s, 3H), 6.80-6.82(d, 2H), 7.10-7.12 (d, 2H), 7.52-7.54 (d, 2H), 7.69-7.71 (d, 2H), 9.97(s, 1H); ^{13}C NMR (125MHz, $CDCl_3$) δ 40.29, 114.02, 119.05, 127.30, 127.90, 131.67, 133.11, 146.02, 153.33, 190.42; Mass Spectrometric analysis (FAB) *m/z* 290 (M^+).

***N*-Methyl-*N*-(*p*-thiocyanatophenyl)-*p*-aminobenzaldehye (16f)**

Yield 79%; ^{1}H NMR (500 MHz, $CDCl_3$) δ 3.40 (s, 3H), 6.95-6.96(d, 2H), 7.22-7.24 (d, 2H), 7.52-7.54 (d, 2H), 7.72-7.74 (d, 2H), 9.807 (s, 1H); ^{13}C NMR (125 MHz, $CDCl_3$) δ 40.22, 110.80, 116.57, 118.56, 125.60, 128.81, 131.61, 132.61, 148.77, 152.83, 190.46; Mass Spectrometric analysis (FAB) *m/z* 268 (M^+).

***N*-(*p*-Chlorophenyl)-*N*-Methyl-*p*-aminobenzaldehye (16g)**

Yield 65%; ^{1}H NMR (500 MHz, $CDCl_3$) δ 3.39 (s, 3H), 6.78 (d,2H), 7.22 (d, 2H), 7.43 (d, 2H), 7.68 (d, 2H), 9.77 (s, 1H); ^{13}C NMR (125 MHz, $CDCl_3$) δ

40.34, 113.85, 126.57, 127.66, 130.03, 130.15, 131.68, 145.50, 153.44, 190.42; Mass Spectrometric analysis (FAB) *m/z* 246 (M+1).

3.6. References

1. Sumalekshmy, S.; Gopidas, K. R. *Chem. Phys. Lett*. **2005**, *413*, 294.
2. Oyama, M.; Nozaki, K.; Okazaki, S. *Anal. Chem.* **1991**, *63*, 1387.
3. (a) Oyama, M.; Higuchi, T.; Okazaki, S. *Electrochem. Commun.* **2000**, *2*, 675. (b) Oyama, M.; Higuchi, T.; Okazaki, S. *J. Chem. Soc., Perkin Trans.* **2001**, *2*, 1287. (c) Goto, M.; Park, H.; Otsuka, K.; Oyama, M. *J. Phys. Chem. A* **2002**, *106*, 8103. (d) Park, H.; Oyama, M. *J. Chem. Soc. Perkin Trans. 2* **2002**, 1335. (e) Oyama, M.; Goto, M.; Park, H. *Electrochem. Commun.* **2002**, *4*, 110. (f) Oyama, M.; Higuchi, T.; Okazaki, S. *Electrochem. Solid-State Lett.* **2002**, *5*, E1. (g) Oyama, M.; Matsui, J.; Park, H. *Chem. Commun.* **2002**, 604. (h) Yano, M.; Ishida, Y.; Tatsumi, M.; Sato, K.; Shiomi, D.; Oyama, M.; Takui, T. *J. Phys. Chem. Solids* **2004**, *65*, 733. (i) Goto, M.; Otsuka, K.; Chen, X.; Tao, Y.; Oyama, M. *J. Phys. Chem. A* **2004**, *108*, 3980. (j) Oyama, M.; Kirihara, K. *Electrochim. Acta* **2004**, *49*, 3801. (k) Yano, M.; Nakanishi, Y.; Matsushita, K.; Tatsumi, M.; Oyama, M.; Sato, K.; Takui, T. *Polyhedron* **2005**, *24*, 2116. (l) Oyama, M.; Imabayashi, T.; Ho, J.-H.; Ho, T.-I. *Electrochemistry* **2006**, *74*, 649. (m) Yano, M.; Fujiwara, A.; Tatsumi, M.; Oyama, M.; Sato, K.; Takui, T. *Polyhedron* **2007**, *26*,

2008. (n) Yano, M.; Okino, Y.; Ichihara, Y.; Tatsumi, M.; Oyama, M.; Sato, K.; Takui, T. *Polyhedron* **2009**, *22*, 2009.

4. Garcia, H.; Roth, H. D. *Chem. Rev.* **2002**, *102*, 3947.
5. Periasamy, M.; Jayakumar, K. N.; Bharathi, P. *J. Org. Chem.* **2000**, *65*, 3548.
6. Saitoh, T.; Yoshida, S.; Ichikawa, J. *Org. Lett.* **2004**, *6*, 4563.
7. Xi, C.; Jiang, Y.; Yang, X. *Tetrahedron Lett.* **2005**, *46*, 3909.
8. (a) Goodbrand, H. B.; Hu, N.-X. *J. Org. Chem.* **1999**, *64*, 670. (b) Lu, J.; Hlil, A. R.; Sun, Y.; Hay, A. S.; Maindron, T.; Dodelet, J.-P.; D’Iorio, M. *Chem. Mater.* **1999**, *11*, 2501. (c) Liu, Y.-H.; Chen, C.; Yang, L.-M. *Tetrahedron Lett.* **2006**, *47*, 9275. (d) Low, P. J.; Paterson, M. A. J.; Goeta, A. E.; Yufit, D. S.; Howard, J. A. K.; Cherryman, J. C.; Tackley, D. R.; Brown, B. *J. Mater. Chem.* **2004**, *14*, 2516. (e) Low, P. J.; Paterson, M. A. J.; Yufit, D. S.; Howard, J. A. K.; Cherryman, J. C.; Tackley, D. R.; Brook, R.; Brown, B. *J. Mater. Chem.* **2005**, *15*, 2304. (f) Wang, X.; Chen, Z.; Ogino, K.; Sato, H.; Strzelec, K.; Miyata, S.; Luo, Y.; Tan, H. *Macromol. Chem. Phys.* **2002**, *203*, 739.
9. (a) Wolfe, J. P.; Wagaw, S.; Marcoux, J.-F.; Buchwald, S. L. *Acc. Chem. Res.* **1998**, *31*, 805. (b) Hartwig, J. F. *Acc. Chem. Res.* **1998**, *31*, 852. (c) Hartwig, J. F. *Angew. Chem., Int. Ed.* **1998**, *37*, 2046.

10. Shida, T. *Electronic Absorption Spectra of Radical Ions*; Elsevier: Amsterdam, 1988, p 209.
11. Shida, T. *Electronic Absorption Spectra of Radical Ions*; Elsevier: Amsterdam, 1988, p 223.
12. (a) Lambert, C.; Nöll, G. *J. Am. Chem. Soc.* **1999**, *121*, 8434. (b) Nelsen, S. F. *Chem. Eur. J.* **2000**, *6*, 581. (c) Lambert, C.; Nöll, G. *J. Chem. Soc., Perkin Trans. 2* **2002**, 2039. (d) Littleford, R. E.; Paterson, M. A. J.; Low, P. J.; Tackley, D. R.; Jayes, L.; Dent, G.; Cherryman, J. C.; Brown, B.; Smith, W. E. *Phys. Chem. Chem. Phys.* **2004**, *6*, 3257. (e) Low, P. J.; Paterson, M. A. J.; Puschmann, H.; Goeta, A. E.; Howard, J. A. K.; Lambert, C.; Cherrymann, J. C.; Tackley, D. R.; Leeming, S.; Brown, B. *Chem. Eur. J.* **2004**, *10*, 83.
13. Kavarnos, G. J.; Turro, N. J. *Chem. Rev.* **1986**, *86*, 401.
14. Galus, Z.; White, R. M.; Rowland, F. S.; Adams, R. N. *J. Am. Chem. Soc.* **1962**, *84*, 2065.
15. Seo, E. T.; Nelson, R. F.; Fritsch, J. M.; Marcoux, L. S.; Leedy, D. W.; Adams, R. N. *J. Am. Chem. Soc.* **1966**, *88*, 3498.
16. Kirchgessner, M.; Sreenath, K.; Gopidas, K. R. *J. Org. Chem.* **2006**, *71*, 9849.
17. (a) Lewis, G. N.; Lipkin, E. *J. Am. Chem. Soc.* **1942**, *64*, 2801. (b) Hasegawa, H. *J. Phys. Chem.* **1962**, *66*, 834. (c) Hall, W. K. *J. Catalysis*

1962, *1*, 53 (d) Dollish, F. R.; Hall, W. K. *J. Phys. Chem*. **1965**, *69,* 2127.

18. Rapta, P.; Fáber, R.; Dunsch, L.; Neudeck, A.; Nuyken, O. *Spectrochim. Acta* **2000**, *56A*, 357.
19. (a) Creason, S. C.; Wheeler, J.; Nelson, R. F. *J. Org. Chem*. **1972**, *37*, 4440. (b) Nelson, R. F.; Feldberg, S. W. *J. Phys. Chem.* **1969**, *73*, 2623.
20 (a) Rapta, P.; Rohde, D.; Hartmann, H.; Dunsch, L. *Tetrahedron Lett.* **2006**, *47*, 7587. (b) Rapta, P.; Zeika, O.; Rohde, D.; Hartmann, H.; Dunsch, L. *ChemPhysChem* **2006**, *7*, 863. (c) Chiu, K. Y.; Su, T. X.; Li, J. H.; Lin, T.-H.; Liou, G.-S.; Cheng, S.-H. *J. Electroanal. Chem.* **2005**, *575*, 95.
21. (a) Strohriegl, P.; Grazulevicius, J. V. *Adv. Mater.* **2002**, *14*, 1439. (b) Shirota, Y. *J. Mater. Chem.* **2000**, *10*, 1. (c) Lindner, S. M.; Thelakkat, M. *Macromol. Chem. Phys.* **2006**, *207*, 2084. (d) Jean, R. *Acc. Chem. Res.* **2009**, *42*, 1719. (e) Preat, J.; Michaux, C.; Jacquemin, D.; Perpète, E. A. *J. Phys. Chem. C* **2009**, *113*, 16821.
22. Gervat, S.; Léonel, E.; Barraud, J.-Y.; Ratovelomana, V. *Tetrahedron Lett.* **1993**, *34*, 2115.
23. Bacher, E.; Bayerl, M.; Rudati, P.; Reckefuss, N.; Müller, C. D.; Meerholz, K.; Nuyken, O. *Macromolecules* **2005**, *38*, 1640.
24. Kajigaeshi, S.; Moriwaki, M.; Tanaka, T.; Fujisaki, S.; Kakinami, T.;

Okamoto, T. *J. Chem. Soc., Perkin Trans. 1* **1990**, 897.

25. Bonesi, S. M.; Erra-Balsells, R. *J. Heterocyclic. Chem.* **1997**, *34*, 877.
26. Lengyel, I.; Cesare, V.; Stephani, R. *Synthetic. Commun.* **1998**, *28*, 1891.
27. Kajigaeshi, S.; Shinmasu, Y.; Fujisaki, S.; Kakinami, T. *Bull. Chem. Soc. Jpn.* **1990**, *63*, 941.
28. Roy, S. C.; Rana, K. K.; Guin, C.; Banerjee, B. *Synlett* **2003**, 221.
29. Sreenath, K.; Suneesh, C. V.; Ratheesh Kumar, V. K.; Gopidas, K. R. *J. Org. Chem.* **2008**, *73*, 3245.

Chapter 4

Cu^{2+} Mediated Generation of Dications of a few Selected Aromatic Amines and Design of a Selective Cu^{2+} Sensor

4.1. Abstract

In this chapter we report the reaction of a few aromatic amines with excess Cu^{2+} *(2 or more equivalents) in acetonitrile. These amines have their first oxidation potentials below 0.7 V vs SCE and second oxidation potentials in the range 0.8-1.2 V vs SCE. In the case of benzidine derivatives* ***3*** *and* ***4****, reactions with excess* Cu^{2+} *yielded stable dications, which were characterized by their absorption spectra. The assignments were confirmed by spectroelectrochemistry. In the case of amines* ***5*** *and* ***6****, the dications were unstable and reacted very fast with water to give oxidized products. Product isolation studies were carried out to confirm product structures. In the case of* ***7****, reaction with* Cu^{2+} *in acetonitrile resulted in a play of colours. We observed that the play of colours can also be seen with* Fe^{3+} *in ACN. However, in 9:1 acetonitrile:water mixture* ***7*** *exhibited colour reaction only with* Cu^{2+}*. In this solvent mixture* ***7*** *could act as a very selective and sensitive colourimetric sensor for the detection of micromolar quantities of* Cu^{2+}*.*

4.2. Introduction

Chapters 2 and 3 of this thesis deal with generation of radical cations from aromatic amines by reaction with Cu^{2+} in acetonitrile (ACN). During the course of this study we observed that with certain aromatic amines and diamines having low oxidation potentials, reaction with Cu^{2+} in ACN can also lead to the formation of the amine dications. A survey of the literature showed that the doubly oxidized states of diamines could exhibit different properties depending on the structure of the diamine. For example, the 1,3-disubstituted diamine derivative **1** upon losing two electrons assumes a diradical-dication type structure, whereas the 1,4-disubstituted diamine **2** assumes a dicationic structure, as shown in Scheme 4.1.

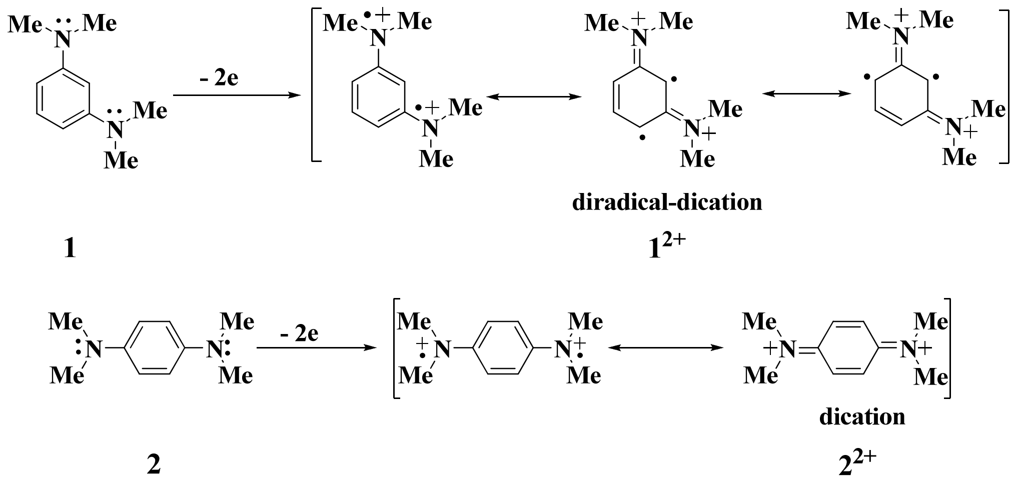

Scheme 4.1

Diradical-dications such as $\mathbf{1}^{2+}$ have attracted considerable interest as they possess multiple open shell electronic structure with high spin multiplicity. These polycations could be used as building blocks in developing new organic materials having unusual spin and magnetic properties.[1] These type of materials could use electron spin, rather than electron charge, as a carrier of information as in conventional electronics. In the field of spin-based electronics, the control of electron spin and its interaction with magnetic materials is of crucial importance. We were unable to generate diradical-dications of the $\mathbf{1}^{2+}$ type by reaction of the parent diamine with Cu^{2+} in ACN. However we could generate dications of the $\mathbf{2}^{2+}$ type by reacting few amines and diamines with Cu^{2+} in ACN and the results of this study are presented in this chapter. The compounds we studied are shown in Chart 4.1.

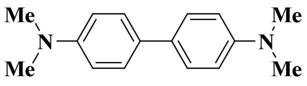

3

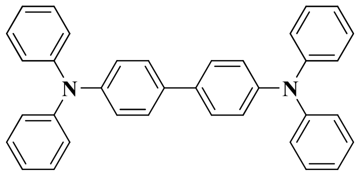

4

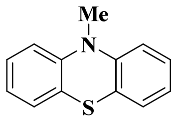

5

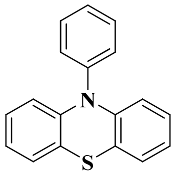

6

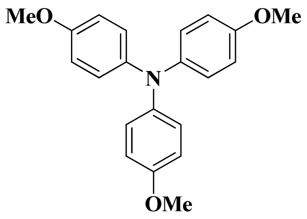

7

Chart 4.1

Dications of a few amine systems were generated previously by electrochemical techniques.[2] For example the absorption spectra of dications of **2** was reported in the literature.[2b] Lambert and co-workers have generated the dication of **7** by spectroelectrochemistry and reported that the dication exhibited a broad and unsymmetrical absorption band at 18,800 cm^{-1} (532 nm) with an oscillator strength of 0.34. They also carried out a AM1-CISD calculation for **7**$^{2+}$ and obtained a transition energy of 15,860 cm^{-1} and an oscillator strength of 0.90, both of which showed distinct deviation from the experimental data.[2c]

Reynolds *et al.* generated dications of few triarylamines (**8a-f**) electrochemically at a platinum anode and observed that these dications undergo cyclization to carbazole (**10a-f**) derivatives as shown in Scheme 4.2.[2d] Yield of these reactions were very low (10-15%) and the mechanism shown in Scheme 4.2 was suggested for product formation.

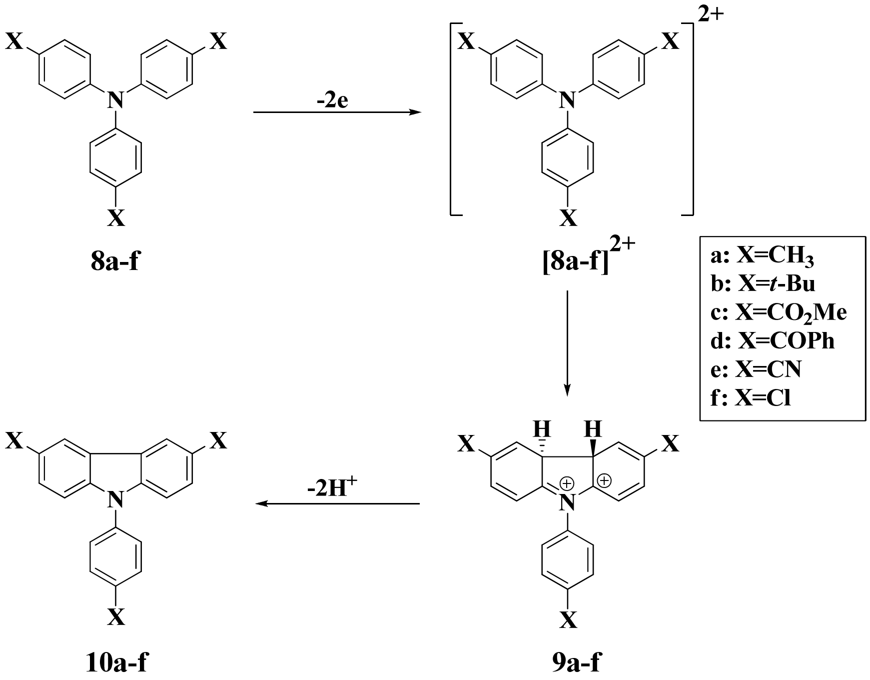

Scheme 4.2

In this chapter we report the reaction of amines **3** to **7** with two or more equivalents of Cu^{2+} in ACN and recorded the absorption spectra of the species formed under these conditions. For diamines **3** and **4** first and second oxidations were completely reversible. For **5** to **7**, first oxidations were completely reversible and second oxidations were not fully reversible. In the case of reversible systems, assignments of the first and second oxidation products were confirmed by spectroelectrochemistry. For **7** we observed that reaction with 0-2 equivalents of Cu^{2+} in ACN leads to a play of colours. We have modified the reaction conditions to design a highly efficient colourimetric sensor for Cu^{2+}. Results of these studies are reported in this Chapter.

4.3. Results and Discussion

Figure 4.1 shows voltammograms of these amines recorded in ACN solution (see experimental section for details). It can be seen that for all these amines the first oxidation potentials ($E_{\mathrm{ox}(1)}$) are ≤ 0.7 V vs SCE and the second oxidation potentials ($E_{\mathrm{ox}(2)}$) are in the range 0.8 to 1.2 V vs SCE. The thermodynamic feasibility of the radical cation and dication formations in ACN for **3** to **7** using Cu^{2+} as oxidant could be analyzed in terms of the free energy changes associated with the electron transfer processes.[3] As mentioned in Chapter 2 of this thesis we have calculated the ΔG^0 values associated with these processes and the calculated values along with experimental oxidation potentials are given in table 4.1.

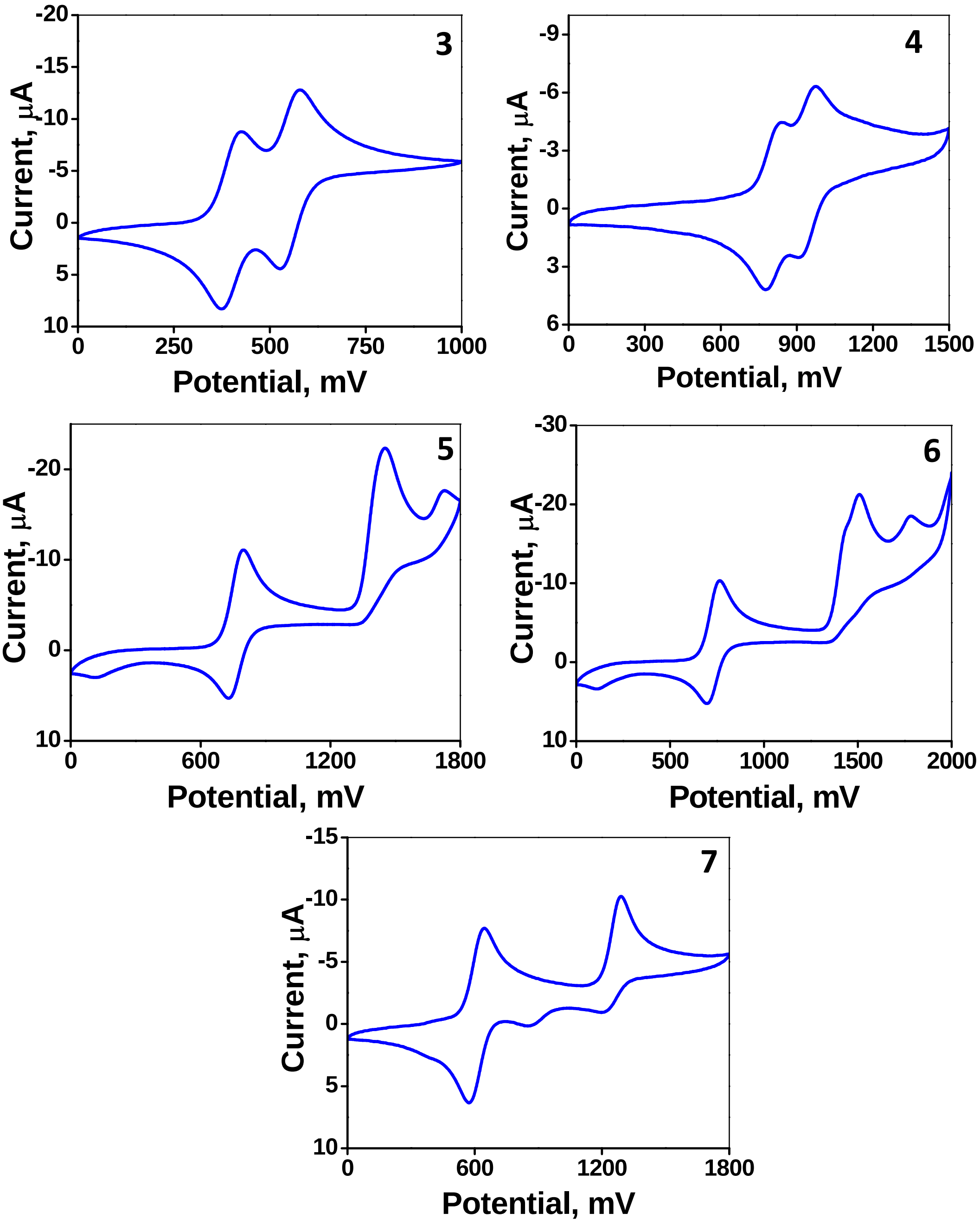

Figure 4.1. Cyclic voltammograms of amines **3** to **7**.

Table 4.1. $E_{ox(1)}$, $E_{ox(2)}$, ΔG^0_1 and ΔG^0_2 for amines **3** to **7**.

Aromatic amine	$E_{ox(1)}$ vs SCE	$E_{ox(2)}$ vs SCE	ΔG^0_1 eV	ΔG^0_2 eV
3	0.32	0.60	-0.70	-0.42
4	0.68	0.82	-0.34	-0.20
5	0.69	1.27	-0.33	+0.25
6	0.66	1.40	-0.36	+0.38
7	0.54	1.17	-0.48	+0.15

It can be seen from Table 4.1 that ΔG^0 is negative for the first oxidations of all amines studied. For the second oxidations ΔG^0 is negative only for **3** and **4**. Although ΔG^0 is positive for the second oxidations of **5** to **7**, these oxidations still take place, albeit very slowly, in ACN (vide infra).

4.3.1. Reaction of *N,N,N',N'*-Tetramethylbenzidine (3) with Cu^{2+} in Acetonitrile

Absorption spectrum of **3** exhibits λ_{max} at 310 nm (Figure 4.2). Upon addition of Cu^{2+} (0-1 equivalents) absorption changes occurred as shown in Figure 4.2. Formation of new structured absorption bands around 470 and 1025 nm could be observed. The new spectrum obtained is identical to the absorption spectrum of $\mathbf{3}^{\bullet+}$, which we reported previously in Chapter 3 (Figure 3.2).

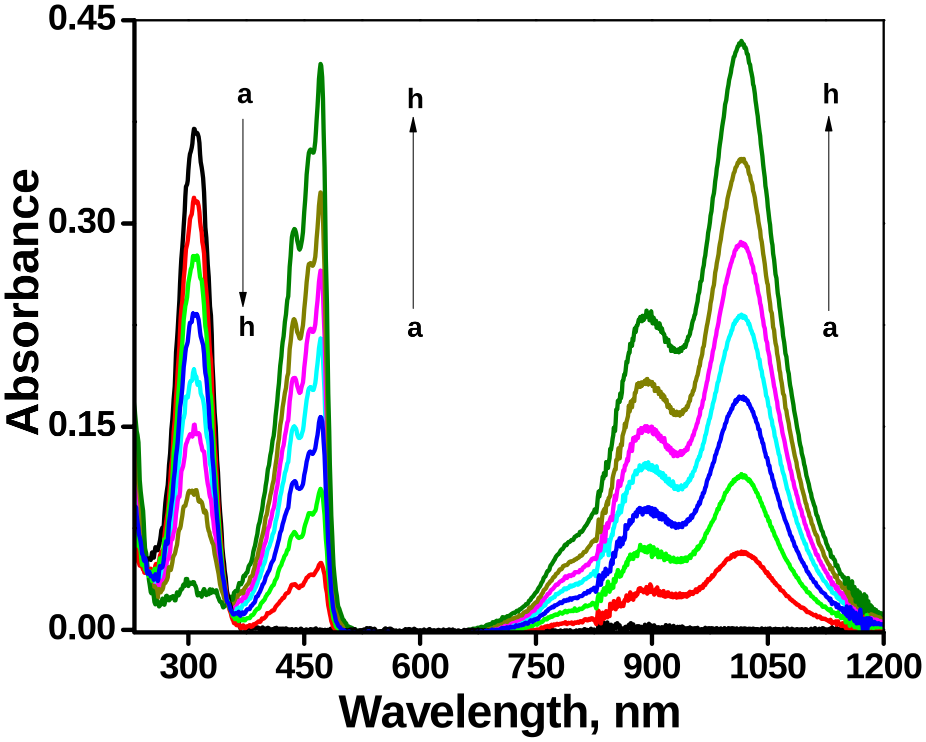

Figure 4.2. Effect of addition of increasing amount of Cu^{2+} (a) 0 (b) 0.15 (c) 0.30 (d) 0.45 (e) 0.60 (f) 0.75 (g) 0.9 (h) 1.05 equivalents to **3** (1 x 10^{-5} M) in ACN.

The band in the 800-1200 nm region was attributed to intervalence charge transfer in $\mathbf{3}^{\bullet +}$. Upon further addition of Cu^{2+} (1-2 equivalents), the intervalence band gradually decreased in intensity and finally disappeared and the 470 nm band increased in intensity and lost its fine structure (Figure 4.3). Since the oxidation of $\mathbf{3}^{\bullet +}$ to $\mathbf{3}^{2+}$ by Cu^{2+} in ACN is thermodynamically allowed, the new band formed at 470 nm is assigned to $\mathbf{3}^{2+}$.

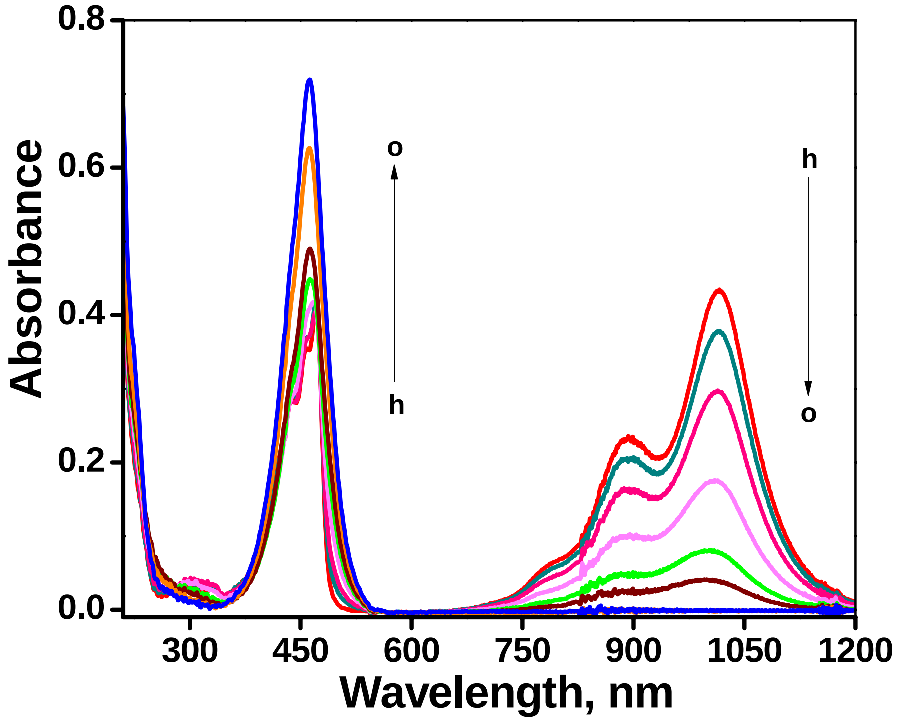

Figure 4.3. Effect of addition of increasing amount of Cu^{2+} to spectrum 4.2 h. (i) 1.20 (j) 1.35 (k) 1.50 (l) 1.65 (m) 1.80 (n) 1.95 (o) 2.10 equivalents of Cu^{2+}.

The process observed in Figure 4.2 and 4.3 can be summarized as shown in Scheme 4.3. The addition of one equivalents of Cu^{2+} produces $\mathbf{3}^{\bullet+}$, and addition of a second equivalent of Cu^{2+} converts $\mathbf{3}^{\bullet+}$ to $\mathbf{3}^{2+}$.

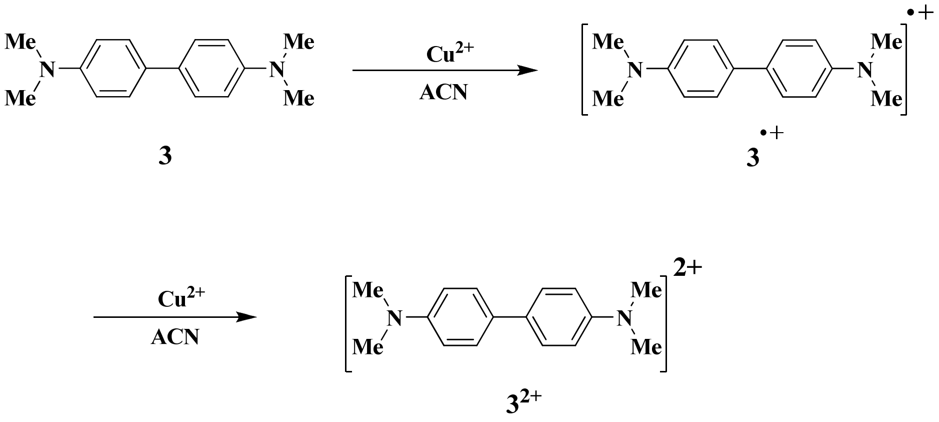

Scheme 4.3

It is to be mentioned that **3**$^{\bullet+}$ and **3**$^{2+}$ were known previously.[4a,b] The assignments of the states, however, was difficult because of conflicting data for the two oxidized states.[4c-g] Part of the problem appears to lie in the similarity of the absorption spectra, which also appear in the same region. Bakac and co-workers have generated **3**$^{\bullet+}$ and **3**$^{2+}$ using the same technique we employed here, but their spectra lacked the NIR region and hence the assignments were not convincing.[4h] In our experiments the assignments were very clear because **3**$^{\bullet+}$ exhibited two bands whereas **3**$^{2+}$ exhibited only one band.

We have further confirmed the above assignments using spectroelectrochemistry. Figure 4.4 shows the spectroelectrochemical response of **3**. Figure 4.4A is the absorption spectrum of the species generated when a potential of 0.32 V is applied to the working electrode. The spectrum is almost identical to Figure 4.2h, which we assign to **3**$^{\bullet+}$. When the applied potential is increased to 0.62 V, the absorption spectrum changed to Figure 4.4B, in which the 470 nm peak has increased in intensity and the 800-1200 nm peak decreased in intensity. The spectrum is similar to that in Figure 4.3m, which is obtained by adding 1.8 equivalents of Cu^{2+} to **3**. Thus the 470 nm band in Figure 4.4B can be unambiguously assigned to the dicationic species, **3**$^{2+}$. It is to be mentioned that in the spectroelectrochemical experiments neutral molecules are present at locations away from the working electrode. Since these locations also fall in the optical path, absorption due to these are also present in the spectrum. This is why we observe the contributions due to **3** (λ_{max} = 310 nm) even in Figure 4.4B, which is obtained after applying 0.6 V.

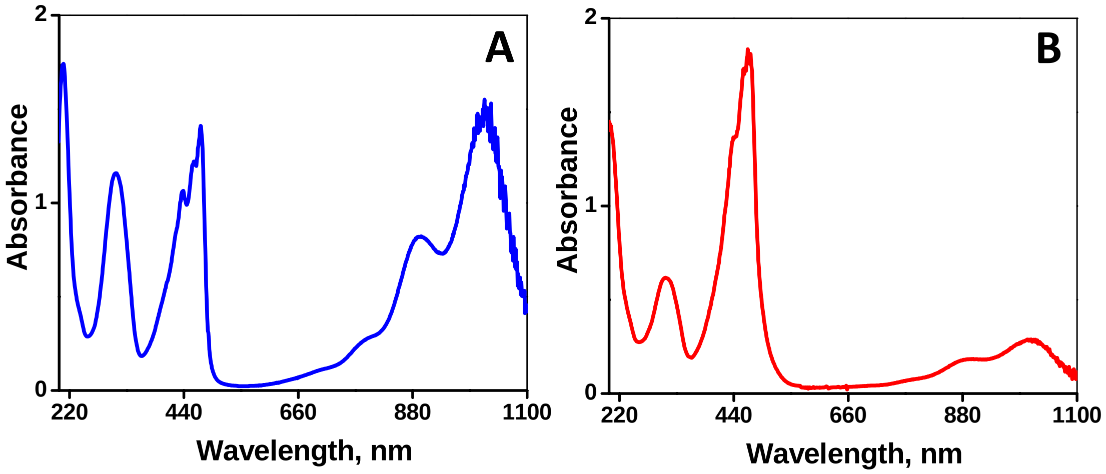

Figure 4.4. Absorption spectra of a solution of **3** in ACN at (A) 0.32 V and (B) at 0.62 V.

4.3.2. Reaction of *N,N,N',N'*-Tetraphenylbenzidine (4) with Cu^{2+} in Acetonitrile

4 exhibited absorption in the 200-400 nm region as shown in Figure 4.5. Upon addition of increasing amounts of $Cu(ClO_4)_2$ (0-1 equivalents), absorption due to **4** decreased and the spectrum corresponding to its radical cation $\mathbf{4}^{\bullet+}$ appeared at 400-580 nm and 800-1600 nm regions (Figure 4.5). Identification of this species is based on our own results reported in Chapter 3 (Figure 3.10).

Further addition of Cu^{2+} (1-2 equivalents) leads to decrease in the absorption corresponding to $\mathbf{4}^{\bullet+}$ at 480 and 1270 nm with concomitant increase in absorbance at 700 nm as shown in Figure 4.6.

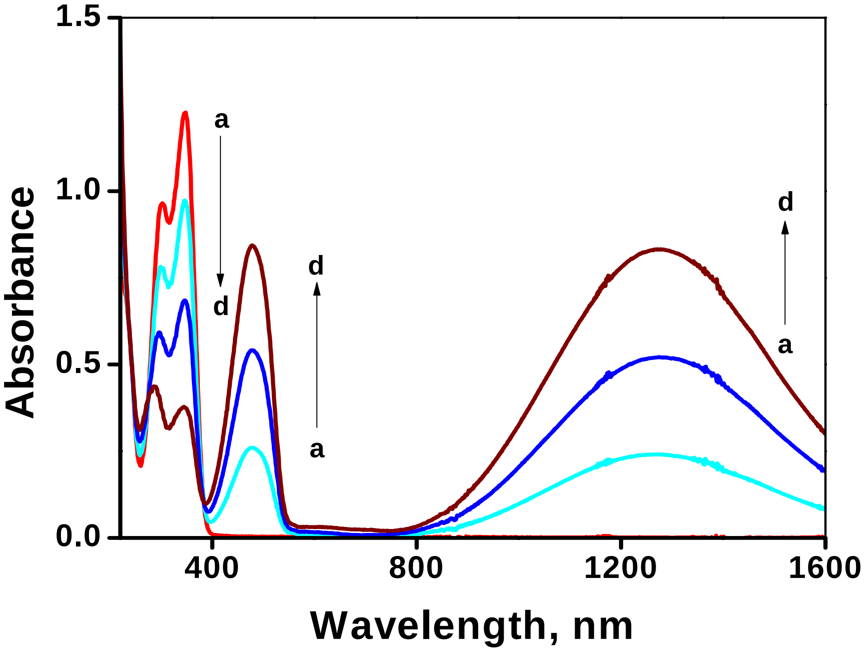

Figure 4.5. Effect of addition of increasing amount of Cu^{2+} (0-1 equivalents) to a solution of **4** (5×10^{-5} M) in ACN.

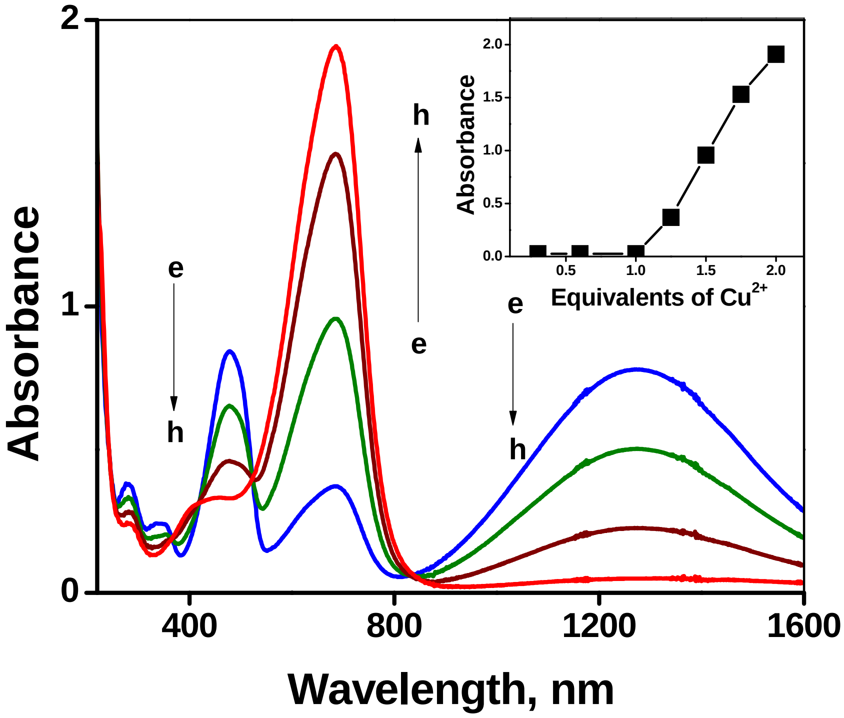

Figure 4.6. Effect of addition of increasing amount of Cu^{2+} (1-2 equivalents) to solution in Figure 4.5d. Inset of figure shows plot of optical density at 700 nm vs $[Cu^{2+}]$.

Based on the observation made in the case of **3**, the new band at 700 nm is assigned to **4**$^{2+}$. Notice that in this case the radical cation and dication absorb at different regions. Hence the assignment of the spectrum is unambiguous. The inset of Figure 4.6 shows a plot of optical density at 700 nm vs [Cu^{2+}]. The absorption due to **4**$^{2+}$ develops only after one equivalent of Cu^{2+} is added and its concentration reaches a maximum at two equivalents of Cu^{2+}, which further confirms the assignments we have made. Thus the oxidation of **4** by Cu^{2+} in ACN is similar to that of **3** shown in Scheme 4.3.

In the case of **4** also we confirmed the above assignments by spectroelectrochemical measurements. Electrolysis of **4** in ACN at its first oxidation potential resulted in decay of absorption spectrum of parent amine with concomitant increase of absorption at 480 and 1270 nm. The spectral profile obtained (Figure 4.7A) is similar to that in Figure 4.5d, which we assigned to **4**$^{\bullet+}$ generated by adding one equivalents of Cu^{2+} into ACN solution of **4**. When potential was increased beyond the second oxidation, intensity of NIR band decreased, along with increase of absorbance at 700 nm. The 700 nm band can thus be assigned unambiguously to the dication **4**$^{2+}$.

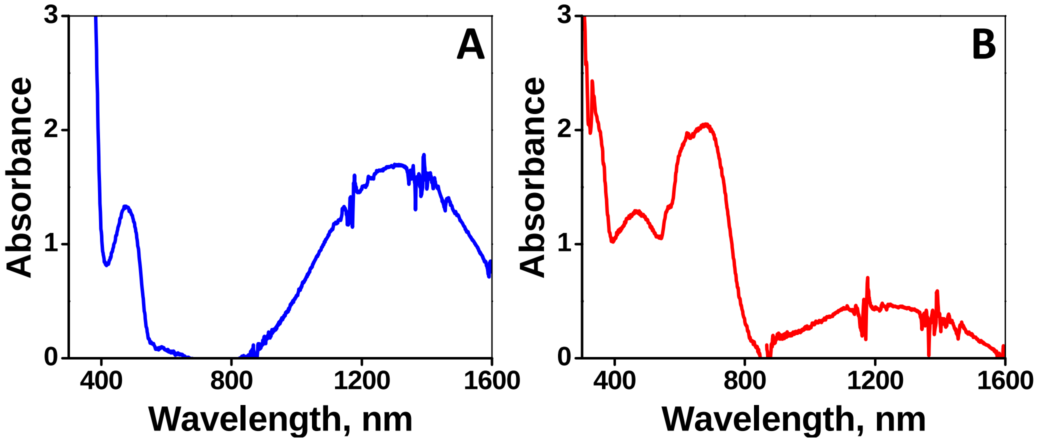

Figure 4.7. Absorption spectra of (A) $\mathbf{4}^{\bullet+}$ (B) $\mathbf{4}^{2+}$ obtained by spectroelectrochemistry in ACN

4.3.3. Reaction of *N*-Methylphenothiazine (5) with Cu^{2+} in Acetonitrile

The absorption spectrum of **5** in ACN consisted of a very intense band at 250 nm and a weak band around 310 nm as shown in Figure 4.8. Upon addition of one equivalent of $Cu(ClO_4)_2$, absorption spectrum corresponding to the radical cation of **5** appeared at 514 nm (Figure 4.8). Details of this assignment were given in Chapter 2 (Figure 2.1).

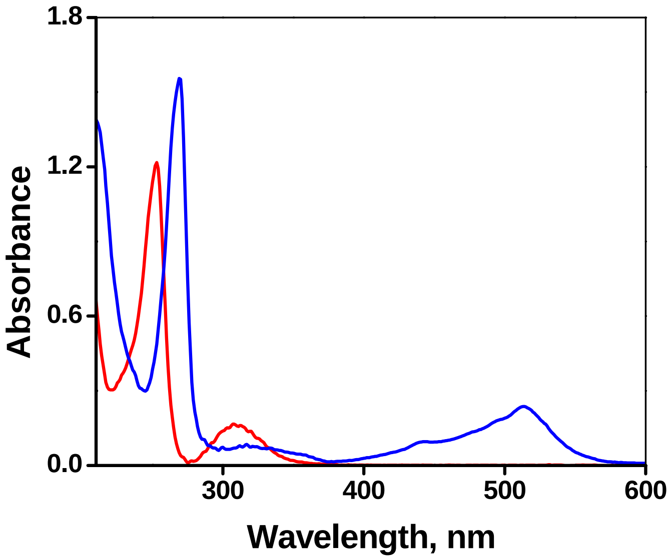

Figure 4.8. Absorption spectrum of **5** in the absence (–) and presence (–) of Cu^{2+}.

The absorption due to **5**$^{\bullet+}$ at 514 nm was very stable. The absorption spectrum was monitored for several hours and only marginal decrease was noticed. We, however, noticed that in the presence of more than one equivalent of Cu^{2+}, the absorption exhibited changes as shown in Figure 4.9. The time-dependent changes in the absorbance at 514 nm was monitored at different concentrations of Cu^{2+} and results are also shown in Figure 4.9. When [Cu^{2+}] was 2 equivalents, decay of the absorption at 514 nm was very slow, but when [Cu^{2+}] was 5 equivalents, the decay was very rapid.

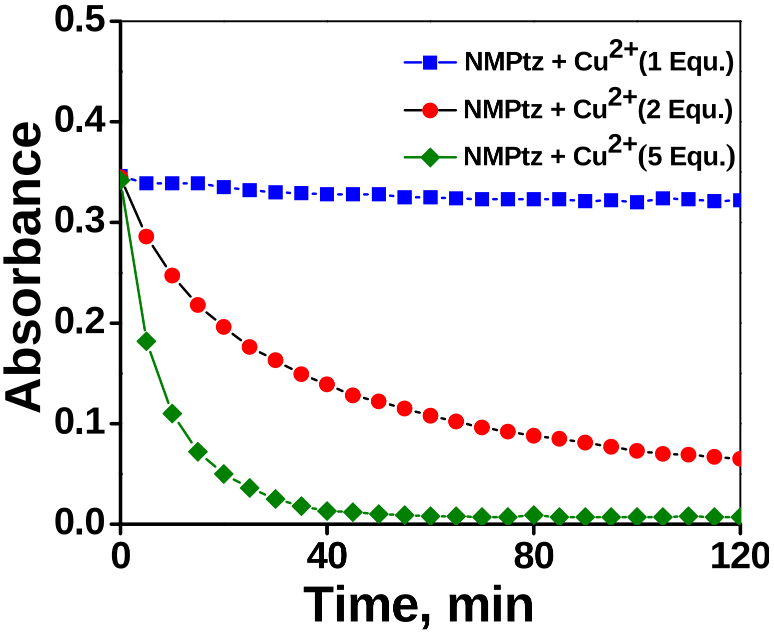

Figure 4.9. The change of absorbance at 514 nm in **5**/Cu^{2+} reaction with time at different Cu^{2+} concentrations.

In order to get a clear understanding of the reaction pathway followed, the spectral profile of **5**$^{\bullet+}$ was monitored in the presence of 5 equivalents of Cu^{2+} and the results are shown in Figure 4.10. It can be seen that the absorption due to **5**$^{\bullet+}$

decreased with concomitant increase in absorptions in the 300-400 nm region. A search of the literature suggested that the new species formed is phenothiazine-5-oxide (**11**, Scheme 4.4).[5]

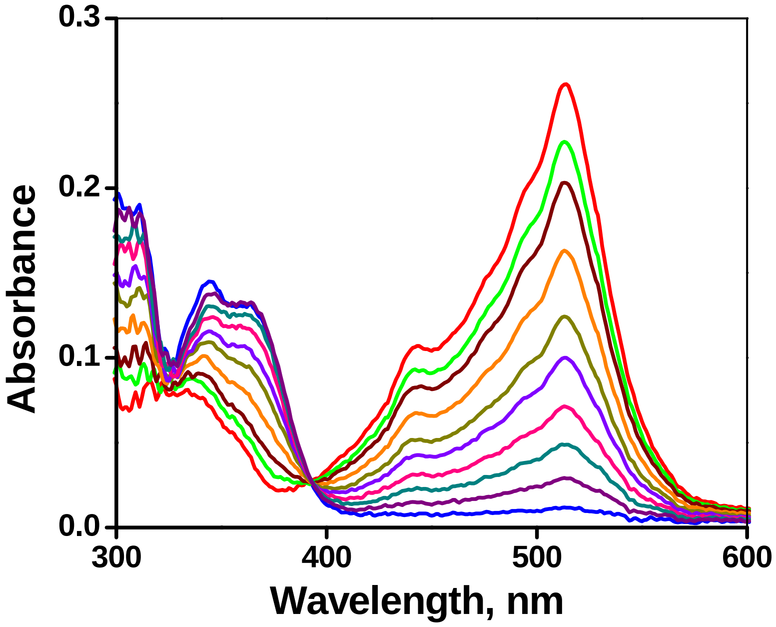

Figure 4.10. Time-dependent changes observed in the absorption spectrum of **5** in the presence of 5 equivalents of Cu^{2+}.

In order to identify the species, the reaction was scaled up and product was isolated (see experimental section). The product was analysed by spectroscopic and analytical techniques and unambigiously identified as *N*-methylphenothiazine-5-oxide (**11**). It was reported previously that $\mathbf{5}^{\bullet+}$ can be oxidized electrochemically to the $\mathbf{5}^{2+}$, which immediately reacts with water to form **11**.[5b] Based on these reports, Scheme 4.4, which involve oxidation of $\mathbf{5}^{\bullet+}$ to $\mathbf{5}^{2+}$ by Cu^{2+}, and subsequent reaction with water is suggested for the conversion of **5** to **11**.

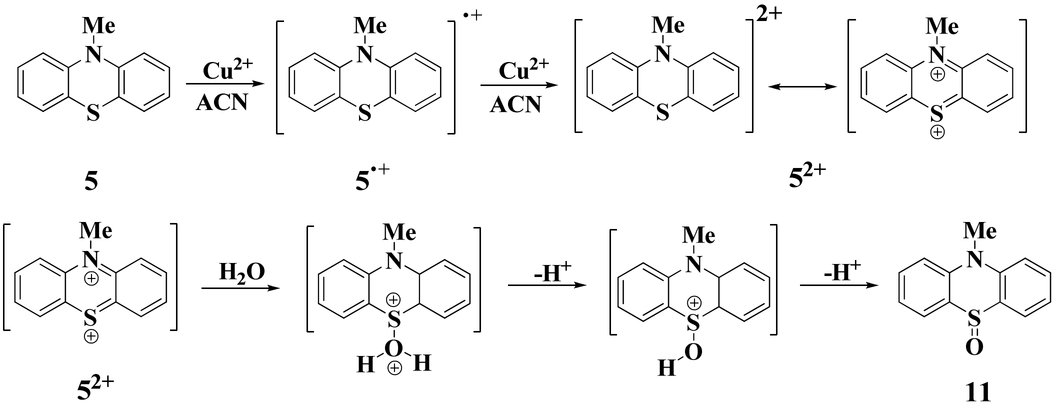

Scheme 4.4

4.3.4. Reaction of *N*-Phenylphenothiazine (6) with Cu^{2+} in Acetonitrile

Behaviour of **6**/Cu^{2+} system was very similar to that of **5**/Cu^{2+}. Figure 4.11 shows absorption spectrum of **6**, in the presence and absence of Cu^{2+}. Absorption maximum of $\mathbf{6}^{\bullet+}$ occurred at 255 and 520 nm and the absorption spectrum did not exhibit any time-dependent changes if [**6**] = [Cu^{2+}]. In the presence of excess Cu^{2+}, absorption due to $\mathbf{6}^{\bullet+}$ decreased and new absorptions shown in Figure 4.12 developed.

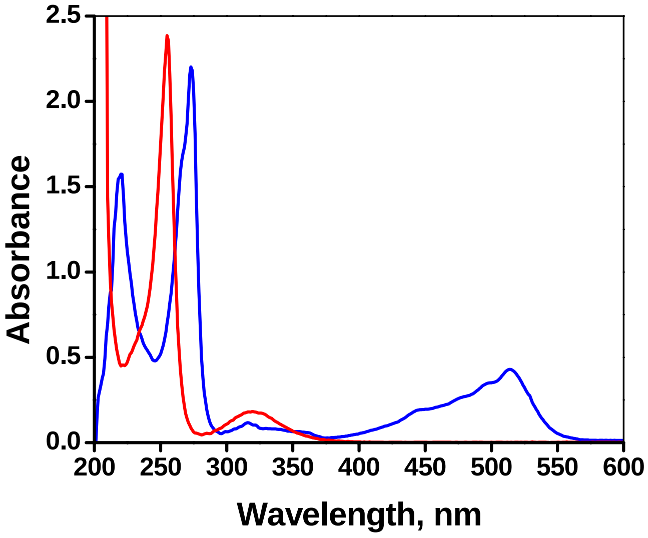

Figure 4.11. Absorption spectrum of **6** in the absence (–) and presence (–) of Cu^{2+}.

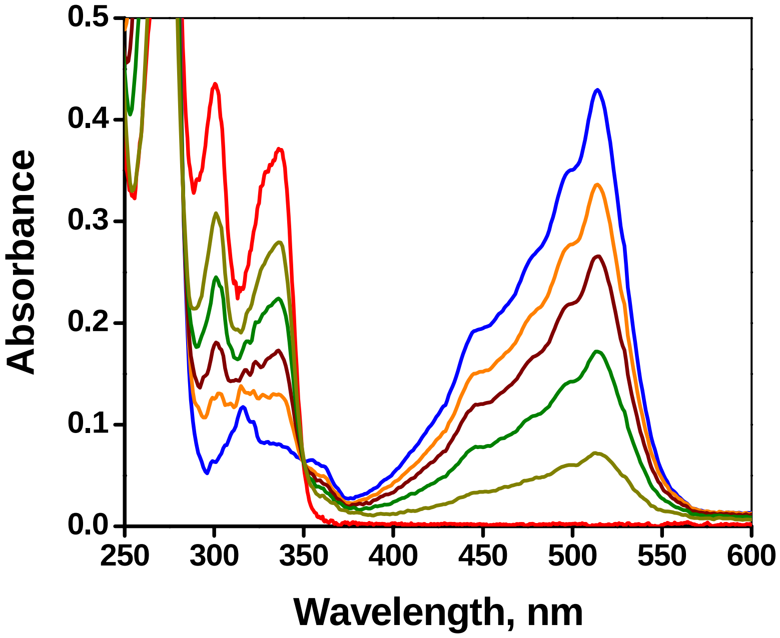

Figure 4.12. Time-dependent changes observed in the in absorption spectrum of **6** in the presence of 5 equivalents of Cu^{2+}.

In this case also the reaction was scaled up and product was isolated and identified as *N*-phenylphenothiazine-5-oxide (**12**) (see experimental section for details). Probable reaction pathway for the formation of **12** is shown in Scheme 4.5.

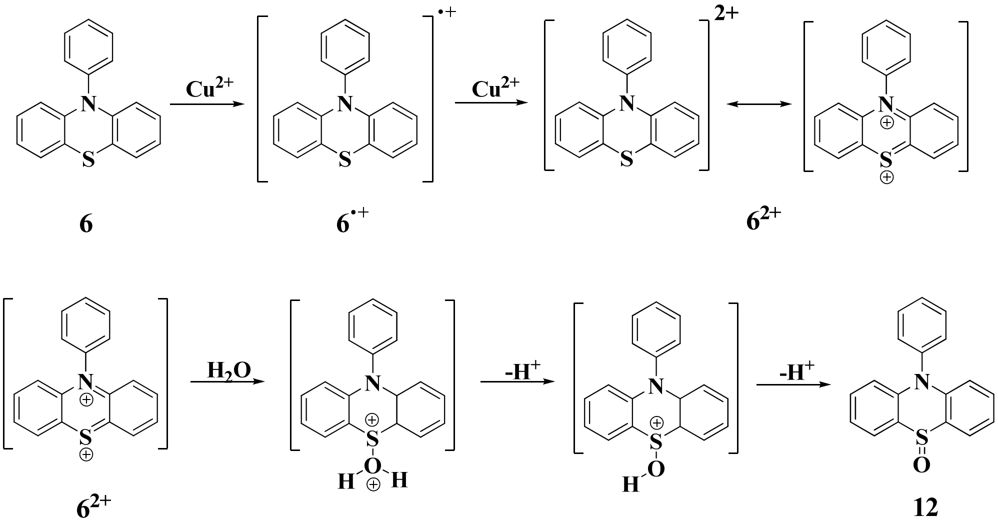

Scheme 4.5

In the case of **6**, the radical cation can in principle undergo a dimerization reaction involving the *para* position of the *N*-phenyl ring. $\mathbf{6}^{\bullet+}$ was actually very stable and did not exhibit any tendency for dimerization reaction.

4.3.5. Reaction of Tris(*p*-anisyl)amine with Cu^{2+} in Acetonitrile

Acetonitrile solution of **7** was colourless and exhibited absorption maximum at 296 nm. Figure 4.13 shows the effect of adding increasing amounts of $Cu(ClO_4)_2.6H_2O$ to **7** (5×10^{-5} M) in ACN.

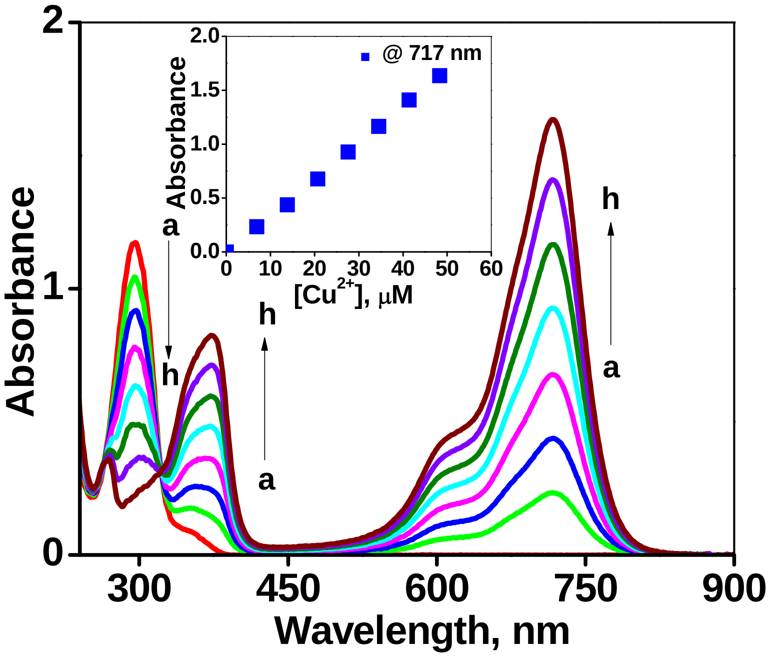

Figure 4.13. Effect of adding $Cu(ClO_4)_2.6H_2O$ to a solution of **7** (5×10^{-5} M) in ACN. $[Cu^{2+}]$ varied from 0 to 1 equivalents. Inset shows variation of absorbance as a function of $[Cu^{2+}]$.

When the Cu^{2+} concentration is in the range of 0-1 equivalents, the absorption due to **7** decreased with concomitant increase in absorption at 717 nm (Figure

4.13). When one equivalent of Cu^{2+} was added, absorption due to **7** disappeared completely, intensity of 717 nm absorption was maximum, and the solution was deep blue in colour. Further addition of Cu^{2+} leads to decrease in the intensity of the 717 nm absorption with concomitant increase in absorption at 520 nm (Figure 4.14). When 2 equivalents of Cu^{2+} was added, the absorption at 717 nm disappeared completely, absorption at 520 nm was maximum, and the solution was deep red in colour. Further addition of Cu^{2+} did not lead to any change in the absorption. Insets of Figure 4.14 show the change in the absorbance at 717 and 520 nm as a function of $[Cu^{2+}]$.

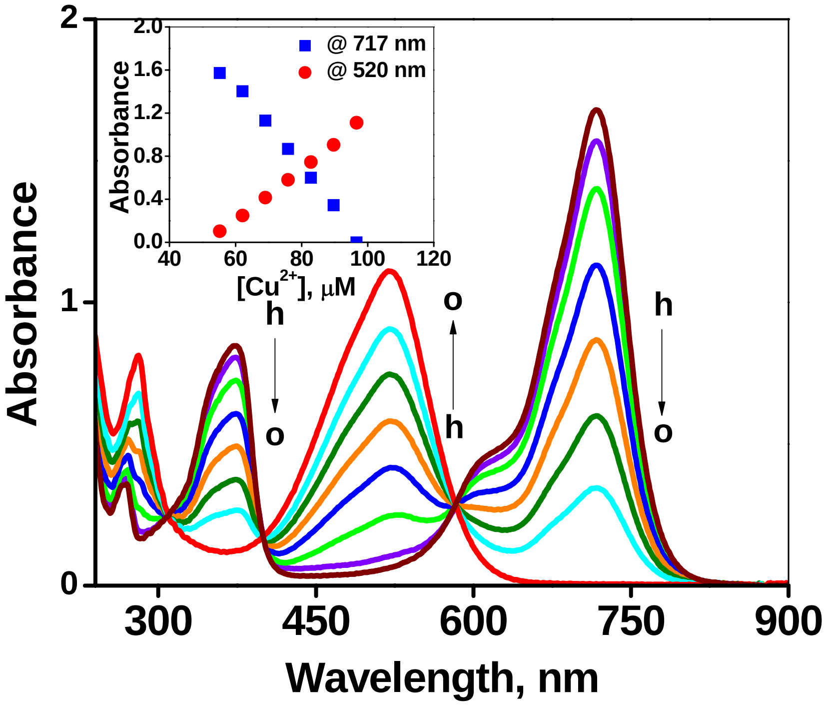

Figure 4.14. Effect of adding $Cu(ClO_4)_2.6H_2O$ to a solution of **7** (5×10^{-5} M) in ACN. $[Cu^{2+}]$ varied from 1-2 equivalents. Inset shows variation of absorbance as a function of $[Cu^{2+}]$.

Based on literature and our own studies the observations in Figure 4.13 and 4.14 are explained using Scheme 4.6. Reaction of **7** with Cu^{2+} leading to formation of $\mathbf{7}^{\bullet+}$ was instantaneous. Formation of the dication by reaction of $\mathbf{7}^{\bullet+}$ with Cu^{2+} was relatively slow and took 10-30 minutes for completion. Hence plots h-o in Figure 4.14 were taken 30 minutes after mixing.

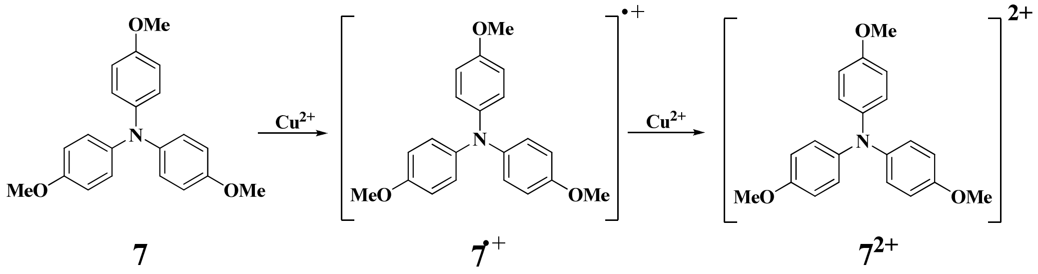

Scheme 4.6

Because of the different absorption bands and change over from one band to another, addition of 0-2 equivalents of $Cu(ClO_4)_2$ to a ACN solution of **7** (5×10^{-5} M) results in a play of colours as shown in Figure 4.15.

Figure 4.15. Play of colours in the reaction of **7** (5×10^{-5} M) with Cu^{2+}. Cu^{2+} concentrations were 0, 0.2, 0.4, 0.6. 0.8, 1.0. 1.2, 1.4, 1.6, 1.8 and 2.0 equivalents.

$\mathbf{7}^{\bullet+}$ obtained by reaction of **7** with one equivalent of Cu^{2+} was very stable. The solution could be kept without decomposition under ordinary laboratory conditions for several weeks. The reaction can be reversed and **7** could be quantitatively recovered by addition of an electron donor such as triethylamine (TEA). Gould *et al.*[6] generated $\mathbf{7}^{\bullet+}$ in ACN by spectroelectrochemistry and reported ε = 45,000 M^{-1} cm^{-1}. Lambert and co-workers using the same technique reported ε = 33,000 M^{-1} cm^{-1} in DCM.[2c] Assuming complete conversion of **7** to $\mathbf{7}^{\bullet+}$, we get ε = 32,800 M^{-1} cm^{-1} in ACN using data in Figure 4.13. Since $\mathbf{7}^{\bullet+}$ is very stable and 100% recovery of **7** was possible upon addition of TEA, we believe that the ε value we report here is very accurate.

As given in Table 4.1 formation of $\mathbf{7}^{2+}$ by reaction of $\mathbf{7}^{\bullet+}$ with Cu^{2+} is endergonic. Although ΔG^0 is slightly positive, dication formation takes place, albeit slowly, in the presence of more than one equivalent of Cu^{2+}, as is established from Figures 4.13-4.15. Lambert and co-workers reported that $\mathbf{7}^{2+}$ exhibited absorption maximum at 532 nm (ε = 20,000 M^{-1} cm^{-1}) in DCM.[2c] In ACN, absorption maximum we obtained was 520 nm (ε = 22,200 M^{-1} cm^{-1}). Because of the difference in absorption maximum it was necessary to confirm our assignment of the 520 nm absorbing species to $\mathbf{7}^{2+}$. This was achieved by adding **7** to a solution of the 520 nm absorbing species obtained by mixing **7** (2.5×10^{-5} M) and $Cu(ClO_4)_2$ (5×10^{-5} M) in ACN (Figure 4.16).

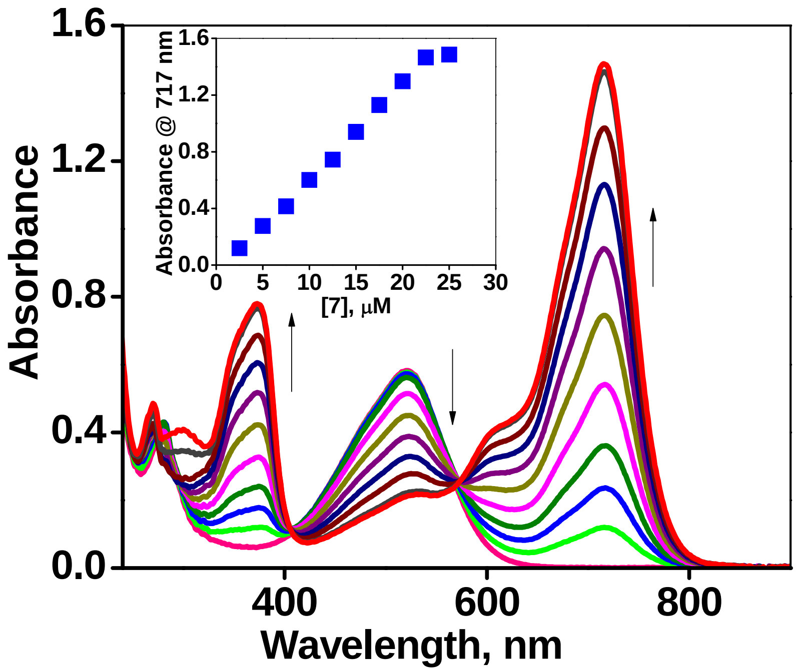

Figure 4.16. Effect of addition of **7** to $\mathbf{7}^{2+}$. Inset shows plot of the absorbance at 717 nm against [**7**]

The 520 nm absorption decreases with increase in the 717 nm absorption due to $\mathbf{7}^{\bullet+}$. Figure 4.16 can be explained using Scheme 4.7.

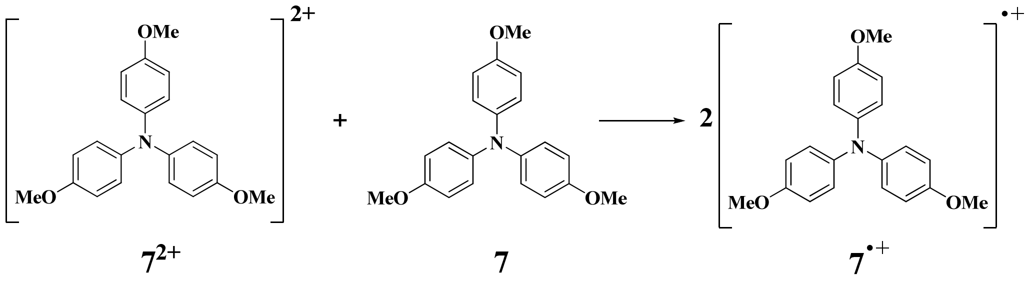

Scheme 4.7

Inset of Figure 4.16 is a plot of the absorbance at 717 nm against [**7**] added. The absorbance due to $\mathbf{7}^{\bullet+}$ was maximum when 2.5×10^{-5} M **7** was added. It may be noted that the absorption due to **7** at 296 nm builds up only after the 520 nm absorption vanishes. Based on this experiment the 520 nm absorption could be unambiguously assigned to $\mathbf{7}^{2+}$. From the absorbance maximum at 717 nm in Figure 4.16, the concentration of $\mathbf{7}^{\bullet+}$ obtained was 4.5 × 10^{-5} M, as against the expected value of 5 × 10^{-5} M, which means that the second oxidation is not completely reversible. This can also be evidenced from the cyclic voltammogram of **7** (Figure 4.1). Lambert and co-workers reported that the second oxidation of **5** is only 83% reversible in DCM. Our results show that reversibility of the second oxidation is better in ACN. The residual absorption at 520 nm (Figure 4.16) is suggestive of a product formation.

4.3.5.1. Use of Tris(*p*-anisyl)amine (7) as a Colourimetric Sensor for Cu^{2+}

The development of selective chemosensors for biologically important metal ions such as Cu^{2+} is an active area of research at present.[7-9] Among the essential heavy metal ions in the human body, Cu^{2+} is third in abundance after Fe^{3+} and Zn^{2+} and it plays very important roles in several biological processes.[10] Although Cu^{2+} is essential for the human body, exposure to high levels of Cu^{2+} for short periods of time can cause gastrointestinal disorders and long term exposures can cause kidney and liver damage.[11] In this context, selective detection of Cu^{2+} using simple techniques is very desirable. Chemosensors for metal ions are generally based on the three-component design consisting of receptor, spacer and signalling unit. Binding of the metal ion at the receptor site would lead to changes in some observable property of the signalling unit.

Synthesis of such sensor systems usually is tedious and may involve several steps. In addition, most of the common receptor units exhibit low to moderate binding affinities for other metal ions also and hence this type of sensor systems are not highly selective for Cu^{2+}. High selectivity, however, can be achieved if the sensor molecule exhibits a specific, reversible reaction with the metal ion.

The play of colours exhibited in the reaction of **7** with Cu^{2+} in ACN (Figure 4.15) prompted us to design a colourimetric sensor for Cu^{2+} based on this reaction. Figure 4.15 itself could be used as basis for the sensor design if no other metal ions produced such colour effects with **7**. In an attempt to see if any other metal ion reacted with **7**, we recorded the absorption spectra of **7** in the presence of several metal ions and the results are plotted in Figure 4.17. It can be seen from Figure 4.17 that Fe^{3+} also is capable of reacting with **7** to give $\mathbf{7}^{\bullet+}$. Although Ag^{+} and Hg^{2+} are better oxidizing metals compared to Cu^{2+} and Fe^{3+}, formation of the blue colour due to $\mathbf{7}^{\bullet+}$ could be noticed in these cases only if the solutions are kept for longer periods (> 12 h).

We have noticed, however, that addition of small amounts of water suppresses the reaction with all metal ions other than Cu^{2+}. As shown in Figure 4.18, when water content in the solution exceeds 3%, only Cu^{2+} shows a response, which could form the basis of selective detection of Cu^{2+} using **7**. We also observed that other ions do not influence the determination of Cu^{2+} in this method.

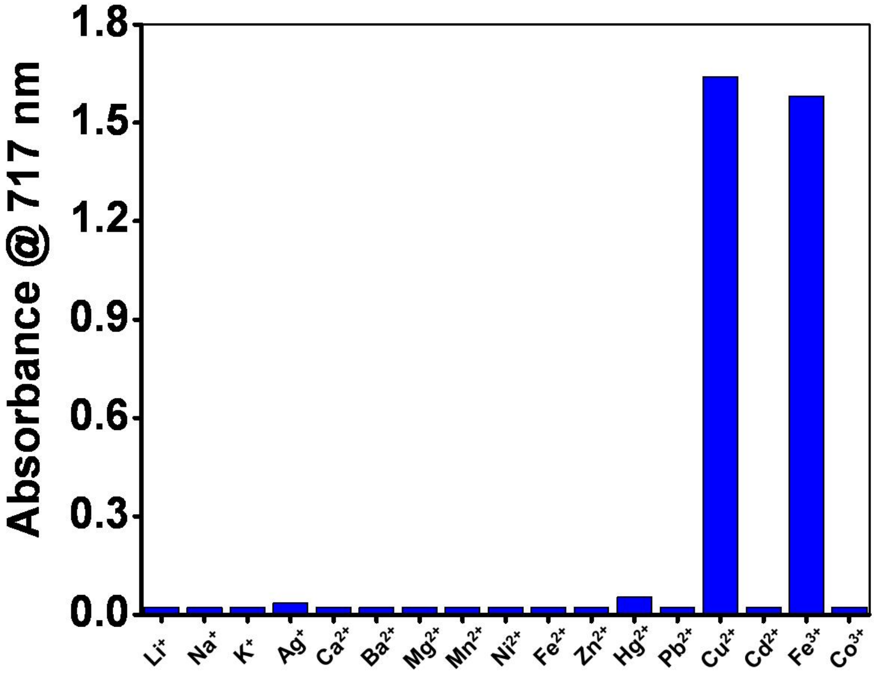

Figure 4.17. Effect of several other metal ions on the absorption properties of **7** in ACN.

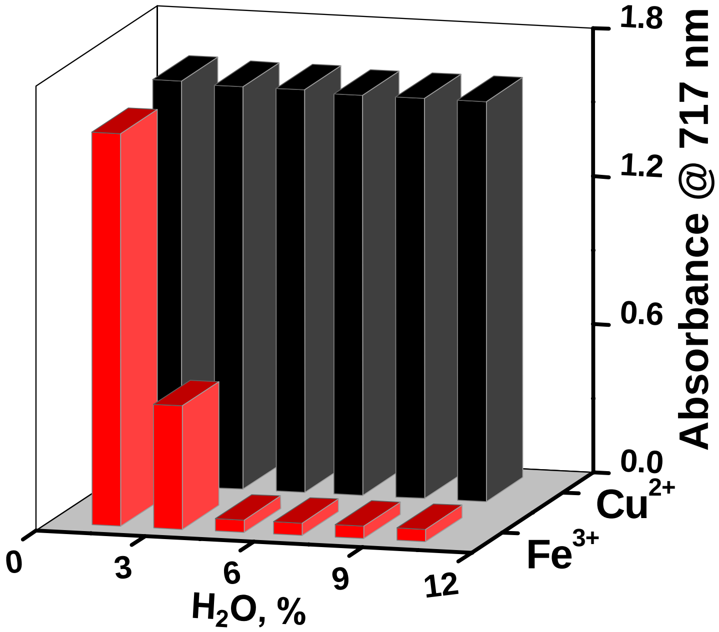

Figure 4.18 Effect of water on Cu^{2+} and Fe^{3+} reaction with **7** in ACN.

Our studies show that ACN containing 10% water is ideally suited for the selective determination of Cu^{2+}. In this solvent mixture, **7** exhibits oxidation peaks at 0.48 and 1.1 V and Cu^{2+}/Cu^{+} redox potential is shifted to 0.65 V vs SCE. $\mathbf{7}^{\bullet+}$ formation would be exergonic (ΔG^0 = -0.225 eV) and dication formation would be highly endergonic (ΔG^0 = +0.4 eV). We observed that **7** is readily converted to $\mathbf{7}^{\bullet+}$ in this solvent mixture and the $\mathbf{7}^{2+}$ is not formed at all, even in the presence of large excess of Cu^{2+}. The 717 nm absorption due to $\mathbf{7}^{\bullet+}$ was linear over a wide range of $[Cu^{2+}]$ as shown by the calibration curve in Figure 4.19. The curve can be used for the quantitative determination of Cu^{2+}. None of the metal ions shown in Figure 4.17 neither exhibited any response to **7** nor interfered with the determination of Cu^{2+}, under these conditions.

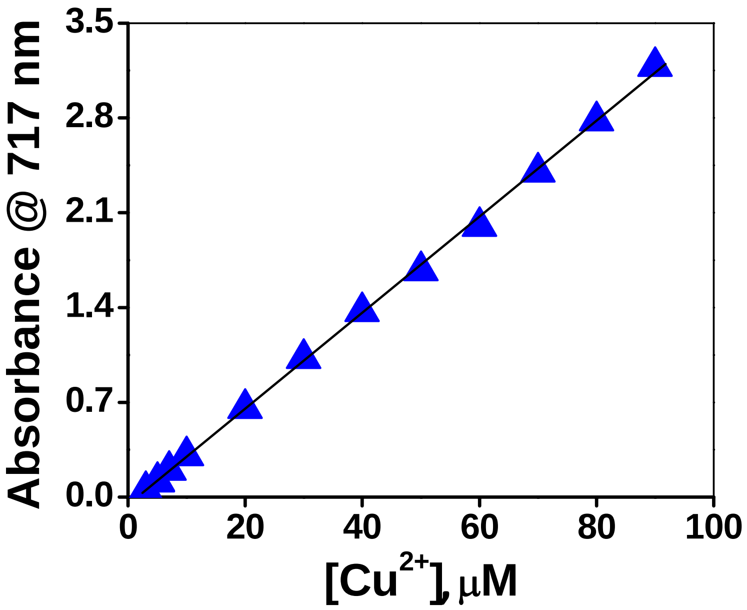

Figure 4.19. Plot of $\mathbf{7}^{\bullet+}$ absorbance at 717 nm vs $[Cu^{2+}]$ in ACN:H_2O (9:1). [**7**] was 5 × 10^{-4} M.

Thus the reaction of **7** with Cu^{2+} can be used as a basis for designing a sensor for Cu^{2+}. Cu^{2+} is capable of oxidizing **7** to $\mathbf{7}^{\bullet+}$ and $\mathbf{7}^{2+}$ in ACN leading to a play of colours. The first oxidation is perfectly reversible for any number of redox cycles whereas the second oxidation is not completely reversible. Among other metal ions tested, Fe^{3+} also could oxidize **7** to $\mathbf{7}^{\bullet+}$ and $\mathbf{7}^{2+}$ in ACN. These observations led to the conclusion that **7** could be used as a highly selective sensor for Cu^{2+}, if the second oxidation by Cu^{2+} and oxidations by Fe^{3+} were suppressed. We observed that both these objectives could be achieved by changing the solvent to ACN:H_2O (9:1) mixture. This solvent composition is suitable for testing Cu^{2+} in biological samples also. In this solvent mixture Cu^{2+} oxidizes **7** to $\mathbf{7}^{\bullet+}$, which is characterized by the strong absorption centered at 717 nm and blue colour. Plot of absorbance at 717 nm vs Cu^{2+} concentration was linear over a wide range and this can be used as a calibration curve for quantitative determination of Cu^{2+}.

4.4. Conclusions

In this chapter we have studied the reaction of few easily oxidizable aromatic amines with excess Cu^{2+} (2 or more equivalents) in ACN. In the case of benzidine derivatives **3** and **4**, these reactions yielded stable dications, which were characterized by their absorption spectra. In the case of amines **5** and **6**, the dications were unstable and reacted very fast with water to give oxidized products. In the case of **7**, reaction with Cu^{2+} in ACN resulted in a play of colours. We observed that in 9:1 ACN:water mixture, **7** could act as a very selective and sensitive colourimetric sensor for Cu^{2+}.

4.5. Experimental Section

4.5.1. Materials

Aromatic amine derivatives **3** and **4** were synthesized as described in Chapter 3 of this thesis and other amines **5-7** were synthesized according to literature procedures. $Cu(ClO_4)_2.6H_2O$ was purchased from Aldrich. Spectroscopic grade acetonitrile was used for electrochemical and spectroscopic studies.

4.5.2. Measurements

The electronic absorption spectra were recorded on a Shimadzu 3101PC UV-Vis-NIR Scanning spectrophotometer and Agilent-8453 Diode array spectrophotometer. Redox potentials of the amines were recorded using a BAS CV50W voltammetric analyser. Solutions of the amines (1×10^{-3} M) in acetonitrile containing 0.1 M tetra-*n*-butylammonium hexafluorophosphate as supporting electrolyte, were thoroughly deaerated before use. A Pt disc electrode was used as working electrode and a platinum wire was used as counter electrode and the potentials were referenced to saturated calomel electrode (SCE). Spectroelectrochemical measurements were carried out using a Pt mesh electrode in a 1mm quartz cuvette.

4.5.3. Synthesis

_N_-Methylphenothiazine-5-oxide (11)

To a solution of **5** (100 mg, 0.47 mM) in ACN (10 mL), $Cu(ClO_4)_2.6H_2O$ (870 mg, 2.35 mM) was added and the solution was stirred overnight. The mixture was diluted with dichloromethane and filtered through a neutral alumina column. Solvent was then evaporated and the residue was recrystallized from 1:8 dichloromethane-hexane mixture to get **11**, 96 mg (89%); ^{1}H NMR (300 MHz, $CDCl_3$): δ 3.77 (s, 3H), 7.25 (t, 2H), 7.39 (d, 2H), 7.62 (t, 2H), 7.39 (d, 2H). Mass Spectrometric analysis (FAB) m/z 230 (M+1).

_N_-Phenylphenothiazine-5-oxide (12)

To a solution of **6** (100 mg, 0.36 mM) in ACN (10 mL), $Cu(ClO_4)_2.6H_2O$ (670 mg, 1.8 mM) was added and the solution was stirred overnight. The mixture was diluted with dichloromethane and filtered through a neutral alumina column. Solvent was then evaporated and the residue was recrystallized from 1:4 dichloromethane-hexane mixture to get **12**, 86 mg (82%); ^{1}H NMR (500 MHz, $CDCl_3$): δ 6.69-6.71 (d, 2H), 7.21-7.24 (t, 2H), 7.37-7.42 (m, 4H), 7.60-7.63 (t, 1H), 7.68-7.71 (t, 2H), 7.98-8.00 (d, 2H); Mass Spectrometric analysis (EI) m/z 292 (M+1).

4.6. References

1. (a) Yoshizawa, K.; Chano, A.; Ito, A.; Tanaka, K.; Yamabe, T.; Fujita, H.; Yamauchi, J.; Shiro, M.; *J. Am. Chem. Soc.* **1992**, *114*, 5994. (b) Yoshizawa, K.; Hatanaka, M.; Ito, A.; Tanaka, K.; Yamabe, T.; *Chem. Phys. Lett.* **1993**, *202*, 483. (c) Yoshizawa, K.; Hatanaka, M.; Matsuzaki, Y.; Tanaka, K.; Yamabe, T. *J. Chem. Phys.* **1994**, *100*, 4453 (d) Ito, A.; Taniguchi, A.; Yoshizawa, K.; Tanaka, K.; Yamabe, T. *Bull. Chem. Soc. Jpn.* **1998**, *71*, 337. (e) Sato, K.; Yano, M.; Furuichi, M.; Shiomi, D.; Takui, T.; Abe, K.; Itoh, K.; Higuchi, A.; Katsuma, K.; Shirota, Y. *J. Am. Chem. Soc.* **1997**, *119*, 6607.
2. (a) Guichard, A.; Bourkba, A.; Poizat, O. *J. Phys. Chem.* **1989**, *93*, 4429. (b) Chaka, G.; Bakac, A. *Dalton Trans.* **2009**, 318. (c) Amthor, S.; Noller, B.; Lambert, C. *Chem. Phys.* **2005**, *316*, 141. (d) Reynolds, R.; Line, L. L.; Nelson, R. F. *J. Am. Chem. Soc.* **1974**, *96*, 1087.
3. (a) Sumalekshmy, S.; Gopidas, K. R. *Chem. Phys. Lett.* **2005**, *413*, 294. (b) Kirchgessner, M.; Sreenath, K.; Gopidas, K. R. *J. Org. Chem.* **2006**, *71*, 9849. (c) Sreenath, K.; Suneesh, C. V.; Ratheesh Kumar, V. K.; Gopidas, K. R. *J. Org. Chem.* **2008**, *73*, 3245. (d) Sreenath, K.; Suneesh, C. V.; Gopidas, K. R.; Flowers, R. A., II. *J. Phys. Chem. A* **2009**, *113*, 6477.
4. (a) Neta, P.; Huie, R. E. *J. Phys. Chem.* **1985**, *89*, 1783. (b) Rao, P. S.;

Hayon, E. *J. Phys. Chem.* **1975**, *79*, 1063. (c) Kiruthiga, K.; Aravindan, P.; Anandan, S.; Maruthamuthu, P. *Res. Chem. Intermed.* **2006**, *32*, 115. (d) Saget, J. P.; Plichon, V. *Bull. Soc. Chim. Fr.* **1969**, 1395. (e) Indelli, M. T.; Ballardini R.; Scandola, F. *J. Phys. Chem.* **1984**, *88*, 2547. (f) Barek, J.; Berka, A.; Novakova, L. *Coll. Czech. Chem. Commun.* **1978**, *43*, 1597. (g) Guichard, V.; Bourkba, A.; Poizat, O.; Buntinx, G. *J. Phys. Chem.* **1989**, *93*, 4429. (h) Szajna-Fuller, E.; Huang, Y.; Rapp, J. L.; Chaka, G.; Lin, V. S. Y.; Pruski, M.; Bakac, A. *Dalton Trans.* **2009**, 3237.

5 (*a*) Warren, R. J.; Eisdorfer, I. B.; Thompson, W. E.; Zarembo, J. E. *J. Pharm. Sci.* **1966**, *55*, 144 (*b*) Bodea, C.; Silberg, I. In *Advances in Heterocyclic Chemistry;* Katritzky, A. R.; Boulton, A. J., Eds.; Academic Press: New York, 1968; Vol. 9, pp 321–460.

6 (a) Gould, I. R.; Ege, D.; Moser, J. E.; Farid, S. *J. Am. Chem. Soc.* **1990**, *112*, 4290. (b) Suneesh, C. V.; Gopidas, K. R. *J. Phys. Chem. C* **2009**, *113*, 1604.

7 (a) de Silva, A. P.; Gunaratne, H. Q. N.; Gunnlaugsson, T.; Huxley, A. J. M.; McCoy, C. P.; Rademacher J. T.; Rice, T. E. *Chem. Rev.* **1997**, *97*, 1515. (b) *Chemosensors for Ion and Molecular Recognition*; Desvergne, J. P.; Czarnik, A. W., Eds.; Kluwer Academic Publishers: Dordrecht, The Netherlands, 1997.

8 (a) Zhao, Y.; Zhang, X.-B.; Han, Z.-X.; Qiao, L.; Li, C.-Y.; Jian, L.-X.;

Shen, G.-L.; Yu, R.-Q. *Anal. Chem.* **2009**, *81*, 7022. (b) Kim, H. J.; Kim, S. H.; Kim, J. H.; Anh, L. N.; Lee, J. H.; Lee, C.-H.; Kim, J. S. *Tetrahedron Lett.* **2009**, *50*, 2782. (c) Martínez, R.; Zapata, F.; Caballero, A.; Espinosa, A.; Tárraga, A.; Molina, P. *Org. Lett.* **2006**, *8*, 3235. (d) Huang, J.; Xu, Y.; Qian, X. *Dalton Trans.* **2009**, 1761. (e) Zhou, Y.; Wang, F.; Kim, Y.; Kim, S.-J.; Yoon, J. *Org. Lett.* **2009**, *11*, 4442. (f) Wu, S.-P.; Huang, R.-Y.; Du, K.-J. *Dalton Trans.* **2009**, 4735. (g) Yin, B.-C.; Ye, B.-C.; Tan, W.; Wang, H.; Xie, C.-C. *J. Am. Chem. Soc.* **2009**, *131*, 14624. (h) Sheng, R.; Wang, P.; Gao, Y.; Wu, Y.; Liu, W.; Ma, J.; Li, H.; Wu, S. *Org. Lett.* **2008**, *21*, 5015. (i) Liu, J.; Lu, Y. *Chem. Commun.* **2007**, 4872.

9 (a) Chen, W.; Tu, X.; Guo, X. *Chem. Commun.* **2009**, 1736. (b) Qi, X.; Jun, E. J.; Xu, L.; Kim, S.-J.; Hong, J. S. J.; Yoon, Y. J.; Yoon, J. *J. Org. Chem.* **2006**, *71*, 2881. (c) Choi, J. K.; Kim, S. H.; Yoon, J.; Lee, K.-H.; Bartsch, R. A.; Kim, J. S. *J. Org. Chem.* **2006**, *71*, 8011. (d) Kim, M. H.; Jang, H. H.; Yi, S.; Chang, S.-K.; Han, M. S. *Chem. Commun.* **2009**, 4838. (e) Kim, H. J.; Hong, J.; Hong, A.; Ham, S.; Lee, J. H.; Kim, J. S. *Org. Lett.* **2008**, *10*, 1963. (f) Xu, Z.; Xiao, Y.; Qian, X.; Cui, J.; Cui, D. *Org. Lett.* **2005**, *7*, 889. (g) Jisha, V. S.; Thomas, A. J.; Ramaiah, D. *J. Org. Chem.* **2009,** *74*, 6667. (h) Ajayakumar, G.; Sreenath, K.; Gopidas, K. R. *Dalton Trans.* **2009**, 1180.

10 (*a*) *Metal Ions in Biological Systems, Properties of Copper*; Sigel, H., Ed.; Marcel Dekker, Inc.: New York, 1981, Vol. 12. (b) Barceloux, D. G. *J. Toxicol. Clin. Toxicol.* **1999**, *37*, 217.

11 (*a*) Huster, D.; Lutsenko, S. *Mol. Biosyst.* **2007**, *3*, 816. (*b*) Georgopoulos, P. G.; Roy, A.; Yonone-Lioy, M. J.; Opiekun, R. E.; Lioy, P. J. *J. Toxicol. Env. Health B* **2001**, *4*, 341.

List of Publications

1. Understanding reactivity patterns of the dialkylaniline radical cation. Kirchgessner, M.; **Sreenath**, **K**.; Gopidas, K. R. *J. Org. Chem.* **2006**, *71*, 9849.
2. Cu(II)-mediated generation of triarylamine radical cations and their dimerization. An easy route to tetraarylbenzidines.

   Sreenath, **K**.; Suneesh, C. V.; Ratheesh Kumar, V. K.; Gopidas, K. R. *J. Org. Chem.* **2008**, *73*, 3245.
3. Phenothiazine attached $Ru(bpy)_3^{2+}$ derivative as highly selective “turn-ON” luminescence chemodosimeter for Cu^{2+}.

   Ajayakumar, G.; **Sreenath**, **K**.; Gopidas, K. R. *Dalton Trans.* **2009**, 1180.
4. Generation of triarylamine radical cations through reaction of triarylamines with Cu(II) in acetonitrile. A kinetic investigation of the electron-transfer reaction.

   Sreenath, K.; Suneesh, C. V.; Flowers, R. A. II.; K.; Gopidas, K. R. *J. Phys. Chem. A* **2009**, *113*, 6477.

Poster Presented at Conference

Generation of aromatic amine radical cations by reaction of aromatic amines with Cu^{2+}. Kinetic and spectroscopic studies and synthetic applications.

Kesavapillai Sreenath, Karical R. Gopidas.

In *National Symposium in Chemistry*, organized by *Chemical Research Society of India (CRSI)* at Pune. February, 5-8 2009.